FINITE ELEMENT ANALYSIS AND OPTIMISATION OF WATERJET COMPONENTS.

A thesis submitted in fulfilment of
the requirements for the Degree of
Master of Engineering in Mechanical Engineering
in the University of Canterbury
by
C. A. ALLAN

Finite Element Analysis and Optimisation of Waterjet Components.

C. A. ALLAN

March 29, 1993

Abstract

This report covers the testing and verification of the plate and shell element library of the Intergraph Finite Element Package, I/FEM and the subsequent use of this package for the modelling and analysis of the reverse duct of a jet unit currently in production by the Jet Division of C.W.F. Hamilton Ltd.

The element testing and verification closely followed by the method used MacNeal and Harder and others, which involved testing the finite elements for every possible type of deformation, and then grading the performance of the element as a result of these tests. The element with the highest overall grade, or the best performance in the types of deformation for which the element will be experiencing in the analysis, was selected for use in the following analysis.

This analysis has been carried out with the aid of an Intergraph "2020" Workstation, running the Intergraph software products I/EMS, or Intergraph/Engineering Modelling System and I/FEM, or Intergraph/Finite Element Modeller.

A plate model of the Model 273 Reverse Duct was constructed from drawings supplied by C.W.F. Hamilton Ltd., and this model was then 'meshed' and after appropriate loads and boundary conditions had been applied, was analysed in I/FEM. The results generated being discussed in the text. A small modification to the plate element model was made at the request of C.W.F. Hamilton Ltd., and the model was re–analyzed, the results discussed in the penultimate chapter.

Further directions for research are suggested in the concluding chapter, which may lead to experimental verification of the finite element model, and also to improved solution accuracy by a modification of the finite element model.

Acknowledgements

Many people have contributed both directly and indirectly to this research project. Particular thanks are given to the following people for their support and knowledge which has been shared:

Dr. R.J. Astley for providing a professional viewpoint of finite element analysis, and for keeping this project along the straight and narrow, despite the troubles that have arisen with various aspects of the research.

Wayne Munro, Gavin Macaulay and Roger Stephen for their help with the various computer and finite element problems that they have been laden with throughout the past year.

Phillip Smith, for his endless patience in setting up, modifying and rebuilding the various computer systems that have been used throughout this project.

Keith Alexander at C.W.F. Hamilton Ltd. for making this project possible, and providing the technical data and drawings necessary for the finite element model and analysis.

Gavin Griffith-Jones and Hamish Coop for their help with some fluid mechanics aspects of the project, and for supplying useful information about the C.W.F. Hamilton Ltd. jet unit that has been analysed during the course of this research project.

Dr A. Carr for the interesting, and very useful course on finite element analysis that is available in the Civil Engineering Department of the University of Canterbury.

A special thanks to my parents for their support, and the other people who have also looked after me during this hectic year, especially the Turner and Vincent families.

Thank you.

Contents

List of Figures

List of Tables

Notation

Mathematical Symbols

$[\ ]$	Matrix
$[\ ]^T$	Transpose of a matrix
$[\ ]^{-1}$	Inverse of a matrix
$\{\ \}$	Column matrix
$\{\ \}^T$	Row matrix

Latin Symbols

$\{\mathbf{a}\}$	Vector of parameters in assumed displacement field.
A	Cross–sectional area
$[\mathbf{B}]$	Strain–displacement matrix
C_{ijkl}	Elastic stiffness tensor
d.o.f.	Degree of freedom
$\{d\}$	Element degree of freedom matrix
D	Plate flexural rigidity
$[\mathbf{D}]$	Elasticity matrix
E	Modulus of Elasticity
$\{\mathbf{F}\}$	Element nodal force vector
$\overline{F_{ij}}$	Prescribed body force tensor
i, j, k	Dummy subscripts
I	Moment of inertia
$[\mathbf{k}]$	Element stiffness matrix
$[\mathbf{K}]$	Global stiffness matrix

L	Length
M_x, M_y, M_z	Bending moments
[N]	Elemental interpolation matrix
Q	Volumetric flowrate
Q_x, Q_y, Q_z	Direct stresses
R	Residual
S	Elasticity matrix
S_{ijkl}	Elastic compliance tensor
t	Thickness
T	Element boundary traction
$\bar{T}$	Prescribed Element boundary traction
u	Surface displacement vector
$\bar{u}$	Prescribed displacement
u, v, w	Displacement components
u_i	Displacement tensor
v_1	Initial velocity
v_2	Final velocity
V_n or Vn	Region of element "n", (includes boundaries)
x, y, z	Cartesian coordinates

Greek Symbols

β	Set of parameters, (Hybrid Stress elements)
δ	Element degree of freedom matrix
Δ	Element displacement field
ϵ	Strain field
ε	Strain field
ε_{ijkl}	Strain tensor
$\varepsilon_x, \varepsilon_y, \varepsilon_z$	Normal strains
η	Duct efficiency factor
ν	Poisson's ratio
θ	Vertical discharge angle
Θ	Modified vertical discharge angle

ϕ	Horizontal discharge angle
Π_p	Potential energy functional
ρ	Density
σ_{ijkl}	Stress tensor
$\sigma_x, \sigma_y, \sigma_z$	Normal stresses
$\{\sigma\}$	Element stress matrix
$\tau_{xy}, \tau_{yz}, \tau_{zx}$	Shear stresses
$\gamma_{xy}, \gamma_{yz}, \gamma_{zx}$	Shear strains

Chapter 1

Introduction

This chapter serves as an introduction to both the masters project as undertaken, and to the content of this thesis. A more correct title for this thesis might be "I/FEM Plate and Shell Element Verification, and Use of these Elements in the Analysis of a Waterjet Component", as this was the direction in which the studies have been pursued.

The first major part of the research was involved with determining the formulation of the plate and shell elements, available in the I/FEM element library, which would be suitable for analysing the complex geometry of the reverse duct of a waterjet unit currently in production. Once the results of these tests had been tabulated an appropriate element, the **QUD** four–noded quadrilateral, was selected and subsequently used for the analysis of the reverse duct.

A review of the roots of the finite element method is presented in chapter two, followed by a section on plate and shell finite elements. The reader is referred to several excellent texts for plate and finite element theory, where plate and finite element theory is covered more fully.

The remainder of the chapter contains two main sections, the first dealing with the plate and shell elements available with the Intergraph I/FEM package. The final section describes alternative methods of formulating plate and shell elements that have been published in recent years, which would result in improved performance and accuracy of the I/FEM package.

As finite element packages become more user–friendly, the engineer, or technician, undertaking an analysis may not wholly understand the errors that can very quickly arise. The main reasons for the testing and verification of the finite element libraries of commercial packages are presented in Chapter Three, followed by the results and conclusions

from the verification of the plate and shell element library of I/FEM.

Chapter Four deals with the analysis of a reverse duct from a C.W.F. Hamilton Model 273 jet unit. Control volume theory is initially used to derive suitable forces and pressures to be applied to a model of the duct.

The following chapter covers the modelling and analysis of the duct that was undertaken at the Mechanical Engineering Department of the University of Canterbury on the Intergraph products, I/EMS and I/FEM.

The reverse duct is analysed for two loadcases, which correspond to the worst loadings likely to be applied in service. The first loadcase is for an emergency, or "crash" stop from 25 knots, while the waterjet is evenly distributed between the two halves of the reverse duct. The second loadcase is similar, except that the jet of water only flows through one side of the reverse duct, severely stressing one side of the duct.

The results from the analysis are depicted in Appendix D, and the results are discussed in Chapter Five.

At the request of C.W.F. Hamilton Ltd. the thicknesses in selected high stress areas of the duct were changed, and the duct was re-analysed. The effect of this local increase in duct thickness is commented upon in Chapter Six, with the plates from this analysis depicted in Appendix E.

Chapter Seven presents the conclusions that have been drawn from this course of study and recommends several directions of research that might be undertaken, based upon the work completed so far.

Chapter 2

Plate and Shell Finite Element Theory

2.1 Introduction

This chapter, and indeed thesis, assumes some prior knowledge of the finite element method, if this is not the case, then the reader is urged to read such excellent texts as Astley, [5], Burnett [15], Cook [22], Gallagher, [33] and Zienkiewicz [104] for a more in–depth derivation of the finite element method.

This chapter is composed of four main parts. The first section deals with a history of the finite element method, with extensive references for those wishing to investigate the roots of the finite element method closely. The second section briefly outlines the steps that are taken in a typical analysis, and discusses the various methods that are used to formulate the force–displacement or stiffness relations.

A brief review of plate bending theory is then presented, followed by the derivation of three of the main conventional (assumed–displacement) plate bending element types, the Kirchoff, Mindlin and Discrete Kirchoff plate bending elements. In each case a comment on a typical element formulation is given.

Shell theory is given a cursory glance in the penultimate section, the reader desiring more detailed information is urged to consult several texts that have been used as references by the author.

In the final section a brief explanation of the element formulations in I/FEM, (as far as the author can deduce), is given, followed by a comment on alternative element formulations that are gaining more widespread use, as the inherent advantages, and superior accuracy of these methods becomes apparent.

2.2 Historical Development

The fundamental idea of the finite element method is the replacement of a continuous function by some piecewise approximation, generally polynomials. This can easily be seen in simple linear, elastic cases where a continuous displacement, or stress field across an object, whether a beam, a plate, or a solid is replaced with a series of piecewise approximations of these fields.

This method in engineering has only really come of age in the last thirty or so years and is now perhaps one of the most useful tools that is readily available to an engineer.

Structural engineering initiated the modern development of the finite element method. Since 1906 researchers have suggested a 'lattice analogy' in which a continuous problem was replaced by a regular pattern of elastic bars, the properties of the elastic bars chosen so as to give joint displacements of the same magnitude as those of the continuum. This analogy between actual discrete elements, (eg. bars and beams), and the corresponding portions of a continuous solid was further developed by Hrennikoff, [43], (1941), McHenry [70], (1943), and also Newmark [77], (1949), as the 'Grillage Method' in the context of aircraft structural design.

The commercial introduction of the 'high-speed' stored-program digital computer in the early 1950's further hastened the development of the finite element method, in that the now well-established methods of framework analysis could be reformulated into matrix format for efficient computation.

Mathematically, the modern finite element method was first proposed in a 1941 lecture by Courant, published in 1943, [23], in which he used the principle of stationary potential energy and piecewise polynomial approximation over triangular sub-regions to study the Saint Venant torsion problem. Similar papers followed by Polya, (1952), and Weinberger, [101], (1956). Greenstadt, [37], (1959), presented the idea of considering a continuous region as an assembly of several discrete parts, and making assumptions about the variables in each region; variational principles being used to find values for these variables.

However, this early mathematical discretisation work was largely ignored by the engineering profession until a more direct virtual work approach was developed independently by such persons as Argyris [2], (1960), and others, notably Turner et.al. [65], (1956), who at the Boeing Aircraft Company, suggested that the skin of a delta wing might be modelled by triangular plane stress elements. These works, published almost simultaneously, marked the beginning of the commercial use of finite elements.

This was a conceptual breakthrough, as it made it possible to realistically model two- and three-dimensional structures as an assembly of smaller two- and three-dimensional

pieces, ie. shells as an assembly of small shells, solids as an assembly of small solids.

The term 'finite element' was actually first used by Clough, [21], (1960), in a paper describing applications in plane elasticity. Since then, developments have proceeded at a prodigious pace. A rigorous mathematical basis has been developed, starting with the publishing of a convergence proof and error bounds in applied mathematics literature by Birkhoff et.al., [32], (1968), and Zlamal, [107], (1968). The first convergence proof in engineering literature was due to Melosh, [71] (1963), who utilised the principle of minimum potential energy.This was further extended as the solution of a problem using Reissner's variational principle by Jones, [58], (1964). A further advance was realised when it was seen that a finite element problem could be redefined as a weighted residual problem of some type, (Szabo and Lee 1969), [96], the Galerkin–Bubnov Method of Weighted Residual method being one of the more popular, and accurate, of these methods. Still later formulation methods have been developed, the "free–formulation" method espoused by Bergan, [11], being a particularly powerful method of developing a wide range of elements, based only upon the satisfaction of a "single–element patch test."

The next obvious problem to consider after plane problems was that of plate bending, and here the researchers found some very real problems, the first attempts being less than successful at modelling problems. It was not until the problems of inter-element compatibility were solved by Bazeley et.al., [35], (1965), that these elements began to give reasonable results.

Initially a major area of application of plate elements was as the bending part of a facet shell element in thin shell modelling, especially in the aerospace industry, and Clough and Johnson, [19], (1968), achieved some success. However modelling a surface using facet shell elements can cause problems, especially in the presence of pronounced curvature and it became clear that curved shell elements would be an improvement. The first shell element developed was an axisymmetric element by Grafton and Strome, [36], (1963), and these were followed by cylindrical and other shell elements by such persons as Gallagher [34], (1969).

Shell elements are still being studied, and various formulations are still being developed in what is probably the most complex area of static linear analysis.

Non-linear analysis is term used to cover one of the other main areas of on-going research in finite element analysis. 'Non-linear' covers a wide range of problems involving either non-linear geometry or materials with non-linear behaviour. Research has been undertaken in geometrically non-linear problems, ie. in which strains are small, but the

displacements are large, since 1960, (Turner et.al., [64]), and in problems involving non-linear materials and material properties, since the early 1960's. Gallagher et.al., [90] , (1962), studied plasticity, and Zienkiewicz et.al., [79], (1968) researched visco-elasticity.

Apart from the static problems discussed above, dynamic problems have, and are, being investigated, and the concept of the 'Consistent Mass Matrix' was introduced by Archer, [1], in 1963. Problems involving vibration and transients were also considered in this period, (Zienkiewicz et.al. [78], 1966, and Koenig and Davids [60], 1969, respectively).

Recent developments in finite element analysis have extended the applicability of the method to model coupled systems of various types, [106], for example the interaction at a fluid–structure boundary or the coupling between various domains such as in metal extrusion between the plastic flow and temperature domains and in soil–fluid interactions such as seepage through a earth dam. In such analyses Bettess and Zienkiewicz developed "infinite" elements, [13], to successfully model the decay behaviour at the boundaries of the problem domain which may, for the purposes of the analysis continue on to infinity. This special type of element has been extended to produce the "mapped infinite element" by researchers, P. Bettess being a prominent name. Astley, [6], recently published works in which a new form of infinite element, the "wave envelope element" has been derived, with excellent results being produced for many problems, especially in acoustics.

Fluid dynamics is another field in which finite element analysis has come of age and is now a major competitor to finite difference methods in the analysis of fluid flows, both incompressible and compressible, Oden, [81], being one of the primary researchers in the development of this branch of finite element analysis.

Still other element types have, and are being developed which have been neglected in this discussion, the boundaries of this very powerful method constantly expanding all the time.

2.3 A Brief Introduction to the Finite Element Method

As can be deduced from the previous section, the finite element method today covers a wide range of engineering problems, from linear to non–linear, static to dynamic, fluids to solids and so on. As linear static finite elements were the only type of elements used in the analysis, attention will be restricted to this type.

When the finite element method was being established in the early 1960's, it was first used as a direct stiffness method, (as opposed to a flexibility method). However, when plate and shell analysis began to dominate research, several other methods came to the fore. In general these other methods employed a variational principle of some type, the

principle of minimum potential energy predominating, however other principles have been, and still are used as the basis of some successful (accurate) elements.

Linear static analysis based upon variational methods can be divided into specific groups, depending on the assumptions that are made about the field variables of the governing variational equation, or indeed which variational equation that the element is based upon. Most of the elements that are discussed in this thesis are compatible–displacement type models, which are based upon an assumed displacement field both within the element and around the element boundary. These are derived from the principle of minimum potential energy.

Hybrid models are based upon some relaxation of the continuity requirements of the governing variational principle, allowing independent field variables within the element and along the boundary. An example of this type of element is the "Hybrid–stress" element, which is based upon a relaxation of the principle of minimum complementary energy, with an independent assumption of stresses within the element, and boundary displacements along the element boundaries.

Other types of element models include "Equilibrium" models, which are based upon an assumed stress field of some type, or prescribed displacements and an assumed equilibrating stress field. (There are two type of Equilibrium finite element models, the latter being similar to the above mentioned Hybrid–stress element).

"Mixed" models are based on the Hellinger–Reissner variational principle, and have displacements, prescribed boundary displacements and surface tractions as field variables.

Some of these alternative formulations are given a brief explanation at the close of this chapter, however most of these methods are not commonly used in commercial finite element packages

A Finite Element Analysis. The following is a brief list of the steps which must be undertaken, to complete a simple linear static finite element analysis of some structure or continuum object.

1. Subdivide the continuum (or structure) into a finite number of discrete elements.

2. Formulate the element properties, for example the field variables that the element is approximating must be piecewise continuous throughout the continuum, and also possess derivatives that are piecewise continuous throughout the continuum. (This second requirement can, and does, cause considerable troubles when formulating a compatible displacement–based plate element).

3. Assemble the elements to form a finite element model of the structure.

4. Apply loads to the model.

5. Specify the boundary conditions on the model.

6. Solve for the nodal (d.o.f.) displacements.

7. Extract the strains and stresses from the displacements.

Steps 1–3 can be collectively called the formation of the global stiffness equation, or the force-displacement relation. In linear elastic analysis these steps involve the most theoretical problems. In a simplistic sense, once this global stiffness equation has been formed, all that remains is for the equation to be solved using matrix manipulations, therefore formation of this relation is the main area which will be considered in this chapter.

2.3.1 Formulation of the Force–Displacement Relations

There are three main methods of formulating the force-displacement relations, these methods being; the Direct Stiffness Method, the Variational Method and the method of Weighted Residuals. The differences between these methods, and the advantages or otherwise, are briefly outlined in the following sections.

Direct Stiffness Method

The direct stiffness method is useful for illustrating the finite element method, as it provides a simple linkage between the real structure, material properties and relationships and the finite element method. However, use of the direct stiffness method is limited, as it is difficult, or impossible, to apply to complex elements and shapes. The following section shows the formation of the finite element stiffness equations using the direct stiffness method.

The direct stiffness method of formulation accomplishes the formulation of the element relationships by the direct combination of the three equations of linear elasticity; the equations of equilibrium, the strain-displacement relationships and the constitutive relationships.

1) The element displacement field, $\{u\}$, is expressed in terms of a finite number of parameters, $\{a\}$, preferably the element joint (node) degrees of freedom, $\{d\}$, by means of an interpolation matrix, $[N]$.

$$\{u\} = [N]\{d\} \tag{2.1}$$

2) The strain field, $\{\varepsilon\}$, is expressed in terms of the d.o.f. $\{d\}$ by differentiation of the displacement field in accordance with the strain–displacement equations of elasticity, for example $\varepsilon = \frac{du}{dx}$ and so on. The strain field is defined as:

$$\{\varepsilon\} = [B]\{d\} \tag{2.2}$$

where $[B]$ is the strain-displacement matrix.

The stresses may then be related to the strains by the use of an elasticity matrix, $[D]$, as follows

$$\{\sigma\} = [D]\{\varepsilon\} \tag{2.3}$$

3) The constitutive law, σ = E ε, is introduced to establish the relationship between the stress field, $\{\sigma\}$, and the d.o.f. $\{d\}$.

$$\{\sigma\} = [D][B]\{d\} \tag{2.4}$$

4) Equations that describe the element joint forces, $\{f\}$, as functions of the stress field, $\{\sigma\}$, are constructed by defining these forces as the statical equivalents of the stresses acting along the element boundaries. Since equations for $\{\sigma\}$ are available in terms of $\{d\}$ (Eq. 2.4), it is now possible to relate {f} to $\{d\}$, with an element stiffness matrix, $[k]$.

$$[k]\{d\} = \{f\} \tag{2.5}$$

5) Assembly - The equations for a series of elements joined at common points (nodes) can now be combined into one large matrix stiffness equation.

$$[K]\{d\} = \{F\} \tag{2.6}$$

Variational Methods

The variational method of solution, for finite element problems, ie. minimisation of some energy expression is probably the most commonly used method available in software today. This method has the advantage of being simple and, for problems that can be described by a minimisation expression, it generally provides accurate results.

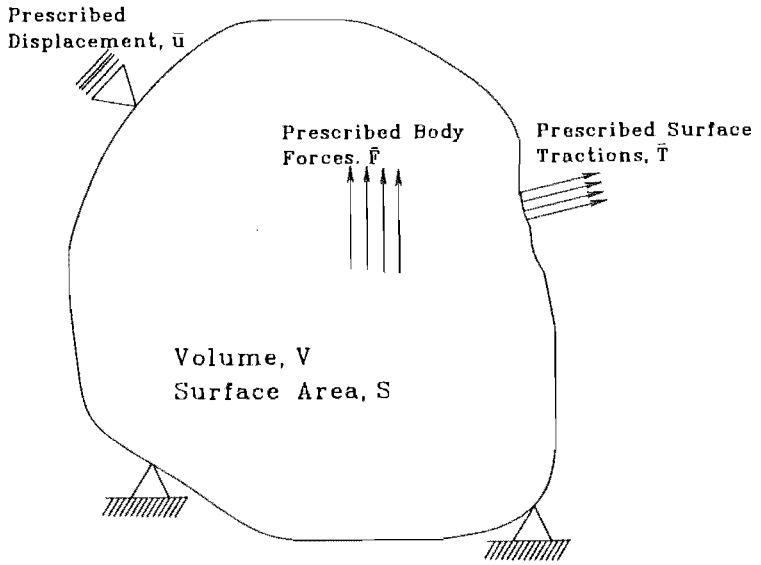

Figure 2.1: Elastic body under the influence of forces

Consider the elastic body shown in figure 2.1, which is under the influence of body forces, prescribed displacements and applied surface tractions.

Now the equations of linear elasticity that apply to this situation are, in matrix notation;

1. The stress equilibrium equations

$$\frac{\partial \sigma_x}{\partial x} + \frac{\partial \tau_{xy}}{\partial y} + \frac{\partial \tau_{xz}}{\partial z} + F_x = 0, \tag{2.7}$$

(The other 2 equations being found by cyclic rotation of the subscripts).

2. The stress–strain relationship

$$\begin{aligned} \{\sigma\} &= [E]\{\varepsilon\} \\ \text{or} & \\ \{\varepsilon\} &= [E]^{-1}\{\sigma\} \end{aligned} \tag{2.8}$$

where $[E]$ is the constitutive matrix.

3. The strain–displacement relationship

$$\begin{Bmatrix} \varepsilon_x \\ \varepsilon_y \\ \gamma_{xy} \end{Bmatrix} = \begin{Bmatrix} \frac{\partial u}{\partial x} \\ \frac{\partial v}{\partial y} \\ \frac{\partial u}{\partial y} + \frac{\partial v}{\partial x} \end{Bmatrix} \tag{2.9}$$

Now to solve this system, one must take into account all the prescribed surface tractions, body forces and displacements.

A simple way of achieving this is to re–formulate the equations of linear elasticity into a "Variational Formulation".

There are three main variational theorems, the principle of minimum potential energy, the principle of minimum complementary energy and the Hellinger–Reissner's variational theorem, each leading towards the formulation of a particular type of finite element. The only variational principle that will be discussed in this section is the principle of minimum potential energy, which can be derived from the principle of virtual displacements.

In the principle of minimum potential energy, the only field variables are the displacements, which must be continuous within the domain being considered.

The *principle of virtual work* states that the total potential energy of the system can be expressed as the sum of the strain energy, (U), and the potential of the applied loads, (V), or

$$\Pi_p = U + V \tag{2.10}$$

The principle of minimum potential energy states that of all displacements of *admissible* form, those which make the potential energy assume a stationary value, satisfy the equilibrium conditions. Thus

$$\partial \Pi_p = \partial U + \partial V = 0 \tag{2.11}$$

Now the strain energy of an elastic body, neglecting initial strains, is defined as

$$U = \frac{1}{2} \int_V \{\varepsilon\}^T \{\sigma\} \, dV \tag{2.12}$$

and the potential of the applied loads as

$$V = - \int_V \{u\}^T \{b\} dV - \int_S \{u\}^T \{t\} dS \tag{2.13}$$

These two expressions are then combined to give the expression for potential energy:

$$\Pi_p = \frac{1}{2} \int_V \{\varepsilon\}^T \{\sigma\} \, dV \; - \; \int_V \{u\}^T \{b\} \, dV \; - \; \int_S [u]^T \{t\} \, dS \tag{2.14}$$

in which the displacement field is

$$\{u\} = \{u, v, w\}^T \tag{2.15}$$

the strain field

$$\{\varepsilon\} = \{\varepsilon_x, \varepsilon_y, \varepsilon_z, \gamma_{xy}, \gamma_{yz}, \gamma_{zx}\}^T \tag{2.16}$$

the stress field

$$\{\sigma\} = \{\sigma_x, \sigma_y, \sigma_z, \tau_{xy}, \tau_{yz}, \tau_{zx}\}^T \tag{2.17}$$

the body forces

$$\{b\} = \{b_x, b_y, b_z\}^T \tag{2.18}$$

the boundary tractions

$$\{t\} = \{t_x, t_y, t_z\}^T \tag{2.19}$$

Now the displacement field can be described in terms of the nodal values, $\{d\}$, by means of the interpolation or shape functions, $[N]$.

Thus

$$\{u\} = [N]\{d\}, \tag{2.20}$$

and the strain field, $\{\varepsilon\}$, is described as

$$\{\varepsilon\} = [B]\{d\}, \tag{2.21}$$

where $[B]$ is the strain–displacement matrix. The stress may be related to the strains by the use of an elasticity matrix, $[D]$, as follows:

$$\{\sigma\} = [D]\{\varepsilon\}. \tag{2.22}$$

The governing FE equations are obtained by minimizing the potential energy to obtain the global system of equilibrium equations:

$$[K]\{d\} - \{F\} = 0 \tag{2.23}$$

where

$$[K] = \int_V [B]^T [D] [B] \, dV \tag{2.24}$$

$$\{F\} = \int_V [N]^T \{b\} \, dV + \int_V [N]^T \{t\} \, dS \tag{2.25}$$

Method of Weighted Residuals

The method of weighted residuals is, in comparison to the direct method of stiffness formulation and even the variational method, of virtually unlimited scope and appears to possess advantages absent from alternative approaches.

A proviso of the variational method of formulation of the force–displacement relations is that the problem must be able to be described by a minimisation expression. This is a major advantage of the method of weighted residuals, in which almost all problems can be solved, irrespective of whether or not they are applicable to a minimisation problem.

Therefore, for certain classes of nonlinear problems the method of weighted residuals may be employed to produce relationships that cannot be obtained with the use of conventional variational principles.

Burnett [15] solely uses this method in his text on finite element analysis, and the reader is urged to refer to this for a more thorough explanation of this method.

To solve a problem using the method of weighted residuals, one presumes that a trial function of some type, which is chosen to approximate the independent variable in a problem of mathematical physics, will not, in general, satisfy the governing differential equation. Therefore, substitution of the trial function into the governing differential equation will result in a *residual*, denoted here by R.

To obtain the best solution, it is required to minimise the integral of these residuals throughout the problem domain, V, or

$$\int_V R \cdot dV = \mathrm{m}inimum \tag{2.26}$$

It is possible to increase the range of possibilities of solution by requiring that a weighted value of the residual be a minimum throughout the domain. This means that the weighted integral of the residuals can achieve a value of zero. Therefore the more general form of the above equation becomes

$$\int_V R \cdot \phi dV = 0, \tag{2.27}$$

where ϕ is a weighting function.

This is the general statement of the Method of Weighted Residuals.

Now there are several methods of choosing the weighting functions, the most popular method being the Bubnov–Galerkin, or simply Galerkin method, which yields equations identical to those obtained by the variational methods of the previous section.

In this method, the weighting functions, ϕ_i, are chosen to be the coefficients, or shape functions, N_i, of the general coordinates, u. Therefore the statement of the Galerkin method of weighted residuals is

$$\int_V N_i \, L\,(u)\, dV \;=\; 0, \quad \text{where } i = 1, 2....n \tag{2.28}$$

and this gives rise to n equations. This equation deals only with points within the problem domain, and therefore does not include the effect of boundary conditions. To produce these boundary conditions, one applies integration by parts to the above equation, yielding integrals both inside and on the domain.

2.4 Plate and Shell Elements

Extensive efforts have been devoted to the formulation of plate bending elements. The requirements of an adequate formulation are often difficult to meet, and for this reason an exceptionally wide variety of alternative formulations have been proposed, for example, Ref [42] lists 88 different plate and shell elements, and 154 references in 1984.

One reason why there is so much difficulty in the formulation of these elements is that the flexure of plates is governed by a fourth-order differential equation, rather than a second-order equation, as is the case in plane stress, plane strain and three-dimensional analysis. Another reason for the difficulty in the analysis of plates and shells is that the thickness of the plate is, in most cases, much less than the other characteristic dimensions of the plate, similarly for the element. This can lead to numerical difficulties in the analysis of the stiffness equations of the plate.

A distinction is made here between plates and shells. A plate is taken to be a bending element, neglecting membrane or in–plane effects.

Shell elements are taken to be (generally) curved elements which include membrane effects, with either singly– or doubly–curved geometry, the different element topology giving rise to corresponding differences in the formulation, in which the membrane and bending actions of the shell are coupled. In shell elements, a bending element and a membrane element can be combined to give the element. However, if only one of these effects is required for a particular problem, they can be used separately, to give a particular bending or membrane element.

In the following section a brief review of the basic equations of current plate theory are presented, which should help the reader to appreciate the problems that beset programmers and analysts with regards to plate and shell elements.

2.4.1 Plate Theory

The theory of the deformation of thin plates is well-covered in many texts, the book of Timoshenko and Woinowsky-Krieger, [100], being particularly good.

Three major types of plate theory are briefly summarized and discussed in this chapter, these being:

1. Kirchoff plate theory,
2. Mindlin–Reissner theory and
3. Discrete Kirchoff theory.

The theory is followed through to the development of an appropriate expression for the strain energy of an element. This expression can then be substituted, together with an expression for the potential energy of the applied loads to the system, into an appropriate potential energy expression and solved by minimisation with respect to the nodal displacements of the system, (the variational method).

These types of plate theory are each illustrated with an applicable finite element formulation. Several alternative element formulations are briefly mentioned at the conclusion of this chapter, to show some of the ingenuity that has been used to produce more accurate plate elements. These elements having been greeted with varying degrees of acceptance by commercial finite element program teams or producers, generally depending on the compatibility with existing finite element codes.

2.4.2 Kirchoff Plate Theory/Formulation

Kirchoff theory is the simplest form of plate flexure theory applicable to thin plates, in which transverse shear deformation is neglected by the imposition of the condition that the angular displacement of a normal to the middle surface equals the slope of the middle surface. Indeed it can be shown that the simplicity of this theory does cause many problems for the development of accurate, compatible plate–bending elements. The requirements for a compatible element were stated in 1965, in a paper by Irons and Draper, [49], and were summarised as:

1. It must be possible to represent element rigid body motions in order to meet equilibrium conditions,
2. It must be possible to represent states of constant stress in order to guarantee convergence with mesh refinement, and

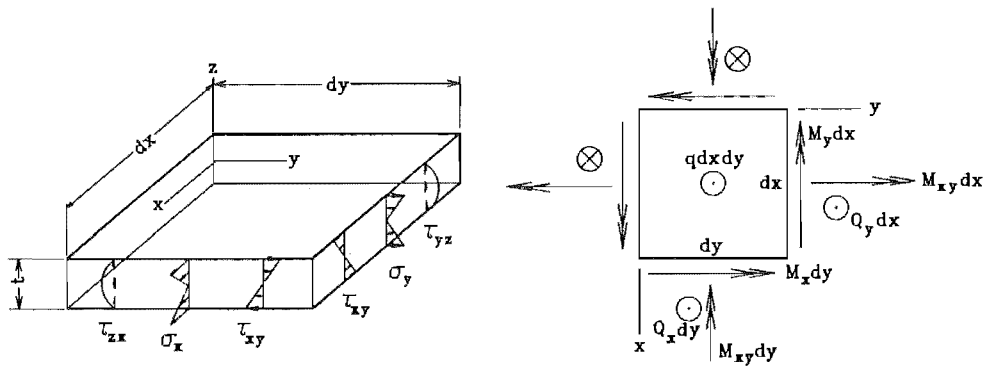

Figure 2.2: Differential plate element.

3. There must be no discontinuities in either slope or displacement between elements, or else the structure will incorrectly deform and lose the bounded nature of the solution.

This causes no small problem as can be seen in the description of various Kirchoff elements at the end of this sub–section, in fact, in order to meet the Kirchoff requirements, an assumed–displacement element must specify more than just the displacement, w, and the nodal rotations, θ_x and θ_y, at two nodes per edge, but also the derivative of the rotations in order to adequately meet the third requirement.

Firstly however, the basic Kirchoff theory will be reviewed.

Consider a differential (rectangular) element of a thin flat plate, of thickness t, as portrayed in figure 2.2. A state of plane stress exists in the plate, ($\sigma_z = \gamma_{xz} = \gamma_{yz} = 0$) and in accordance with the usual assumptions of thin plate flexure the normal stresses, (σ_x, σ_y) vary linearly (with z) across the thickness and are associated with bending moments M_x and M_y. Shear stress τ_{xy} also varies linearly with z and is associated with the twisting moments, M_{xy} per unit length. The positive sense of these moments is as shown in the figure.

Deformations

The deformation of a plate differential element under Kirchoff theory obeys several simple rules.

1. Deflections are small.

2. Points on the midsurface, ($z = 0$), move in only the z direction as the plate is bent.

3. Lines straight and perpendicular to the midplane remain so after deformation.

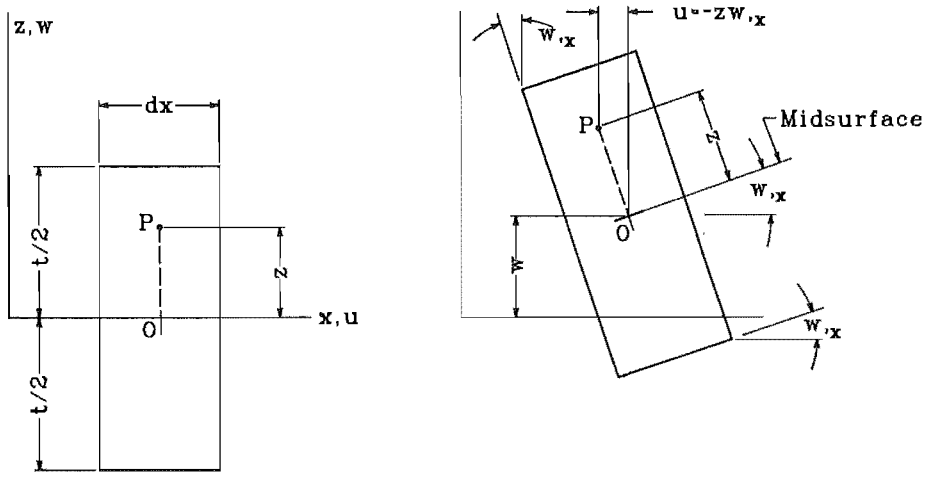

Figure 2.3: Deformation of a differential plate element: Kirchoff theory.

With reference to figure 2.3, the displacement of a point, P, (not on the midplane), can be described by the equations:

$$\begin{aligned} u &= -zw_{,x} \\ v &= -zw_{,y} \end{aligned} \tag{2.29}$$

And the strain–displacement equations are:

$$\{\varepsilon\} = \left\{ \begin{array}{c} \varepsilon_x \\ \varepsilon_x \\ \gamma_{xy} \end{array} \right\} = \left\{ \begin{array}{c} u_{,x} \\ v_{,y} \\ u_{,x} + v_{,y} \end{array} \right\} = \left\{ \begin{array}{c} -zw_{,xx} \\ -zw_{,yy} \\ -2zw_{,xy} \end{array} \right\} \tag{2.30}$$

Now the stress–strain equations for a linear homogeneous, isotropic material neglecting initial strains are:

$$\left\{ \begin{array}{c} \sigma_x \\ \sigma_y \\ \tau_{xy} \end{array} \right\} = \left[\begin{array}{ccc} E/(1-\nu^2) & \nu E/(1-\nu^2) & 0 \\ \nu E/(1-\nu^2) & E/(1-\nu^2) & 0 \\ 0 & 0 & E/(2(1+\nu)) \end{array} \right] \left\{ \begin{array}{c} \varepsilon_x \\ \varepsilon_y \\ \gamma_{xy} \end{array} \right\} \tag{2.31}$$

Integration of the stresses across the thickness yields bending moments, M_x, M_y and M_{xy} and transverse shear forces Q_x, Q_y as shown in the following equations.

$$M_x = \int_{-t/2}^{t/2} \sigma_x z dz \quad M_y = \int_{-t/2}^{t/2} \sigma_y z dz \quad M_{xy} = \int_{-t/2}^{t/2} \tau_{xy} z dz$$

$$Q_x = \int_{-t/2}^{t/2} \tau_{zx} dz \quad Q_y = \int_{-t/2}^{t/2} \tau_{yz} dz \tag{2.32}$$

It should be noted that the above expressions are moments per unit length and forces per unit length. When these expressions are integrated across the thickness of the plate, the total differential moments, and shears, are given by $M_x dy$, $\sigma_x dy$

Stresses can also be calculated to be

$$\begin{aligned} \sigma_x &= \frac{M_x z}{t^3/12} \qquad \sigma_y = \frac{M_y z}{t^3/12} \\ \tau_{xy} &= \frac{M_{xy} z}{t^3/12} \end{aligned} \tag{2.33}$$

Moment-Curvature Relationships

Substitution of the stress–strain relations into the above equations gives the relationship between the moments and curvatures.

$$\begin{Bmatrix} M_x \\ M_y \\ M_{xy} \end{Bmatrix} = - \begin{bmatrix} D & \nu D & 0 \\ \nu D & D & 0 \\ 0 & 0 & (1-\nu)D/2 \end{bmatrix} \begin{Bmatrix} -w_{,xx} \\ -w_{,yy} \\ -2w_{,xy} \end{Bmatrix} \text{ or } \{M\} = [D_K]\{\kappa\} \tag{2.34}$$

where the flexural rigidity of the plate, $D = (\mathrm{E}t^3)/(12(1-\nu^2))$, E is Young's Modulus, t the thickness and ν Poisson's Ratio.

Kirchoff Element Stiffness Matrix

The element stiffness matrix for a Kirchoff finite element is formulated using the following general formulae:

$$U = \int_V \frac{1}{2} \{\varepsilon\}^T [E] \{\varepsilon\} dV \tag{2.35}$$

where $\{\varepsilon\}^T = \{-zw_{,xx} \; -zw_{,yy} \; -2zw_{,xy}\}$.

For a rectangular plate element, with edges parallel to the x- and y–axis, this becomes

$$U = \int_A \frac{1}{2} \{\kappa\}^T [D_K] \{\kappa\} dA \tag{2.36}$$

where $\{\kappa\}^T = \{w_{,xx} \; w_{,yy} \; 2w_{,xy}\}$

The midplane displacement is expressed in terms of the nodal d.o.f., $\{d\}$:

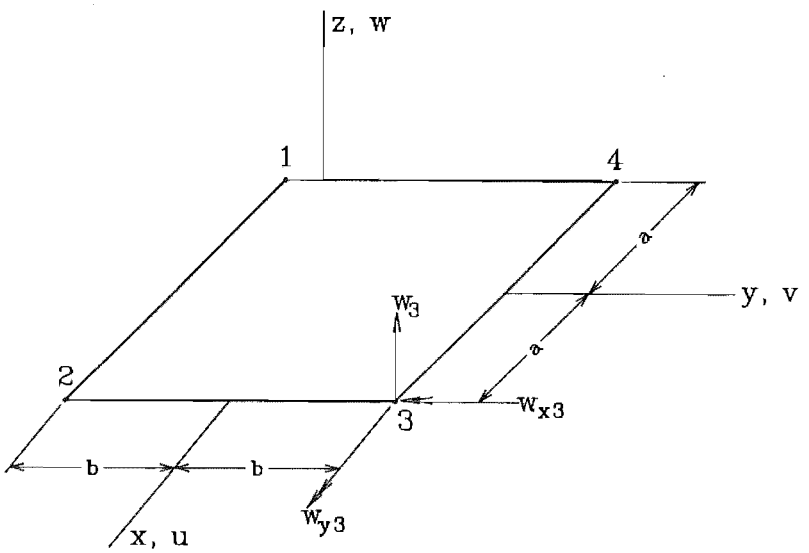

Figure 2.4: Adini, Clough, Melosh rectangular element.

$$\{w\} = [N]\{d\} \tag{2.37}$$

where $\{d\} = \{w_1 \;\; w_{,x1} \;\; w_{,y1} \ldots w_n \; w_{,n1} \; w_{,n1}\}^T$ for an n–noded Kirchoff element.

This then being differentiated to yield the curvatures, $\{\kappa\} = [B]\{d\}$. Substitution of this relation into the formulae for strain energy, then gives the element stiffness matrix, $[k]$

$$U = \frac{1}{2}\{d\}^T[k]\{d\} \tag{2.38}$$

where $[k] = \int_A [B]^T[D_K][B]dA$.

Examples of Kirchoff Element Formulations

This section is divided into two logical parts, the first dealing with rectangular elements and the second dealing with triangular elements. Within each part there is a further subdivision, with "single field" formulations being considered first, and then the slightly more involved subdomain formulations.

Rectangular single field formulations. One of the first successful Kirchoff plate elements was the Adini, Clough Melosh rectangle, or ACM rectangle, (see figure 2.4). This element was derived using an single interpolation field of the type

$$w = \{1\ x\ y\ x^2\ xy\ y^2\ x^3\ x^2y\ xy^2\ y^3\ x^3y\ xy^3\}\{a_1\ a_2 \ldots a_{12}\}^T \tag{2.39}$$

and had for the d.o.f. w, $w_{,x}$ and $w_{,y}$ at each vertex.

This element, although successful, did have a problem in that the normal slope along the midsides of the rectangle was non–continuous, (slope continuity being enforced at the corners of the element), therefore the element was non–conforming. This was not a serious fault, as it has been shown that, similar to the BCIZ1 triangle mentioned later in this section, the completeness of the element interpolation field guaranteed convergence, [53], although not monotomic convergence and indeed, the element possessed very good accuracy in almost all plate–bending problems.

Other elements utilising alternative interpolation fields have been devised, which meet inter–element compatibility requirements. An example of one such successful element is the 16 d.o.f. Bogner, Fox, Schmidt rectangular plate element, [27], which has a translational, (w), two rotational, $(-w_{,x}, w_{,y})$ and a "twist" degree of freedom , $(w_{,xy})$, at each vertex.

Rectangular subdomain formulations. Among the more well known of the quadrilateral plate elements is that depicted in figure 2.5, the so–called "de Veubeke" quadrilateral, [29], in which the element is formed by dividing the rectangle into four subtriangles. The degrees of freedom within each subtriangle are the displacements and rotations at each vertex, as well as a normal rotation d.o.f. on the midside of each outer edge. This element is utilised in the latest version of the PC finite element program, ALGOR.

Similar to the de Veubeke quadrilateral is the Q19 element developed by Clough and Felippa, [18], which is formed from four subtriangles, which are themselves formed of three subtriangles. The element is called a Q-19 because the Quadrilateral has 19 basic degrees of freedom, the seven internal degrees of freedom being eliminated by a static condensation process prior to assembly into a complete structure. The result is a 12 d.o.f. quadrilateral, with a translation and two rotations specified at each vertex, with linear variation of normal slopes along the exterior edges, therefore ensuring inter–element compatibility.

Triangular single field formulations. Triangles, as opposed to rectangles, created more difficulties in the search for a fully compatible plate bending element. The interpolation field of the element must be able to fully express all the necessary deformation patterns of the element. When one considers the ideal simple three–noded triangular element, as depicted in figure 2.6 it has nine d.o.f., three at each vertex, these being w, $w_{,x}$ and $w_{,y}$, and therefore requires nine terms in the interpolating polynomial function. However,

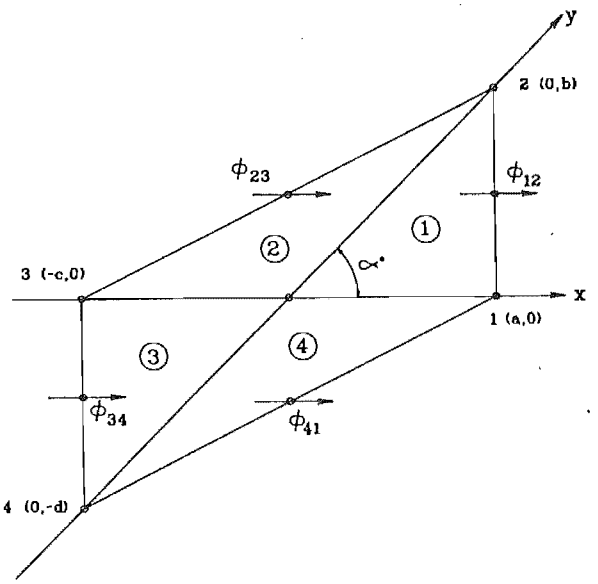

Figure 2.5: The de Veubeke compatible quadrilateral element.

from the Pascal's triangle a complete polynomial contains either 6 terms, (quadratic), or 10 terms, (cubic). Therefore for a fully–compatible three–noded triangle, this means that ten terms must be utilised, or some arbitrary adjustment must be used to make do with an interpolation field of nine terms.

Several formulation methods were tried for 'single field' displacement–based elements with nodal degrees of freedom similar to the element depicted in figure 2.6, where the interpolating polynomial function covers the total area of the element.

One of the initial approaches involved modifying the interpolation field by removing a term, ("A" element of Adini, 1961). The term removed was the xy term, and this was not acceptable, as it removed a constant strain shape from the available deformation fields, which were therefore

$$w = \{1\ x\ y\ x^2\ y^2\ x^3\ x^2y\ xy^2\ y^3\}\{a_1\ a_2 \ldots a_9\}^T \tag{2.40}$$

Because of the lack of this constant strain shape it could not be guaranteed that the element would converge to the correct solution. The next 'fix' tried was combining two polynomial terms, to create a $(x^2y + xy^2)$ term, ("T" element of Tocher, 1962). The deformation field being

$$w = \{1\ x\ y\ x^2\ xy\ y^2\ x^3\ (x^2y + xy^2)\ y^3\}\{a_1\ a_2 \ldots a_9\}^T \tag{2.41}$$

This was also unacceptable, as it would, for some element shapes, cause a singular local–global coordinate transformation matrix, $[A]$ in the relation $\{d\} = [A]\{a\}$.

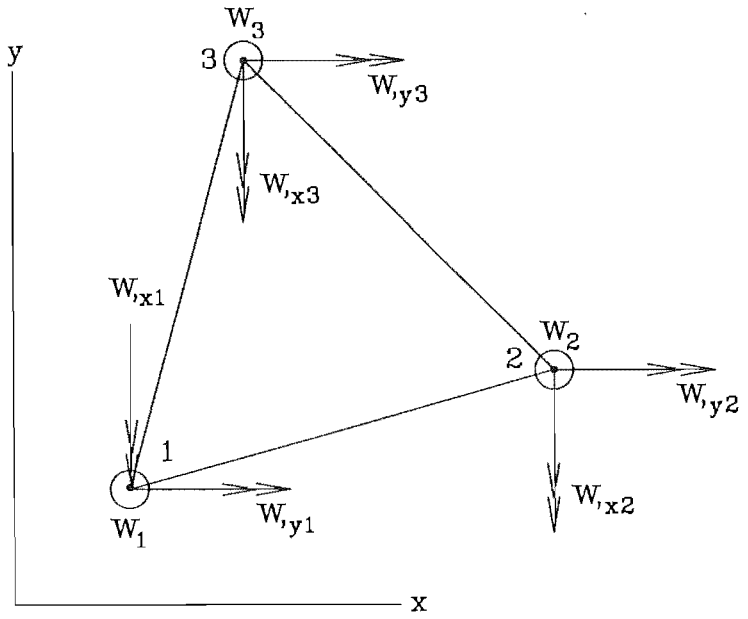

Figure 2.6: The ideal triangular element.

Another approach tried by Tocher, 1962, was that of a four–noded triangle, the T-10, with three nodes at the vertices of the triangle, and a fourth node at the centre of the element, which had the out–of–plane displacement, w, as a degree of freedom, (similar to figure 2.6, with an extra node). This element was not acceptable, as it violated the inter–element angular displacement continuity requirements and the results from even elementary testcases were very poor.

These, and similar elements derived around this time, all behaved poorly due to either incompleteness of the interpolation polynomial, incompatibility (as above), lack of invariance with regard to element orientation or singularity. It was then realised that it was impossible to form a completely acceptable assumed–displacement plate bending element with 9 degrees of freedom.

It is interesting to note at this point a closely related element, the BCIZ1 triangle, mentioned in a paper by Bazeley et.al., [35], which is formed using rational functions in area coordinates and has nine degrees of freedom. This element, whilst being an incompatible element and failing the patch test for a general mesh of elements, provides results of acceptable quality or accuracy, in fact better than the results generated by a much more complicated compatible element mentioned in the same paper, which utilised both polynomial and rational shape functions in area coordinates. This complicated compatible was later modified by smoothing the derivatives of the shape functions, to create the "A-9" element of Razzaque, [89], which gave similar results to the BCIZ1 triangle in test

problems. (Other elements have also been formulated using this "smoothing" of element functions, for example - least squares smoothing was applied to shear terms in the strain matrix which suffer from spurious effects in an eight-noded serendipity plane stress element in Ref. [55], resulting in elimination of the spurious modes which normally afflict this element). The BCIZ1 triangle has also been recently reformulated with modified shape functions, [95], based upon a relaxed C^1–continuity requirement called the "interpolation test", the resulting element passing the patch test and providing good numerical results in several testcases.

In search of compatible displacement elements, the number of d.o.f. can be expanded, until the number of d.o.f and the complete number of terms in the interpolating polynomial coincide, however this does not happen until the polynomial contains 21 terms, a quintic polynomial.

A point which must be considered here is that when does the computational effort expended in creating a fully compatible acceptable element become uneconomic, when other simpler elements, (ie. the BCIZ1 triangle), will provide results of approximately the same accuracy. In fact it has been noted in Ref. [94] that "*...few cases have been discovered... in which the 3DOFI element* (BCIZ1 triangle) *fails to give results of acceptable engineering accuracy*". This is possibly one of the reasons why this quintic element, and other complex elements plate–bending have not gained wider exposure in currently available finite element packages.

Triangular subdomain formulations. The simplest possible fully compatible triangular plate element is one called the Clough–Tocher or HCT triangle, which was developed using what is called a 'subdomain formulation' for the triangular element. The reason for this name can be seen in figure 2.7. Basically the element is divided into subregions and independent displacement fields are assumed for each subregion, the d.o.f. on the common boundaries of these subregions being equated to reduce the number of d.o.f. of the element.

Clough and Tocher, [20], employed this approach in an element composed of three nine d.o.f. subtriangles. This fully compatible element was arranged so as to give a quadratic variation of displacement along each exterior edge of the triangle.

An improved version of this element, the LCCT-12 has also been formulated by Clough and Felippa, [18], using three 10 d.o.f subtriangles. The initial 30 d.o.f. being reduced to 12, (three at each vertex, and a midside normal slope on each exterior edge), by the imposition of compatibility constraints in the interior of the element.

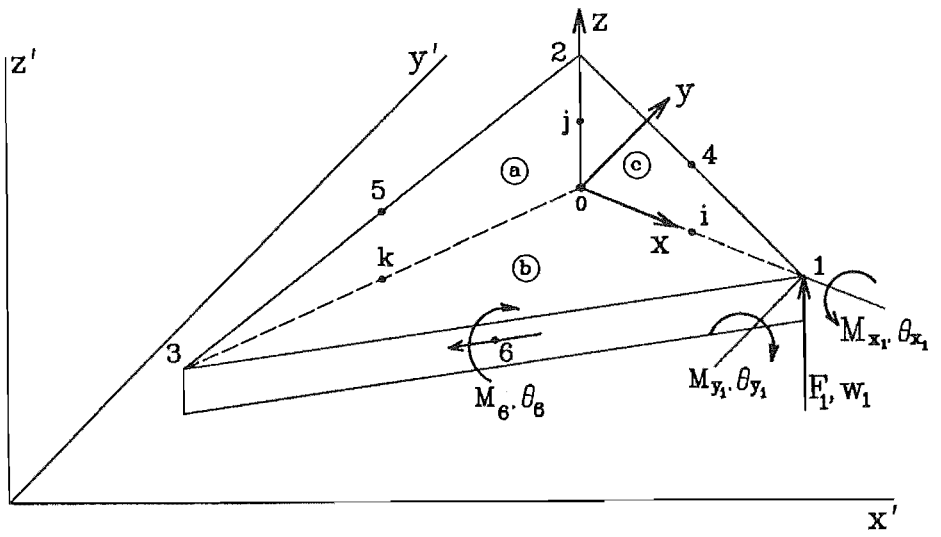

Figure 2.7: HCT triangular element.

Another method of formulation of an HCT–type triangular element involves using interpolation functions and triangular coordinates within each subtriangle, which leads to simpler local–global transformation matrices, and therefore simpler matrix inversions to create the stiffness matrix.

2.4.3 Mindlin Theory/Formulation

As stated at the beginning of the Kirchoff theory section, the difficulty in developing acceptable plate (and shell) elements is due to the simplistic nature of Kirchoff theory, which requires C^1 of the displacement functions. Mindlin[1] plate theory, however, accounts for both bending and transverse shear deformation and requires only C^0 of the displacement functions, therefore it may be used to analyze thick plates as well as thin plates. There is however a complication, when Mindlin elements are used for very thin plates they may be less accurate than Kirchoff elements, which do not allow for transverse shear deformation. This is due to numerical difficulties with the shear terms overwhelming the bending terms in the stiffness matrix and causing "shear locking,". This will be discussed later, after the basic theory is covered.

Deformations

The deformation of plates, according to Mindlin theory obeys the following rules:

[1] While this modification of the Kirchoff theory is often credited to Mindlin, it had previously been independently derived by Reissner, and therefore should probably be called Reissner–Mindlin theory.

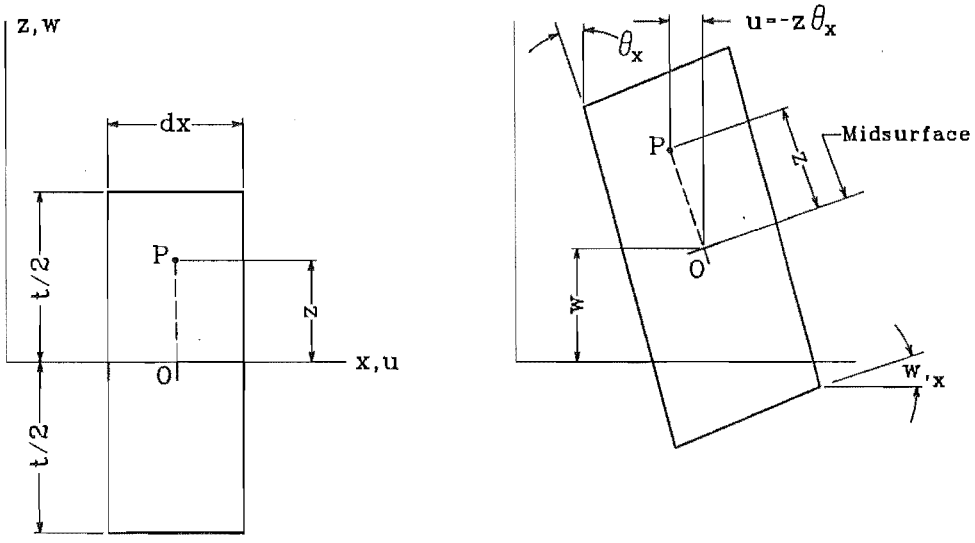

Figure 2.8: Deformation of a differential plate element: Mindlin theory.

1. Deflections are small,
2. Lines straight and perpendicular to the midplane remain straight, but not necessarily normal after deformation,
3. Stresses normal to the surface (membrane stresses) are negligible.

Note: The following Mindlin theory is based on that in Ref [41].

The displacement of an arbitrary point, P, not on the midplane, (see figure 2.8), can be described by the equations

$$\begin{aligned} u &= -z\theta_x \\ v &= -z\theta_y \end{aligned} \tag{2.42}$$

Note: $\theta_x \neq w_{,x}$, $\theta_y \neq w_{,y}$.

Mindlin Element Stiffness Matrix

Deflections and normal rotations for an n–noded Mindlin element are specified by independent shape function interpolations:

$$w = \sum_{i=1}^{n} N_i w_i$$

$$\theta_x = \sum_{i=1}^{n} N_i \theta_{xi} \qquad \theta_y = \sum_{i=1}^{n} N_i \theta_{yi} \tag{2.43}$$

where w, θ_x and θ_y are the corresponding displacements and rotations at node i, and N_i is the shape function associated with node i.

Curvature–displacement relations are then written as

$$\epsilon_b = \sum_i B_{bi} d_i, \tag{2.44}$$

in which the curvatures are expressed as

$$\epsilon_b = \{\theta_{x,x} \quad \theta_{y,y} \quad \theta_{x,y} + \theta_{y,x}\}^T \tag{2.45}$$

The curvature–displacement matrix associated with node i may be written as

$$B_{bi} = \begin{bmatrix} 0 & N_{i,x} & 0 \\ 0 & 0 & N_{i,y} \\ 0 & N_{i,y} & N_{i,x} \end{bmatrix} \tag{2.46}$$

and the unknowns at node i are

$$d_i = \{w_i \quad \theta_{xi} \quad \theta_{yi}\}^T \tag{2.47}$$

Shear strain–displacement relations are written as

$$\epsilon_s = \sum_i B_{si} d_i, \tag{2.48}$$

in which the shear strains are written as

$$\epsilon_s = \{w_{,x} + \theta_x \quad w_{,y} + \theta_y\}^T \tag{2.49}$$

The shear strain–displacement matrix associated with node i may be written as

$$B_{si} = \begin{bmatrix} N_{i,x} & N_i & 0 \\ N_{i,y} & 0 & N_i \end{bmatrix} \tag{2.50}$$

The moment–curvature relationships are given as

$$\sigma_b = D_b \epsilon_b \tag{2.51}$$

where the bending moments are

$$\sigma_b = \{M_x \quad M_y \quad M_{xy}\}^T \tag{2.52}$$

and the matrix of flexural rigidity for an isotropic material is

$$D = \frac{Et^3}{12(1-\nu^2)} \begin{bmatrix} 1 & \nu & 0 \\ \nu & 1 & 0 \\ 0 & 0 & (1-\nu)/2 \end{bmatrix} \tag{2.53}$$

where E is Young's Modulus, ν is Poisson's ratio, and t is the plate thickness.

The shear force–shear strain relationships are given as

$$\sigma_s = D_s \epsilon_s \tag{2.54}$$

where the shear forces are

$$\sigma_s = \{Q_x \quad Q_y\}^T \tag{2.55}$$

and the matrix of shear rigidity for an isotropic material is

$$D = \frac{Et\kappa}{2(1+\nu)} \begin{bmatrix} 1 & 0 \\ 0 & 1 \end{bmatrix} \tag{2.56}$$

where κ is a shear modification factor, usually taken as $\frac{5}{6}$ for homogeneous isotropic plates.

Therefore the total strain energy can be expressed as

$$U = \frac{1}{2}\int_A \epsilon_b^T [D_b] \epsilon_b dA + \frac{1}{2}\int_A \epsilon_s^T [D_s] \epsilon_s dA \tag{2.57}$$

This can then be substituted into the potential energy expression, and minimised with respect to the nodal values d_i to obtain the stiffness equation for the system.

Isoparametric formulation. The very useful manipulation of "Isoparametric formulation" can be used on Mindlin elements. This is where, if the element is of general shape, it can be mapped to a square element defined by edges of $\eta, \xi = \pm 1$, where η and ξ are generalised mapping coordinates. The element stiffness matrix is then integrated using some numerical integration rule [2], commonly the Gaussian–Quadrature rule, at a specified number of "Gauss" points. The element stiffness matrix equation then becomes

[2] Numerical integration is used because analytic integration of the general curved shape would require rather complex formulae, which would yield no noticeable improvement in accuracy.

$$[k] = \int_{\xi}\int_{\eta}[B]^T[D_M][B]Jd\eta\, d\xi \tag{2.58}$$

where J is the determinant of the Jacobian matrix.

For more detailed information on the 'Isoparametric' formulation of elements, see Ref. [56], Chapter 6 of Cook, [22], and Chapter 8 of Zienkiewicz, 4th ed., vol 1, [104].

Accuracy of General Mindlin elements

Mindlin elements, in general, suffer from 'shear locking', in which the transverse shear of the element is overly constrained, and therefore the shear stiffness matrix terms become very large in comparison to the bending stiffness terms. This leads to serious numerical problems, and the deflections may in extreme cases become negligible. Shear locking can be avoided by adopting a reduced- or selective integration rule to generate the element stiffness matrix, $[k]$, or else by redefining the transverse shear interpolation. When this is done the Mindlin formulation plate elements produce very good results for the normal range of plate–bending problems.

An undesirable side–effect of using reduced or selective integration for evaluating the shear strain energy of the element is that it may give rise to spurious zero energy modes and 'rank deficiency' of the element matrix.

Shear–locking and spurious modes associated with discretization of the transverse shear strain energy have been investigated extensively in many published papers. Some references read by the author include [26], [39], [41], [99], [98] and [45], much important research being done by groups in conjunction with T.J.R Hughes and E. Hinton.

Methods of combating these failings of Mindlin elements include using Hybrid and mixed formulations, mechanism suppression techniques, smoothing techniques, [57], and of late "free–formulation" techniques, [12] and [11]. An interesting, although rather complicated analysis of locking and rank deficiencies utilising symbolic Fourier analysis was undertaken by Park and Flaggs, [83], [82], [84], who developed a successful plate bending element by the assumed natural–coordinate strain method.

More comments upon the accuracy of Mindlin elements can be found in the paper on the "Heterosis" element by Hughes and Cohen, [44], and in the "Finite Element Handbook", [59].

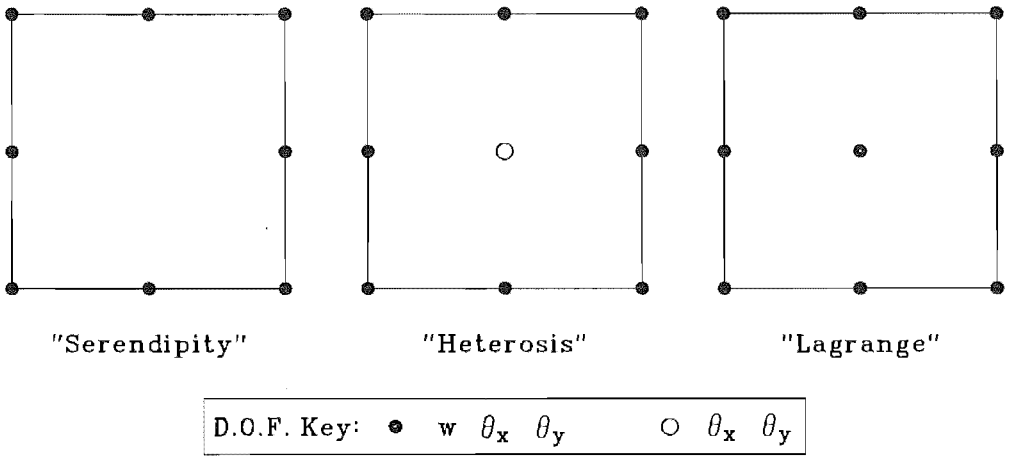

Figure 2.9: Mindlin elements.

Examples of Mindlin Formulations.

The Heterosis Element. The 'Heterosis' element, (depicted along with related Mindlin elements in figure 2.9), is currently the best Mindlin plate element formulation, if not the best conventional, (assumed displacement), plate element available. It is formulated by modifying a quadratic (eight-noded) serendipity element with the inclusion of a centre node with two d.o.f. θ_x and θ_y , therefore the element has nine-nodes with 26 d.o.f. Details of this element stiffness matrix formulation, and that of a consistent load vector can be found in Ref.[44].

The element, because of the isoparametric formulation, must be integrated using numerical integration, a selective gaussian quadrature rule being used. A rule of 3 x 3 gauss points being used in the calculation of the bending stiffness, and a 2 x 2 gauss point rule being used for the calculation of the transverse shear stiffness.

The heterosis element does not exhibit locking, erratic convergence characteristics, or mechanisms, and therefore can be used with confidence for any plate analysis problem.

2.4.4 Discrete Kirchoff Theory/Formulation

An element of this type, the Discrete Kirchoff Triangle, or DKT, was first described in a technical report by Oden and Wempner, (1967), and extensively published by Wempner, Oden and Kross, [31], [102]. Since then other Discrete Kirchoff type elements have been published, see Refs. [50], [24], [25], [8], [10], [74]. These elements in every case proving to perform accurately. Indeed a survey of plate-bending elements in 1980 concluded that

the DKT was one of the best elements for the analysis of thin plates [52].

The essential step in the element formulation of a Discrete Kirchoff element is the enforcement of zero transverse shear strain at specific points and along the edges of the element. This is done by assuming a Mindlin theory of deformation over the entire element, and then applying Kirchoff theory at the nodes around the exterior of the element. The position of the nodes need not be at the vertices of an arbitrarily shaped triangle or rectangle, indeed some elements, notably the Semi–Loof elements of Irons, [47], enforce these "Kirchoff constraints" at specially defined "Loof" nodes.

Deformations

The displacement coordinates of a point are given by Mindlin theory:

$$\begin{aligned} u &= z w_{,xx} \\ v &= z w_{,yy} \end{aligned} \tag{2.59}$$

Independent shape function interpolations are used for the element deflections and rotations, see figure 2.10, similar to those used for Mindlin elements, with the out–of–plane deformation being expressed as a polynomial expression of some type, the shape functions of the BCIZ1 nonconforming triangle being used here.

$$\begin{aligned} w &= \sum_{i=1}^{9} N_i w_i \\ \theta_x &= \sum_{i=1}^{6} N_i \theta_{xi} \qquad \theta_y = \sum_{i=1}^{6} N_i \theta_{yi} \end{aligned} \tag{2.60}$$

This gives 21 initial degrees of freedom, which must be reduced to 9 for the final element. This is done by imposing the "Kirchoff constraints".

Kirchoff Constraints

At each of the vertices, the transverse shear strains, γ_{yz} and γ_{zx} are set to be equal to zero. This yields six equations:

$$\begin{aligned} \theta_{xi} &= -w_{,xi} \\ \theta_{yi} &= -w_{,yi} \quad \text{for } i = 1,2,3 \end{aligned} \tag{2.61}$$

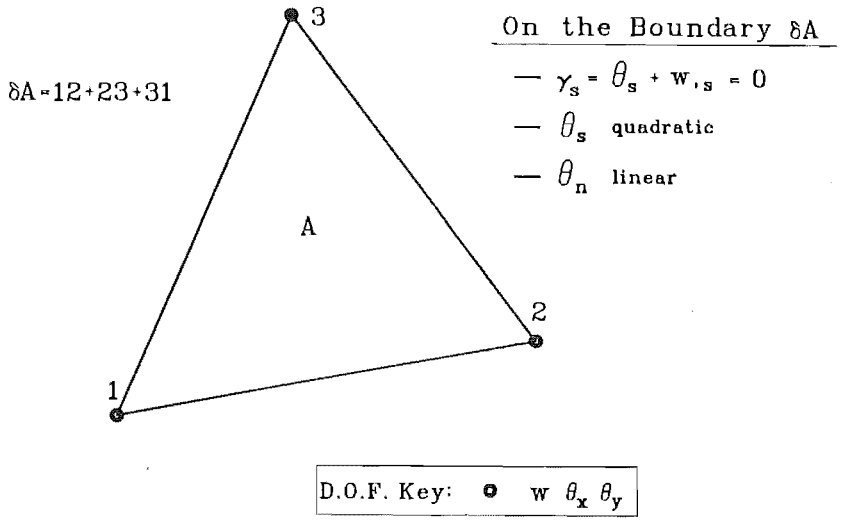

Figure 2.10: A Discrete Kirchoff Triangle.

At the midside nodes, the transverse shear strain vanishes: This gives three equations.

$$\theta_{si} = w_{,si} = 0 \quad \text{for } i = 4, 5, 6 \tag{2.62}$$

Normal slopes are constrained to a linear variation along the sides of the element. This gives another three equations of the form:

$$\begin{aligned} \theta_{n4} &= \frac{1}{2}(w_{,n1} + w_{,n2}) \\ \theta_{n5} &= \frac{1}{2}(w_{,n2} + w_{,n3}) \\ \theta_{n6} &= \frac{1}{2}(w_{,n3} + w_{,n1}) \end{aligned} \tag{2.63}$$

These twelve constraints are then combined with the nine nodal d.o.f. to give a transformation which expresses the twelve nodal d.o.f. θ_{xi} and θ_{yi} in terms of the nine nodal d.o.f., $w_i, w_{,xi}$, and $w_{,yi}$.

$$\{\theta_{x1}\ \theta_{y1}\ \theta_{x2} \ldots \theta_{y6}\}^T = [T]\{w_1\ w_{,x1}\ w_{,y1}\ w_2 \ldots w_{,y3}\}^T \tag{2.64}$$

where $[T]$ is the 12 x 9 transformation matrix from rotational d.o.f. to standard Kirchoff nodal d.o.f.

Discrete Kirchoff Element Stiffness Matrix

The strains are expressed in terms of the nine nodal d.o.f. using the strain–displacement relations of Mindlin theory, (whilst not including the γ_{yz} and γ_{zx} terms as this formulation is using Kirchoff theory), and the transformation matrix, $[T]$, from above.

$$\{\varepsilon\} = z \begin{bmatrix} N_{1,x} & 0 & \dots & 0 & N_{6,x} & 0 \\ 0 & N_{1,y} & \dots & 0 & 0 & N_{6,y} \\ N_{1,y} & N_{1,x} & \dots & 0 & N_{6,y} & N_{6,x} \end{bmatrix} [T] \begin{Bmatrix} w_1 \\ w_{,x1} \\ w_{,y1} \\ w_2 \\ \vdots \\ w_{,y3} \end{Bmatrix} \quad \text{or} \quad \{\varepsilon\} = z[B_\theta][T]\{d\}$$

After integrating through the thickness, the strain energy expression becomes

$$U = \frac{1}{2}\{d\}^T[k]\{d\} \tag{2.65}$$

where $[k] = \int_A [B]^T[D_K][B]dA$ and $[B] = [B_\theta][T]$.

Comments on Discrete Kirchoff Elements

The Discrete Kirchoff triangle. The Discrete Kirchoff Triangle, (DKT) is used successfully in a number of finite element packages, and is in all cases a most acceptable element. It passes all patch tests, does not lock or have spurious modes. Several variations on the theme have been produced since the concept was introduced, these ranging from the original complicated formulation of Wempner, to the simpler formulations of Stricklin, [50], and Batoz, [52].

Other versions of the DKT have varying degrees of freedom, from the 9 d.o.f. version presented here, to a 15 d.o.f. version formulated by Batoz and Dhatt, [9] and up to 27 d.o.f., [25]. Later formulations of the element have included explicit expressions for the stiffness matrix of the element, [8] and later [54], which allow much more efficient coding, with a corresponding decrease in the computing time required.

The Discrete Kirchoff Quadrilateral. A variation on the DKT theme, the DKQ or Discrete Kirchoff Quadrilateral, [10], has been produced in recent times. This uses much the same method of formulation as the above DKT element, with explicit formulation of the stiffness matrix. While the results from this element are good, the convergence is not monotomic, or as good as some other elements tested at the time.

The Semi–Loof Element. The Semi–Loof element of Irons was first published in literature in 1976, [47], and since then has gained a wide acceptance because of the accuracy attainable by this element.

What follows is a brief note on the formulation of the Semi–Loof quadrilateral element. It should be noted that this is not the only Semi–Loof type element available, indeed the commercial finite element program, PAFEC, uses both this element and a similar six–noded triangular element for plate–bending and shell problems.

The basis for the Semi–Loof element is an eight–noded isoparametric quadrilateral element. The eight nodes have three translatory degrees of freedom, u_x, u_y and u_z, for nodal variables, with another eight *loof* nodes placed at the Gauss points along the side having one rotational degree of freedom, as can be seen in figure 2.11. A further degree of freedom, a *bubble* function, $w = (1 - \xi^2)(1 - \eta^2)$, is added in a direction normal to the element, at $(\eta = \xi = 0)$, to enable a quadrilateral element to pass the patch test. This brings the total number of degrees of freedom to 43. The eight corner and midside nodes, with the translatory degrees of freedom are adequate to describe the membrane deformations of the shell fully, but are not acceptable to provide slope continuity between elements, hence the need to specify the normal rotations at the Loof nodes. To reduce the total number of degrees of freedom, eleven constraints can be introduced. Eight of these constraints take the form of the Discrete Kirchoff constraints, or in other words the shear strain is constrained to be equal to zero at the Gauss points. Two further constraints are supplied by manipulation of the shear strains at the central node, $(\eta = \xi = 0)$. This takes the form of

$$\int \hat{X}_9 \cdot \gamma \; d(area) = \int \hat{Y}_9 \cdot \gamma \; d(area) = 0 \tag{2.66}$$

which is integrated over the Gauss points, where $\gamma = \hat{X}\gamma_{XZ} + \hat{Y}\gamma_{YZ}$, and $\hat{X}_9$ and $\hat{Y}_9$ are the unit vectors at the central node.

The final degree of freedom is removed by constraining the bubble function. Consider the bubble function, which has negative curvature in the η and ξ directions. It is then postulated that the total curvature, $\partial^2 W/\partial X^2 + \partial^2 W/\partial Y^2$ is negative almost everywhere. As there is no rotation, $U = V = 0$. The shear corresponding to the slope W_X is $\gamma_{XZ} = W_X + U_Z$, so that the expression in the shears that corresponds to the total curvature, in the same way, is

$$\frac{\partial \gamma_{XZ}}{\partial X} + \frac{\partial \gamma_{YZ}}{\partial Y} = \nabla \cdot \gamma \tag{2.67}$$

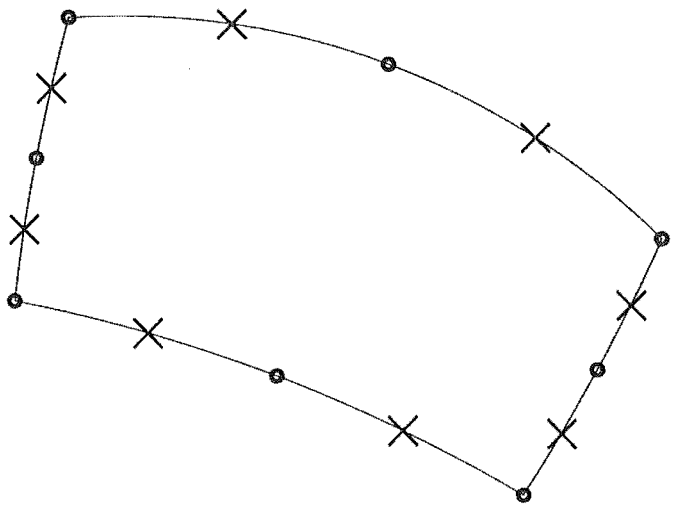

Figure 2.11: The Semi–Loof quadrilateral element.

Therefore the constraint is taken to be

$$\int \nabla \cdot \gamma \; d(area) = 0 \tag{2.68}$$

Now, if the thickness is constant, this constraint can be transformed using Green's theorem, to

$$\int (thickness)\, \gamma_{XZ} \; d(boundary) = 0 \tag{2.69}$$

As can be seen from the above theory, the Semi–Loof element is rather complicated, the constraints being applied numerically. This does lead to inaccuracies as the element is significantly distorted. Another disadvantage of this element is that it contains one spurious mode, however this is rarely activated, and in general the element is well behaved and demonstrates good convergence.

2.4.5 Shell theory

Recommended Reading. The reader is referred to some excellent texts by Flugge, [28], Kraus [61] and Seide [93] and also the paper by Bushnell, [16], for a more detailed explanation of shell theories.

Shell Geometry

Shells are generally curved surfaces, which can be described by the position of the midplane of the surface, and the thickness of the shell, which is almost always very thin in comparison

to the other characteristic dimensions of the shell. The midplane of the surface is described either by two mutually perpendicular *principal radii of curvature*, or by vectors, whose components are curvilinear coordinates.

Shell Finite Elements

There are three recognized ways of analyzing a shell using finite elements. These are:

1. A facet shell representation, where the curved surface is modelled as a number of simple flat elements.
2. Curved shell elements, formulated from some classical shell theory.
3. Mindlin–type shell elements, formed by the degeneration of a solid element into a shell element.

Facet Shell Elements. In general, elements of this type are easy to formulate, pass patch tests and do not give rise to non–zero strains for rigid body motions. The geometric approximation of facet shell elements may give rise to erroneous results, especially for problems which are sensitive to geometric perturbations, however as the mesh is refined in these sensitive areas, one can be confident that the finite element solution will converge to the correct result.

A simple element of this type can be formed by combining a plate element of some type with a membrane element, as can be seen in figure 2.12. A simple example of an element of this type is described in a paper by Clough and Johnson, [19], and also in Chapter 10.8.2 of Astley, [5], and in Chapter Three of Zienkiewicz, [105]. The simple shell elements in the I/FEM finite element package are formulated in this way.

The membrane element commonly used in facet shell elements is the Constant Strain Triangle, (CST), however this element causes the resultant shell element to exhibit rather slow convergence, and several authors have formulated improved elements with more advanced membrane elements, such as the Linear Strain Triangle, (LST).

More complicated facet shell elements, generally with correspondingly better results, can be formed by combining more advanced plate–bending and membrane elements. A recent example of one such element, an 18 degrees of freedom triangular shell element proposed by Carpenter et.al., [75], being formulated by combining a DKT bending element and a degenerate linear strain triangle plane–stress element. This element performs creditably, being of similar accuracy to the advanced 9–node Lagrangian "γ–element" of Belytschko, [97], whilst still being reasonably simple to formulate. It should be noted,

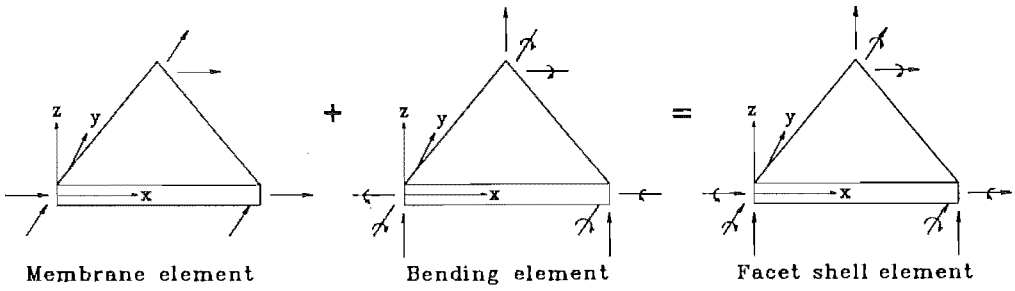

Figure 2.12: A facet shell element, formed by the combination of a plate bending element and a membrane element.

however, that due to the reduced integration of the plane-stress element that is employed in the formulation, zero-energy modes can occur.

Curved Shell Elements. Curved shell elements are by nature of their formulation more complicated than flat plate elements. Apart from the shell theory that is used to describe the deformations of the surface, the geometry of the surface itself requires some involved expressions. This leads to the element requiring at least C^1 continuity, (as do Kirchoff-type plate-bending elements), which we have seen is not easy to achieve.

Classical shell theory deals with *thin* shells, and if one desires to analyze thick shells, the shell theory must be modified to account for transverse shear deformation, similar to the modifications of Kirchoff plate theory by Reissner and Mindlin.

Curved thin shell elements may or may not behave correctly, (accurately), due to the approximations of the shell theory used in the formulation. Many discussions have been published on the acceptability or otherwise of the various approximations of shell theory, and conclusions have, in many cases, pointed to the unacceptability of a particular shell theory.

A broad division is also made between shallow shell theory, and deep shell theory. Many elements use shallow shell theory because, as the mesh of an arbitrarily shaped shell is refined, the element tends towards a facet-type element, ie. shallow. (The non-conformities caused by the parabolic surfaces of adjacent elements of the shell being neglected). The analysis of deep shell problems using shallow shell theory based elements may lead to incorrect solutions depending on the method of formulation, this being discussed more fully in the paper by Idelsohn, [46]. Difficulties arose in many early finite elements based on deep shell theories because they did not provide strain-free rigid body motions, nor correct representation of the coupling between the bending and membrane actions of the shell, (apart from the then unrecognized 'membrane locking' problems).

Morris, [73], lists three criteria that the constitutive equations from a shell theory must meet, these being:

1. *Consistency. The set of constitutive equations should be consistent with the principles of energy and equilibrium.*

2. *Rigid displacement invariance. The equations should remain invariant under rigid body displacements. This does not mean that the strain measures necessarily produce zero strain for this kind of motion, but that the constitutive equations give rise to zero strain energy.*

3. *Coordinate invariance. The equations should be stated by a rule which holds equally well in all coordinate systems. This condition can be easily satisfied if the appropriate equations are stated in tensorial form or by the aid of direct notations not employing coordinates at all.*

Morris goes on to say that the traditional shell theories of Love and Novozhilov do not give satisfactory compliance with these requirements. Even today there is still no common agreement on the best shell theory to be used for an analysis, although consistent Kirchoff–type deep shell theories, such as those of Sanders, Koiter and Budiansky and Sanders are generally accepted as providing correct solutions, [76].

It has been argued that the shell theory does not have to be exact, as the result of a finite element analysis is not exact, however in Chapter 2 of Ref. [4], Morris states that this is not an acceptable course to take, and that one should be confident that *"errors which do arise come from the numerical approximation and not from an unsuitable shell theory."*

Successful (accurate) early elements have been formulated, the "SHEBA" family of elements (Argyris and Scharpf, [3]), being an example, however with 18 degrees of freedom at each node, these elements are rather complicated for use in difficult geometric situations, such as cusps, as well as being computationally expensive.

A simple and successful curved shell element developed recently by Murthy and Gallagher, [74], and is based upon the Discrete Kirchoff theory covered previously. The three–noded triangular element has 27 degrees of freedom, 9 at each vertex. The nodal freedoms are U, $U_{,x}$, $U_{,y}$, V, $V_{,x}$, $V_{,y}$, W, $W_{,x}$, $W_{,y}$, where U, V and W are respectively the tangential and normal components of the displacements in the curvilinear coordinate (x, y) system.

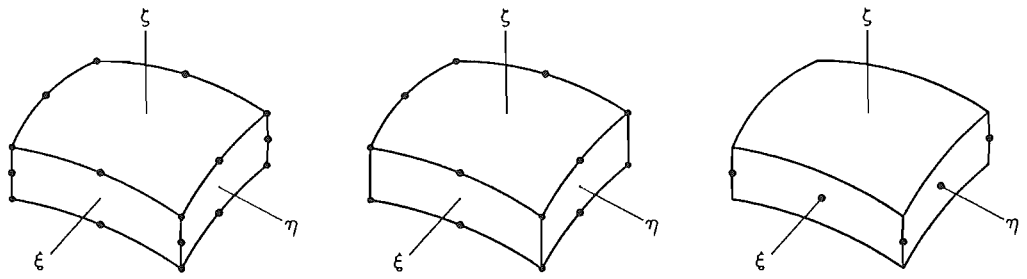

Figure 2.13: Degeneration of a cubic isoparametric solid element to an eight–noded shell element.

Degenerate Solid Elements. For more discussion on the use of solid elements in the analysis of shells, the reader is pointed to some useful references, [91], [80], [85], which trace the use of thick shell (solid) elements of curved, arbitrary shape in the analysis of thick and thin shell structures, and also the implementation of reduced and selective integration techniques in these elements, leading to improved solution accuracy.

An example of this type of element is described, as this is perhaps the simplest method of illustrating the formulation.

The basis of this typical element is a solid cubic isoparametric element, with three nodes per external edge, which is degenerated to an eight–noded shell element, as illustrated in figure 2.13.

Several assumptions are made throughout the formulation of the element, in order to simplify, and improve the accuracy of the final element. The first such assumption is that the strains in the direction ζ, (approximately normal to the midplane of the element), are negligible. This means that the order of interpolation through the thickness of the element can be reduced, being reduced to a linear interpolation, (a node on both the upper and lower surfaces) in this example[3]. This results in a marked improvement in the accuracy of the element, as the stiffness matrix becomes less ill–conditioned. (The condition of the matrices is due to the terms, or more particularly the numerical differences in the terms, the differences being proportional to the spatial dimension in the particular direction).

Another effect of this reduction in the number of nodes, and degrees of freedom, is that there are less equations to be solved. Economy is important in commercial finite element analyses, as both computer time and storage space cost, therefore this degeneration of the solid element is also financially useful.

A recent example of a highly accurate and efficient degenerate element is presented in a paper by Belytschko et.al., [97], where a nine–noded Lagrange element is formed

[3] In extreme cases the nodes are coalesced into one node on the midplane, forming a 'super–parametric' element.

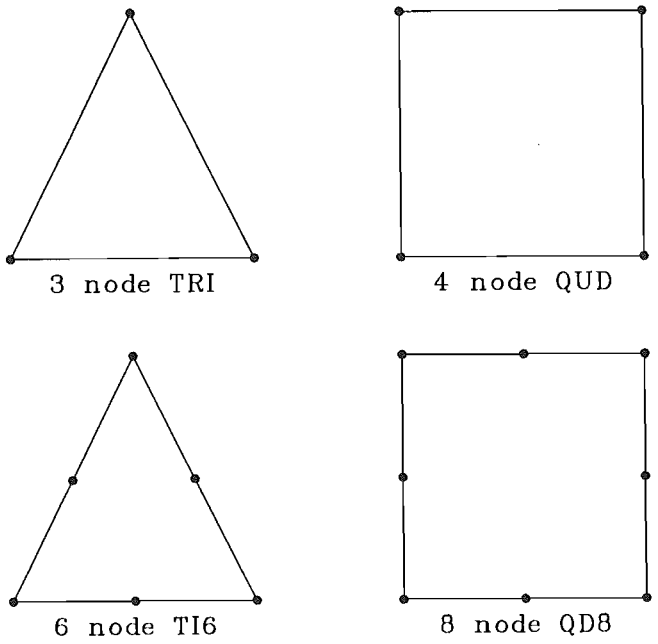

Figure 2.14: Intergraph I/FEM plate and shell elements.

by degeneration of an 18 node brick element. "Mode control" is used in this so–called "γ–element", which results in elimination of spurious modes and avoidance of membrane locking, and because of the use of uniform reduced integration, the storage requirements of the element are much less than a conventional selective reduced integration, again resulting in a more economic element.

An alternative approach to the analysis of shell structures is using solid elements with added incompatible modes, similar to the incompatible modes added to the four–noded I/FEM plate element in the following section. Ref [88] mentions an example of this, the eight–noded brick element, with three added modes to improve the bending response of the element.

2.5 Plate and Shell Elements Available in I/FEM

The Intergraph/Finite Element Modeller, or I/FEM, offers a basic range of plate and shell elements, as depicted in figure 2.14.

The I/FEM documentation produces very little useful information about the formulation of the plate and shell elements that are available in the package, especially with regard to the higher–order shell elements.

2.5.1 Low–Order Shell Elements.

The shell elements in I/FEM use a local coordinate system for stress recovery, which is in general defined as the projection of the global $x-$axis on the element. In particular cases where the element is orthogonal, or nearly orthogonal to the $x-$axis, the global $y-$axis is used for the projection.

Stresses are recovered at the element centroid, and then projected to the nodes, where they are calculated using a simple or weighted averaging scheme. This is a poor method of calculating stresses, as more accurate results are generated by evaluating the Jacobian matrix, [J], and the strain–displacement matrix, [B], and computing the stresses at each Gauss point and then extrapolating this computed value to the nodes to arrive at the nodal stress values, [17]. For more discussion upon the optimal location of the stress sampling points, see Chapter 6.13 of Cook, [22], and also Refs. [7] and [40].

The TRI three–noded shell element. The three–noded TRI element is a facet shell element. It is formulated by combining a membrane element, (the constant strain triangle), and a plate bending element, the Zienkiewicz (BCIZ1) triangle in much the same manner as the element described in Chapter 10.8.2 of Astley, [5].

As the bending and membrane parts of this element are uncoupled, only the membrane element, (the CST or Constant Strain Triangle), or the bending element, (the BCIZ1 triangle), may be used if required.

The QUD four–noded shell element. The QUD shell element is comprised of two parts, a bending part and a membrane part. The bending contribution is from four cross–lapped Zienkiewicz plates.

The membrane contribution is from a membrane isoparametric element with two in–plane translational degrees of freedom at each corner node, and *"with two additional shape functions"*. As far as the author can deduce, the formulation of this element is similar to the **"QM6"** element proposed by Taylor et.al. [88].

The basis for the quadrilateral is the bilinear isoparametric element, with edges at $\eta, \xi = \pm 1$, and the displacement interpolation modified by the addition of two incompatible modes, therefore the displacement field will be of the following type:

$$u = \sum_{i=1}^{4} u_i N_i(\eta, \xi) + \sum_{i=1}^{2} a_i P_i(\eta, \xi)$$

$$v = \sum_{i=1}^{4} v_i N_i(\eta, \xi) + \sum_{i=1}^{2} b_i P_i(\eta, \xi) \tag{2.70}$$

where $N_i(\eta, \xi) = \frac{1}{4}(1 - \eta_i\eta)(1 - \xi_i\xi)$, $P_1 = (1 - \eta^2)$, $P_2 = (1 - \xi^2)$ and η and ξ are the natural coordinates of the element.

The elements are derived using the Mindlin–Reissner assumptions, as specified in the section on Mindlin theory, which means that they should provide acceptable results for a much larger range of shell thicknesses than Kirchoff elements.

These assumptions are valid when deflections are a few tenths of the plate's thickness and at least one transverse dimension is large compared to the thickness, thereby negating shear deflections.

Bending and membrane effects are uncoupled in the QUD element.

2.5.2 High–Order Shell elements.

The information on these elements is rather sparse, apart from the statement that these elements are true shells, and some statements of basic shell element properties, for example that bending and membrane behaviour is coupled.

Both of the shell elements are formulated using Reissner–Mindlin theory, ie. transverse shear strain is taken into account, which means that they can be used for both thick and thin shells.

The only other clue to the identity of these elements was from the results generated in the element verification testcases, which is covered in the next chapter, and references to several papers for each element.

The TI6 six–noded shell element. The I/FEM documentation produces very little useful information about this element except for the statement that the accuracy of high–order triangles is much better than that of the low–order triangles.

The documentation lists a paper by MacNeal, [66], in which a six–noded triangular element is formulated using an assumed strain method. The membrane strains of this element are evaluated by assuming a strain field, (instead of a displacement field), and relating this strain field to the nodal displacements by line integration of the strain field along straight line segments between pairs of nodal points. The resulting element proves to be accurate and converge to the correct solution for several testcases, and is used in MSC/NASTRAN as the 'TRIA6' curved shell element.

The QD8 eight–noded shell element. The QD8 element is a shell element, and the information given in the finite element package documentation about these high–order elements is rather limited. For example: *"Higher order plates are true shells, unlike low–order plates. Bending and membrane effects are coupled. Their accuracy is far better than the accuracy of low order triangles."*

It appears, from the results generated in the element verification testcases which are covered in the following chapter, that this element is a reduced or selectively integrated isoparametric serendipity shell element. The "Finite Element Handbook", [59], has this to say about such elements.

"The element is simple and works well if it is not distorted.... It contains two spurious kinematic modes, but these modes are rarely activated in practical circumstances."

These comments seem to describe the behaviour of the element that was encountered in the element verification tests, which are described in the following chapter.

2.6 Element Formulations based on Modified Principles

Table 2.1 summarises the different finite element categories based upon their variational principle. Several of these methods are briefly commented upon in the following text.

Free formulation Another class of alternative formulation that has recently been derived is the "free formulation". The only requirement for elements derived in this manner, is that the displacement patterns that the element possesses must contain the fundamental deformation modes, (rigid body and constant strains), and be linearly independent. For more information on this powerful method of formulation, the reader is pointed towards references by the research group headed by Bergan, [12] and [11].

Equilibrium Models. Equilibrium models are based on an assumed equilibrating stress field.

The equilibrium–type finite elements provide an upper bound solution to finite element problems which, when combined with a conventional assumed–displacement method (which provide a lower bound solution), can provide a measure of the accuracy of a solution, [30]. This re–analysis by another method, and elements is time–consuming to say the least, financially unviable.

Finite Element Method	Variational Principle	Assumed Functions Inside the Element	Along Interelement Boundaries	Unknowns in Final Equations
Displacement (Conforming)	Minimum Potential Energy	Continuous Displacements	Displacement Continuity	Nodal Displacements
Equilibrium	Minimum Complementary Energy	Continuous and Equilibriating Stresses	Equilibrium Boundary Tractions	a) Generalised Displacements b) Stress Parameters
Hybrid Stress Method	Modified Complementary Energy	Continuous and Equilibriating Stresses	Assumed Compatible Displacements	Nodal Displacements
Hybrid Displacement Method (1)	Modified Potential Energy	Continuous Displacements	Assumed Compatible Displacements	Nodal Displacements
Hybrid Displacement Method (2)	Modified Potential Energy	Continuous Displacements	Assumed Equilibriating Boundary Tractions	Nodal displacements and Boundary Forces
Reissner's Principle	Reissner Method as modified by Hermann	Continuous Stress and Displacement Functions	Combinations of Boundary Tractions and Displacements	Combinations of Displacements and Tractions
Generalised Displacement Method	Modified Potential Energy	Continuous Displacements	Lagrangian multipliers (stresses)	Nodal Displacements and Lagrangian multipliers
Generalised Equilibrium Method	Modified Complementary Energy	Continuous and Equilibriating Stresses	Lagrangian multipliers (displacements)	Nodal Displacements and Lagrangian multipliers

Table 2.1: Classification of finite element methods.

Hybrid Stress Elements. The Hybrid Stress method is based upon a modification of the principle of complementary energy, in which the energy functional is, in matrix notation;

$$\Pi_c = \sum_n \left\{ \int_{Vn} \frac{1}{2} \sigma^T S \sigma dV - \int_{\partial Vn} \tilde{u}^T T dS + \int_{S\sigma n} \tilde{u}^T \bar{T} dS \right\} \tag{2.71}$$

where Vn is the domain of the element, ∂Vn is the boundary of the element and $S\sigma n$ is the boundary of the domain satisfying stress equilibrium.

The stresses are interpolated in terms of a set of undetermined parameters, β. This interpolation is comprised of two parts; the first in β must satisfy stress equilibrium within the element, while the second part corresponds to a particular solution with prescribed body forces, $\bar{F}_i$.

$$\sigma = P\beta + P_F \beta_F \tag{2.72}$$

where the second term is prescribed, and thus β_F is known. (The remainder of this derivation will ignore this second term).

The element boundary tractions are related to the assumed stresses, σ, by a coordinate

transformation, N;

$$T = N\sigma \tag{2.73}$$

Substituting

$$T = NP\beta \tag{2.74}$$

The interelement compatible boundary displacements, $\bar{u}$, are interpolated in terms of the nodal displacements, v;

$$\bar{u} = Lv \tag{2.75}$$

where the interpolation, L, is applied along the external boundary.

The energy functional can then be written as;

$$\Pi_{me2} = \sum_n \left\{ \frac{1}{2}\beta^T \int_{Vn} P^T S P dV \beta - \beta^T \int_{\partial Vn} (NP)^T L dS v + v^T \int_{S\sigma n} L^T \bar{T} dS \right\} \tag{2.76}$$

which can be rewritten as:

$$\Pi_{me2} = \sum_n \left\{ \frac{1}{2}\beta^T H \beta - \beta^T G v + v^T \bar{Q}_T \right\} \tag{2.77}$$

where

$$H = \int_{Vn} P^T S P dV \tag{2.78}$$

$$G = \int_{\partial Vn} (NP)^T L dS \tag{2.79}$$

$$\bar{Q}_T = \int_{S\sigma n} L^T \bar{T} dS \tag{2.80}$$

Now since σ is assumed independently within each element, the stationary condition of the functional with respect to β is directly obtained for each element as

$$H\beta - Gv = 0 \tag{2.81}$$

or

$$\beta = H^{-1} G v \tag{2.82}$$

Substituting

$$\Pi_{me2} = \sum_n \left\{ -\frac{1}{2} v^T G^T H^{-1} G v + v^T \bar{Q}_T \right\} \tag{2.83}$$

Defining

$$K = G^T H^{-1} G \tag{2.84}$$

Thus

$$\Pi_{me2} = -\sum_n \left\{ \frac{1}{2} v^T K v - v^T \bar{Q}_T \right\} \tag{2.85}$$

Finally the stationary condition of the functional, Π_{me2}, with respect to v becomes

$$\sum_n \left(K v - \bar{Q}_T \right) = 0 \tag{2.86}$$

Here K represents the Element Stiffness Matrix and $\bar{Q}_T$ is the Consistent Load Vector. The only matrices needed are G, H^{-1} and the vector $\bar{Q}_T$.

A major advantage of the Hybrid Stress elements over some other alternative formulations is that they may be incorporated into a conventional assumed–displacement finite element package, without the user knowing any difference, as the external degrees of freedom used in the formulation are the nodal displacements.

Chapter 3

Element Verification

3.1 Introduction

A fact which must be stressed when dealing with finite element analysis is that it is an approximate method of analysis – it may yield answers which are, in most cases as close to exact as is required for the purposes of design, but it may also give answers which are totally wrong.

Apart from errors by the engineer, the elements are the major source of inaccuracy, the rest of the calculations are exact except for their lack of precision, for example, rounding errors.

The reasons for the errors in the analysis may be as simple as an incorrect unit used in an analysis, or it may be more insidious, for example, an element type may only provide correct answers for a particular shape or loading. This type of error is quite serious, as the user of a finite element package may have, through a series of simple analyses built up a false assurance in the ability of their program to provide accurate results.

Most texts on finite elements include a section, if not a chapter, on the errors or inaccuracies that are involved in the use of a finite element method. Typical quotes on the accuracy of finite elements are:

"...a competent analyst must have sound engineering judgement and experience, and that doubts raised in the course of an analysis should be taken seriously." from Cook, [22],

and

"In any practical analysis problem, perhaps the most difficult job facing the analyst is to assess the magnitude of the errors implicit in the analysis technique." from Ref. [4]

This is the reason why the user of any new or untested finite element package should undertake a comprehensive series of element verification tests.

Element verification is simply the testing of the performance of an element to ascertain the accuracy, or lack of, in a particular application so one can have confidence in the results generated by an analysis.

The following section comments upon the errors that may arise in a finite element formulation, and which will lead to incorrect solutions in an analysis.

3.2 Errors in the Element Formulation.

In the process of element verification one must test for:

Elementary (or basic) defects in the element formulation. It is entirely possible that an element may be deficient by nature of incorrect assumptions in the formulation. This is a very serious sort of error and any element possessing this type of error should never progress beyond the development stage. Thankfully this type of error is usually picked up rather quickly, due to extensive testing in the development of the element, similar to the tests that are described in the remainder of this chapter.

Two main defects that might occur in a new element formulation, depending on the method used are:

- Violation of the rigid-body property, ie. a rigid-body displacement of any element must give rise to zero strain energy.
- Non-invariance to node numbering, ie. the result generated must not depend on the way the element nodes are numbered.

Presence of spurious mechanisms. For more detailed information on spurious modes, it is suggested that the reader look at Refs. [14], [87] and [105].

Mechanisms, which are also called instabilities, 'kinematic' modes, 'hourglass' modes or zero-energy modes, will lead to an inaccurate solution of the stiffness equations due to an incorrect evaluation of the energy of the system. The cause of mechanisms can be traced back to the stiffness matrix of the element, where an eigenvalue analysis of the matrix will warn the user that the matrix is 'rank deficient'.

Rank deficiencies can lead to (locally) singular stiffness equations, ie. the number of unknowns is greater than the number of equations in the stiffness equation, which although not preventing a solution from being arrived at, they will obviously lead to a less than accurate solution.

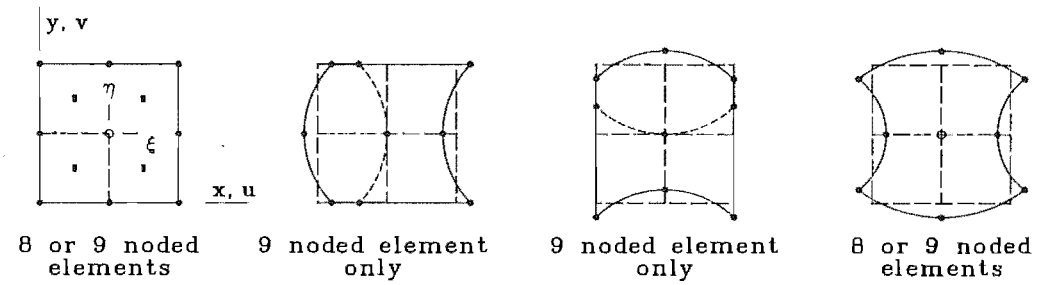

Figure 3.1: Examples of spurious mechanisms.

In some cases the presence of spurious mechanisms may be tolerable, an example of such a case being a mechanism which only occurs in a single element, and cannot occur when several elements are joined together. Although this is allowable, it would be preferable if no such mechanisms were possible in an element.

Rank deficiency problems are generally due to an inadequate order of Gaussian quadrature used for evaluation of the shear strains of an element, in an effort to avoid the shear locking, which is mentioned next, and has been shown to occur in reduced integrated four- and nine-noded isoparametric plane strain elements, [14].

Some examples of spurious mechanisms can be seen in figure 3.1.

Shear Locking. Shear locking is the term used to describe a numerical problem that commonly occurs in the analysis of fully-integrated Mindlin plate and shell elements, where the shear contribution overwhelms the bending contribution of the element stiffness matrix.

An extreme case of this is called 'machine locking', where, because of the finite word length of a particular system, the magnitude of the bending stiffness becomes negligible in comparison to the shear stiffness.

One must check for the presence of locking for:

- Particular loadings, eg. a point load on the end of a cantilever beam of two element depth, or the deformation of a single element structure on an essentially rigid foundation.

- Particular (irregular) element shapes, for example, how does a quadrilateral element perform as the shape is changed from a square to an elongated rectangle, or even to a trapezoidal shape.

3.3 Parameters that affect element accuracy

The main parameters that affect the accuracy of an element, and therefore must be tested for in any series of verification tests are listed in this section.

Each of these parameters are tested in the series of testcases on the I/FEM quadrilateral element library, in an effort to determine the best type of element for the analysis of the reverse duct that follows in Chapter Five.

1. Loading - The problem set should provide significant loading for each of the types of deformation which the elements can exhibit.

2. Element geometry - Each element has a standard shape, which may be the only shape the developer has tested. In the case of a quadrilateral element the standard shape is a square, in the case of a triangular element the standard shape is usually an isoceles right triangle. Care should be taken to test non–standard element shapes, as are shown in figure 3.2.

3. Problem geometry - Geometric parameters which affect more than one element can also affect element accuracy. Curvature is a very important such parameter. It is not just sufficient to test single curvature, but one must also test double curvature, as some elements perform well in the former but very poorly in the latter problem. The slenderness ratio and manner of structure support affect the conditioning of the stiffness matrix and therefore can be used to check element failures related to precision.

4. Material properties - Poisson's ratio has a strong effect on element accuracy in plane strain problems as it's value approaches 0.5. Such values should be included in problems if the use of nearly incompressible materials is contemplated.

3.4 Element verification method

The first step in element verification is to search through the finite element package documentation, or any academic papers that have been produced upon the release of the element with some package. Journals such as *'Computers and Structures"* and the *"International Journal for Numerical Methods in Engineering"* are most useful in this respect. This literature search will generally be of some assistance in determining the formulation of the elements that are able to be used in the package, but it may also be not much use

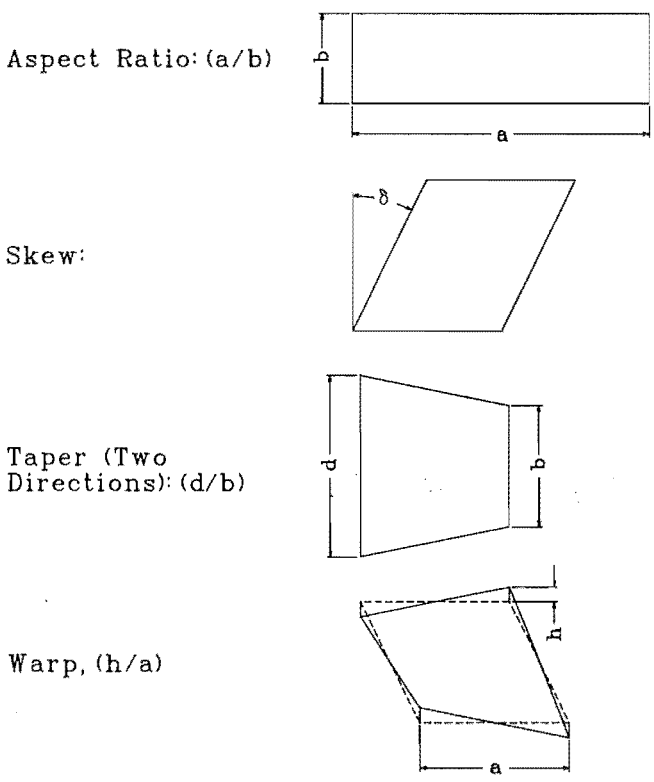

Figure 3.2: Types of geometric distortion from a square plate.

at all. For example, in the I/FEM Reference Manual we find the following description of the QD8 eight-noded quadrilateral:

"High-order plates are true shells, unlike the low-order plates. Bending and membrane effects are coupled. Their accuracy is far better than the accuracy of low order triangles."

To extract any more information than this from the reference manual is rather a difficult task, and it may end up being more constructive by undertaking a comprehensive series of element verification tests, as is outlined in the following section.

The method undertaken in this project involves testing each element for all the possible modes and geometric distortions. The results are then tabulated and a grade assigned to each result. The overall grade then shows the suitability, or otherwise, of the element for use in a finite element package or analysis.

3.5 The test problems

The following section describes the testcases that were used to grade the quadrilateral elements of the Intergraph I/FEM product. Only the quadrilateral elements were tested, as a model utilising quadrilateral elements should be more economical to solve than a triangular model of similar accuracy.

This series of tests are described in detail by MacNeal, [68], Batoz, [8], and White, [103], among others.

3.5.1 Patch test

Every set of element tests should include the patch test. Two variations of the patch test, a constant membrane stress and a constant bending curvature test are used in this element verification. Displacement boundary conditions are used in both of the tests, as they are easier to specify than force and moment boundary conditions. The rectangular five element patch used for this test is shown in figure 3.3.

The principle virtue of the patch test is that, if an element produces correct results for the test, then any problem solved with that element will converge towards the correct solution as the mesh is refined. The reason for this is that the stress within each element tends to a uniform value in the limit. Many authorities, including B.M. Irons[48], feel that any element that fails the patch test should not be trusted.[1] On the other hand, passing the patch test does not guarantee a satisfactory rate of convergence for the element to be of any practical use.

[1] However, if the basis functions of an element meet the completeness criterion, the element may well

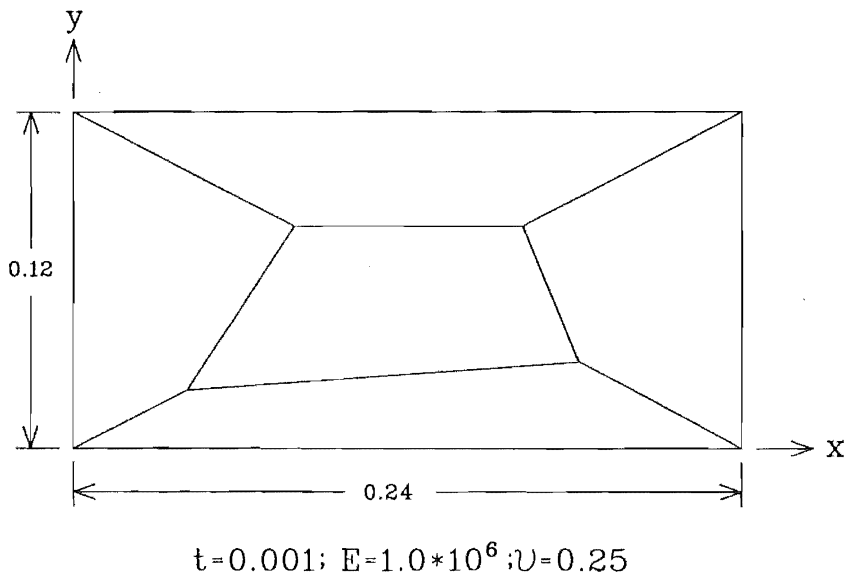

Figure 3.3: Patch test for plates.

Table 3.1: Patch test geometry.

Location of inner nodes:		
	x	y
1	0.04	0.02
2	0.18	0.03
3	0.16	0.08
4	0.08	0.08

Table 3.2: Theoretical Solutions - Patch Test.

(a) Membrane plate patch test

Boundary conditions: $u = 10^{-3}(x + y/2)$
$v = 10^{-3}(x/2 + y)$

Theoretical solution:
$\epsilon_x = \epsilon_y = \gamma = 10^{-3}$; $\sigma_x = \sigma_y = 1333$; $\tau_{xy} = 400$

(b) Bending plate patch test

Boundary conditions: $w = 10^{-3}(x^2 + xy + y^2)/2$
$\theta_x = \partial w/\partial y = 10^{-3}(x/2 + y)$
$\theta_y = -\partial w/\partial x = 10^{-3}(-x - y/2)$

Theoretical solution:
Bending moments per unit length:
$m_x = m_y = 1.111 * 10^7$; $m_{xy} = 10^{-7}$
Surface stresses:
$\sigma_x = \sigma_y = \pm 0.667$; $\tau_{xy} = \pm 0.200$

3.5.2 Straight cantilever beam

The straight cantilever beam is a frequently used test problem, which can be applied to beam, plate and solid elements. The test is simple, and covers all the principal deformation modes, (constant and linearly varying strains and curvatures), by the application of unit loads at the free end of the beam. The theoretical solutions to this testcase are given in table 3.3. A particularly useful test is that of the straight cantilever beam modelled with trapezoidal elements, which tests shear locking.

Batoz, [8], comments that the critical test for a (single) quadrilateral is usually the case of a plate under twist moments with one side fully clamped, which activates differential bending. This test is similar to the twist subcase included here, with the beam being subdivided into six elements.

3.5.3 Curved beam

In the curved beam testcase combinations of the principal deformation modes can be evoked by a single in-plane or out-of-plane loads. Because of the non-rectangular element shape this case also tests the effect on accuracy of slight element irregularity.

converge towards the correct solution, for example, the non-conforming BCIZ1 triangle.

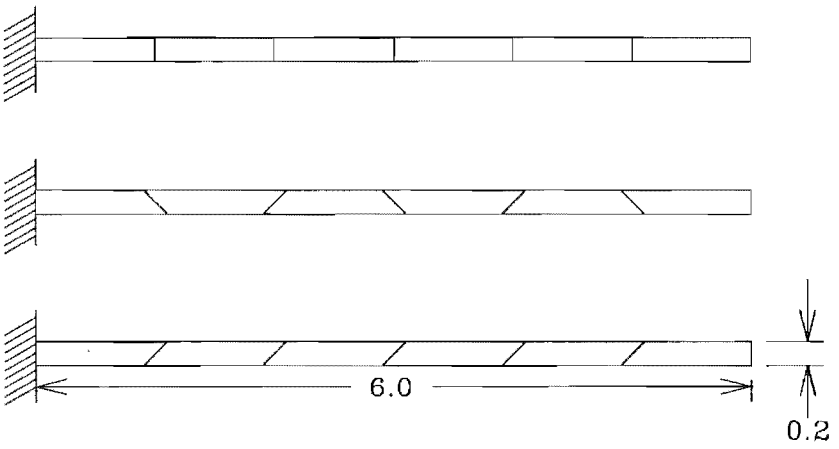

Thickness=0.1; E=1.0*10^7 ; υ=0.30
Loading: unit forces at free end.

Figure 3.4: Straight cantilever beam testcases.

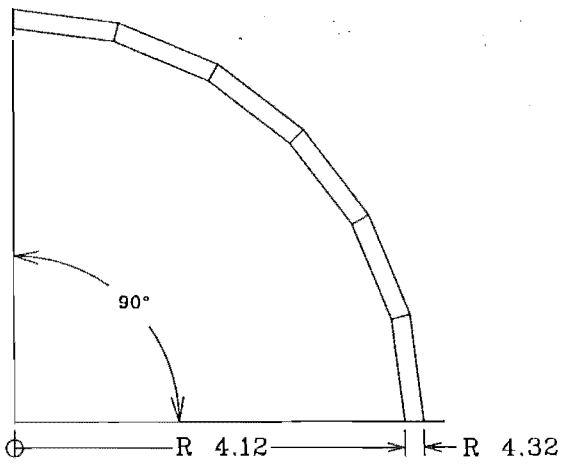

Thickness=0.1; E=1.0*10^7 ;υ=0.25;
Loading: unit forces at tip.

Figure 3.5: Curved beam testcase.

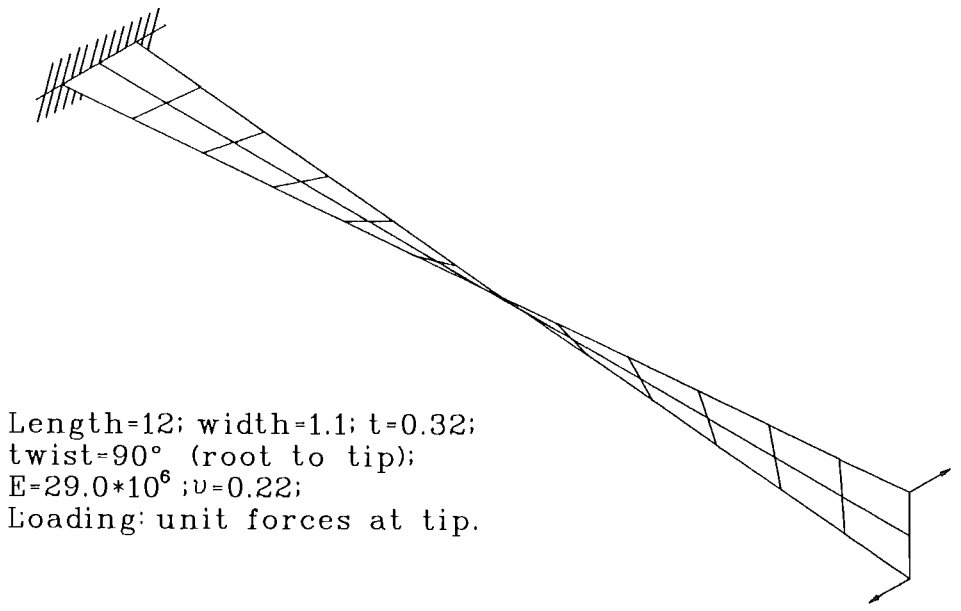

Figure 3.6: Twisted beam testcase.

3.5.4 Twisted beam

This testcase tests the effect of warp on the elements. It should be noted that there is only a small amount of warp, 7.5 degrees on each element, but even this causes some surprising results.

The comments by Batoz for the twist subcase of the straight cantilever beam testcase apply in this testcase as well.

Table 3.3: Theoretical Solutions - Beam Testcases.

Tip loading direction	Displacement in direction of load		
	Straight beam	Curved beam	Twisted beam
Extension	$3.0 * 10^5$	-	-
In-plane shear	0.1081	0.08734	0.005424
Out-of-plane shear	0.4321	0.5022	0.001754
Twist	0.03208	-	-

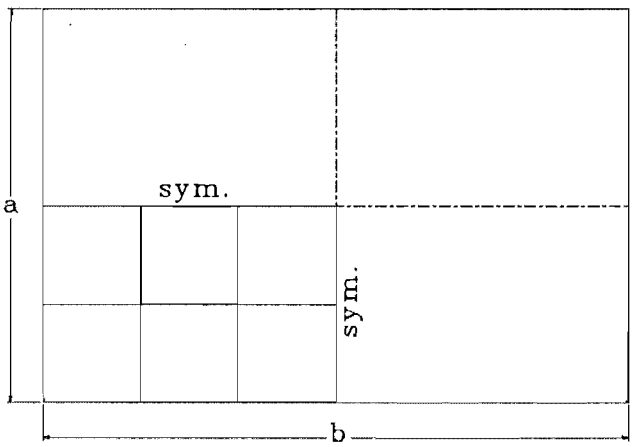

a=2.0; b=2.0 or 10.0; t=0.0001;
$E=1.7472*10^7$; $\upsilon=0.3$;
Boundaries=simply supported or clamped;
Loading:uniform pressure, $q=10^{-4}$ or
central load, $P=4.0*10^{-4}$.

Figure 3.7: Rectangular plate testcase.

3.5.5 Rectangular plate

This test originated with the evaluation of the original NASTRAN elements, and has become a de facto standard test and is frequently seen in technical literature. The particular geometry that is used for the test is shown in figure 3.7. Theoretical results for lateral displacement at the center are provided in table 3.4 for the all combinations of boundary supports, aspect ratio and loading conditions listed.

This is the first problem in which convergence with decreasing mesh spacing will be studied.

Table 3.4: Theoretical Solutions - Rectangular Plate Testcases.

Boundary supports	Aspect ratio b/a	Displacement at center of plate	
		Uniform Pressure	Concentrated force
Simple	1.0	4.062	11.60
Simple	5.0	12.97	16.96
Clamped	1.0	1.26	5.60
Clamped	5.0	2.56	7.23

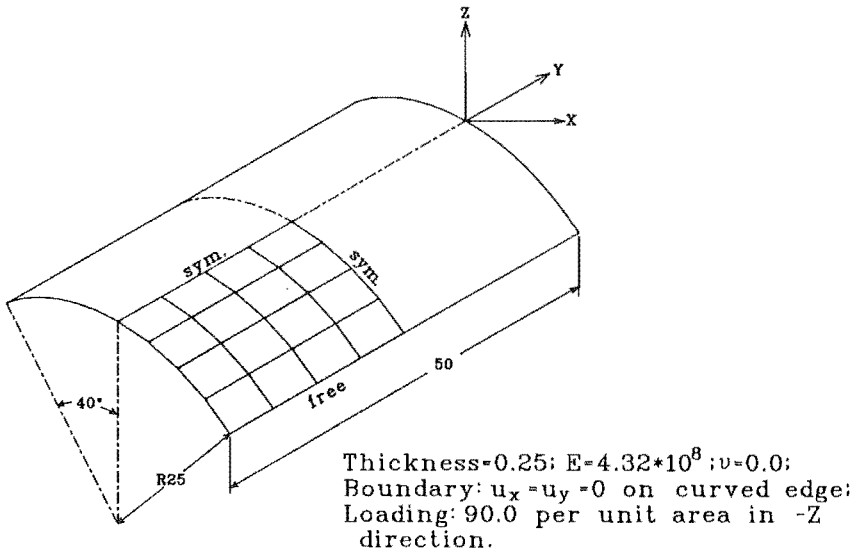

Figure 3.8: Scordelis–Lo roof testcase.

3.5.6 Scordelis-Lo roof

The Scordelis-Lo roof has achieved the status of a defacto standard test problem. The most frequently given test result is the vertical displacement of the midpoint of the free edge. While the value for the midside vertical displacement attributed to Ref. [92] is 0.3086, the author could not find this testcase, or result, in this paper and therefore assumed that this value was approximately correct. However further investigation revealed a tortuous past. Ashwell in Chapter Six of Ref [4] comments that the analysis method described by Scordelis et.al. is based on the work of Gibson [2], in which the shell geometry is shallow, however the load components were calcuated as if the shell was deep, and also that the value of Poisson's ratio is incorrect, (using $\nu = 0.3$ instead of zero). Ashwell goes on to note that several different values have been used as the solution, however the values quoted use a value of $3 * 10^6$ lb/sq.in for Young's Modulus, wheras the problem as specified by MacNeal and Harder uses a value of $4.32 * 10^8$. Even further discussion of this problem can be found in the paper by Idelsohn, [46].

To enable some meaningful comparisons a value of 0.3024 has been used for normalization of the results, as in [68]. Both membrane and bending behaviour are tested in this problem, which is depicted in figure 3.8.

[2]The author, upon reading Ref. [92], found that shell theory used in the described computer program for shell analysis was in fact based upon a numerical integration of the "Donnell–Jenkins" shell equation.

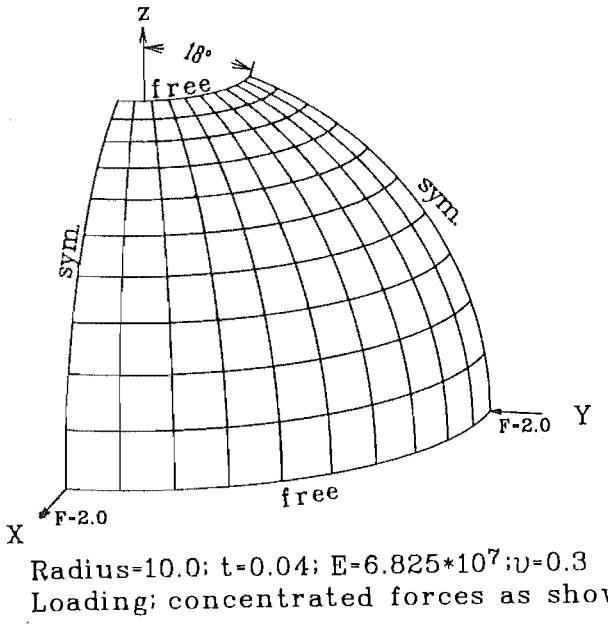

Figure 3.9: Spherical shell problem.

3.5.7 Spherical shell

This problem is more correctly a hemispherical shell, (see figure 3.9), as the equator is a free edge, with four point loads alternating in sign at 90 degree intervals on the equator. The hole at the top has been introduced to avoid the use of triangles near the axis of revoution. While both bending and membrane effects contribute to the result in this problem, this particular testcase shows whether or not membrane locking effects an element. Also, since the membrane strains are small over most of the shell, this problem tests whether or not an element can represent inextensional bending modes.

Convergence is studied by varying the mesh size.

A theoretical lower bound for a slightly different configuration, in which the hole at the axis is closed, [72], has been computed as being 0.0924, however a value of 0.0940 has been used for normalisation of the results, as in [68].

3.5.8 Thick-walled cylinder

This problem has been chosen to test the effect of a nearly incompressible material. Plane strain is the assumed condition which, along with the radial symmetry confines the material in all but the radial direction and intensifies the numerical difficulty caused by near incompressibility.

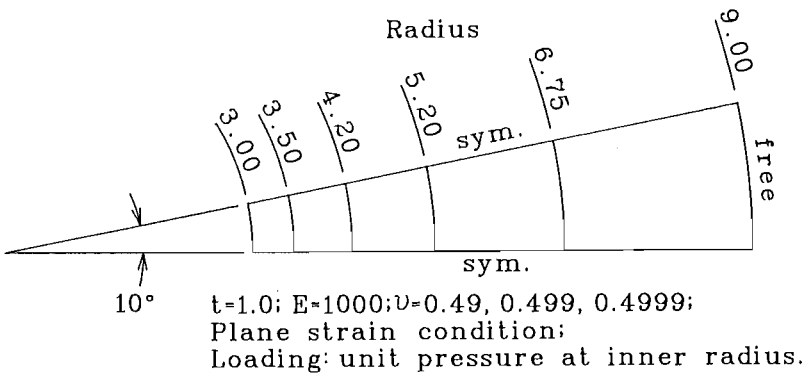

Figure 3.10: Thick–walled cylinder testcase.

Table 3.5: Theoretical Solution - Thick–Walled Cylinder Testcase.

Poisson's Ratio	Radial deflection $r = R_1$
0.49	5.0399 x 10^{-3}
0.499	5.0602 x 10^{-3}
0.499	5.0623 x 10^{-3}

The formula used for radial displacement can be found in Ref. [100].

$$u = \frac{(1+\nu)pR_1^2}{E(R_2^2 - R_1^2)}\left[\frac{R_2^2}{r} + (1-2\nu)r\right]$$

where p = pressure, R_1 = inner radius and R_2 = outer radius.

3.6 Element Verification Results

Tables of the results from these element verification tests can be seen in Appendix A.

3.6.1 Patch Test Results

The results for the QUD four–noded quadrilateral were as expected, with the element passing the membrane patch test exactly, and with some error in the bending patch test, as would be expected with Zienkiewicz non-conforming triangles being used in the element formulation.

The QD8 higher order quadrilateral elements passed the membrane patch test, or 'Constant-stress' patch test, and the bending, or 'Constant-curvature' patch test exactly,

Table 3.6: Results - Patch test.

	Maximum error in stress	
	QUD	QD8
In–plane loading	0.00%	0.00%
Out–of–plane loading	19.56%	0.00%

as would be expected for any conforming plate and shell elements available in a modern finite element package.

3.6.2 Straight Cantilever Beam Results

The QD8 eight-noded elements performed better in all the deformation modes than the QUD four-noded elements, even though in the twisting testcase the improvement over the truly poor QUD result is minimal. MacNeal, [69], comments that the cantilever beam test is failed badly by most four–noded elements, especially those without drilling freedoms.

Also noted was the very poor result for the trapezoidal shaped QUD elements in the in-plane shear testcase. This is most probably due to the formulation of the element. The QUD plate element is formulated by combining a membrane isoparametric element with two additional shape functions, and a bending quadrilateral element, which is itself formulated from four cross-lapped Zienkiewicz triangles. This particular trapezoidal sub–test shows the effect of 'shear locking', with the four–noded membrane isoparametric element being particularly severly affected.

Another effect that may contribute to the poor result is that the aspect ratio of the sub–triangles of the bending element will be tending towards a large value, possibly leading to numerical 'noise' and therefore poor results, [86].

White et.al., [103], claims that poor performance of elements in the twisting subcase is due to the Kirchoff assumptions that are employed in the formulation of (some of) the elements[3] and the fact that the thickness of the beam, (and therefore element), is equal to one–half the width. He continues on to say that Kirchoff–based elements perform poorly for width–to–thickness ratios as high as ten.

MacNeal, in Ref. [67], attributes the poor performance of the four–noded trapezoidal membrane element under this sort of test to the fact that the linear stress capability of

[3]The Kirchoff assumption of neglecting transverse shear deformation will lead to a large error in the result for low characteristic dimension–to–thickness ratios.

Table 3.7: Results - Straight cantilever beam testcases.

Tip loading direction	Normalized tip displacement in direction of load	
	QUD	QD8
	(a) *Rectangular elements*	
Extension	1.000	1.000
In-plane shear	0.993	1.000
Out-of-plane shear	0.979	0.998
Twist	0.006	0.010
	(b) *Trapezoidal elements*	
Extension	1.000	1.000
In-plane shear	0.222	0.999
Out-of-plane shear	0.952	0.995
Twist	0.006	0.010
	(c) *Parallelogram elements*	
Extension	1.000	1.000
In-plane shear	0.786	1.000
Out-of-plane shear	0.924	0.998
Twist	0.004	0.010

such elements is limited to inplane bending along the principal directions of rectangles and parallelograms.

3.6.3 Curved Beam Results

The QD8 element passes this testcase for both in-plane and out-of-plane loadings, the QUD element however, does not perform as well, barely passing for in-plane loading, showing the effect of shear locking, but failing in the out-of-plane subcase, the influence of the aspect ratio of the sub–triangles of the plate bending element doubtless contributing towards the poor results noted. White et.al., [103], again attributes poor performance of some elements in this testcase to the Kirchoff assumptions that are employed in the formulation of the element as twisting is a major component of the out–of–plane loadcase.

3.6.4 Twisted Beam Results

The I/FEM shell elements all produced poor results in this testcase, failing badly, with the QUD element producing better results than the QD8 element. In some respects this

Table 3.8: Results - Curved beam testcase.

Tip loading direction	Normalized tip displacement in direction of load	
	QUD	QD8
In-plane (vertical)	0.888	1.013
Out-of-plane	0.717	0.962

Table 3.9: Results - Twisted beam testcase.

Tip loading direction	Normalized tip displacement in direction of load	
	QUD	QD8
In-plane	1.411	1.782
Out-of-plane	1.431	1.807

testcase is similar to the twisting of the straight cantilever beam that has already been commented upon.

Haftka and Robinson, [38], found that conventional four–noded membrane quadrilaterals responded particularly badly to this type of deformation, with the results for a linear strain quadrilateral element widely scattered, even for small out-of-plane distortions.

The reason for the poor performance of the higher order quadrilateral elements in this testcase can only be attributed to the formulation employed, and that the isoparametric mapping functions cannot adequately describe the deformation of the element, when they are also required to account for the curved boundaries of the element. (This same effect will occur for the membrane part of the four–noded shell element).

In Ref. [68] the failure of the QUAD2 element in this test is attributed to a misalignment of moments at interelement boundaries, leading to an unresisted moment about the normal to the surface of the element. In this case however, due to a lack of such explicit information, it can only be concluded that both quadrilateral elements are very sensitive to warping of the geometry.

3.6.5 Results for rectangular plate

In this series of testcases the QUD element proved to be superior to the QD8 element, producing a more stable solution that appeared to converge to the analytic solution as given in [100]. The QD8 element results were very unstable, ie. they dipped to a value far below that of the analytic solution and only converged very slowly for increasing mesh

Figure 3.11: Results: Simply Supported plate under concentrated loading.

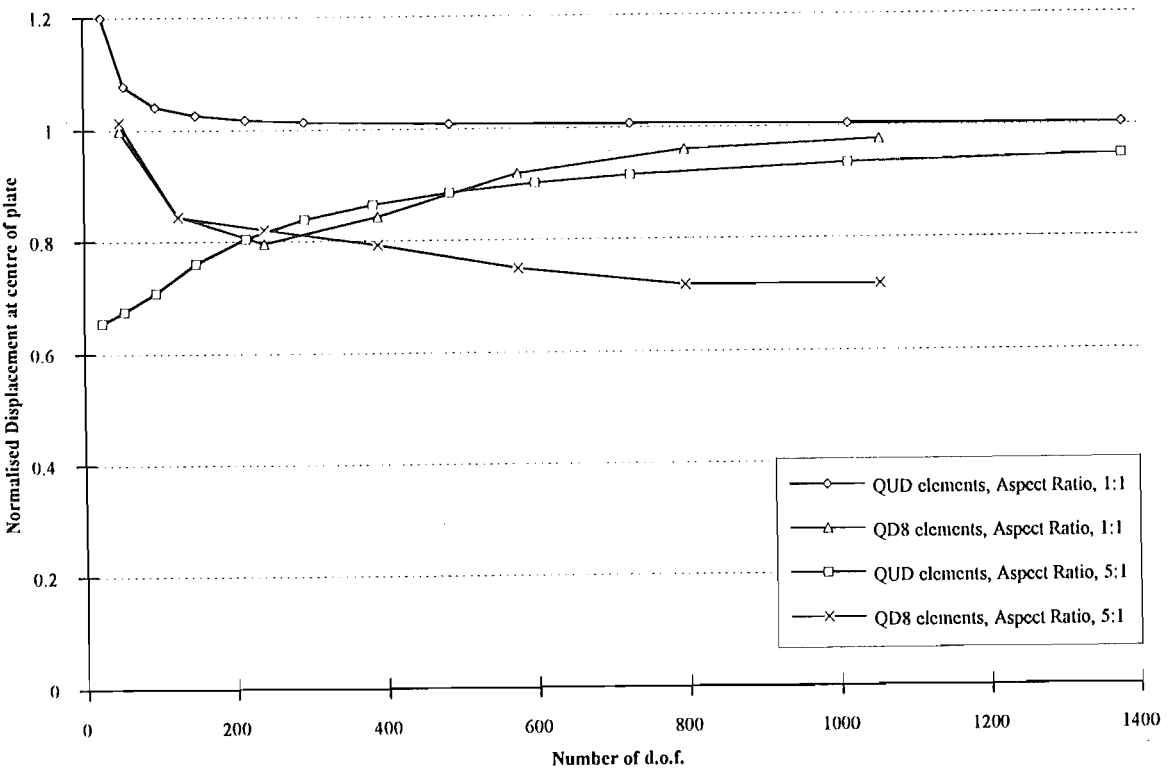

density, especially in the subcases with clamped boundary conditions. It would appear that membrane locking effects are predominating when clamped boundary conditions are used, the boundary conditions acting as excessive constraints on the behaviour of the QD8 element.

In the series of graphs, the convergence of the QUD and QD8 shell elements can be seen. The percentage error of the solution is plotted with the total number of degrees of freedom as the abscissa of the problem, to show the efficiency of the various elements in providing a correct solution.

3.6.6 Results for Scordelis-Lo roof

The deflection of a reference point, the midside of the free edge, is plotted against the total number of degrees of freedom. It can be seen that both quadrilaterals have a monotomic convergence trend, with similar efficiency in achieving the normalised solution, (and overshooting slightly).

It is noted that the QUD element converges slowly to the normalized solution for this

Figure 3.12: Results: Simply supported plate under uniformly distributed loading.

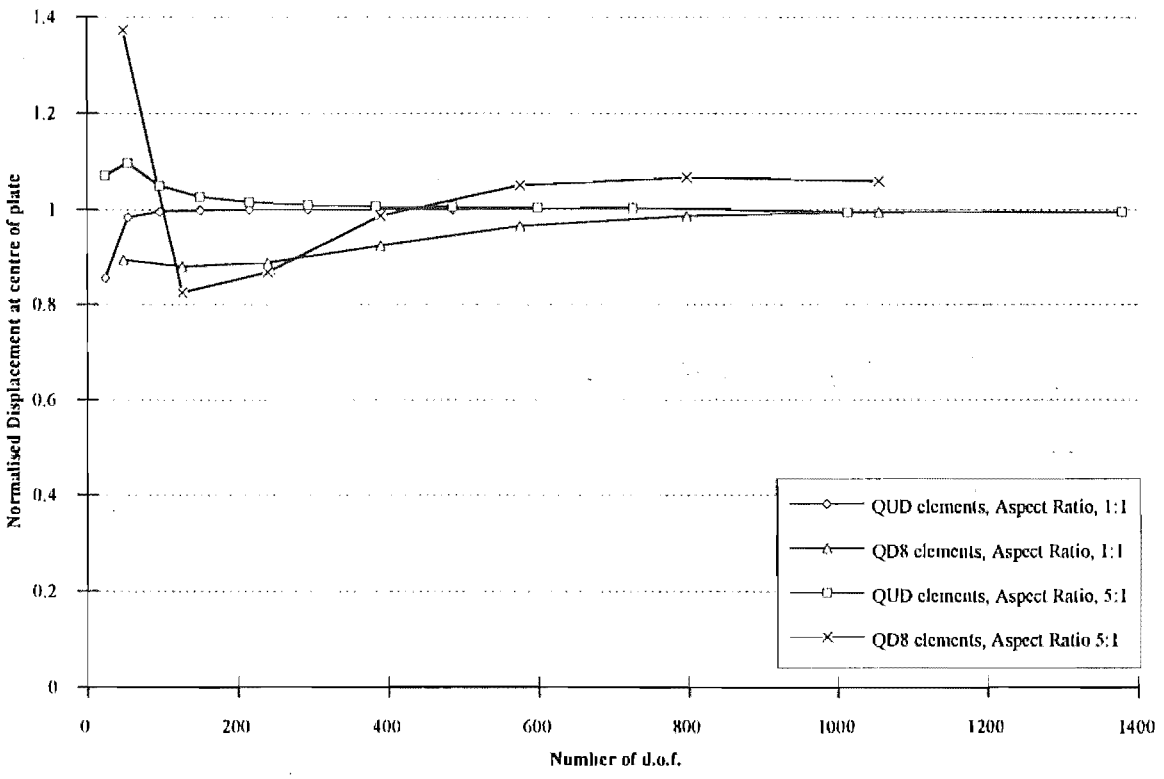

Figure 3.13: Results: Clamped plate under concentrated loading.

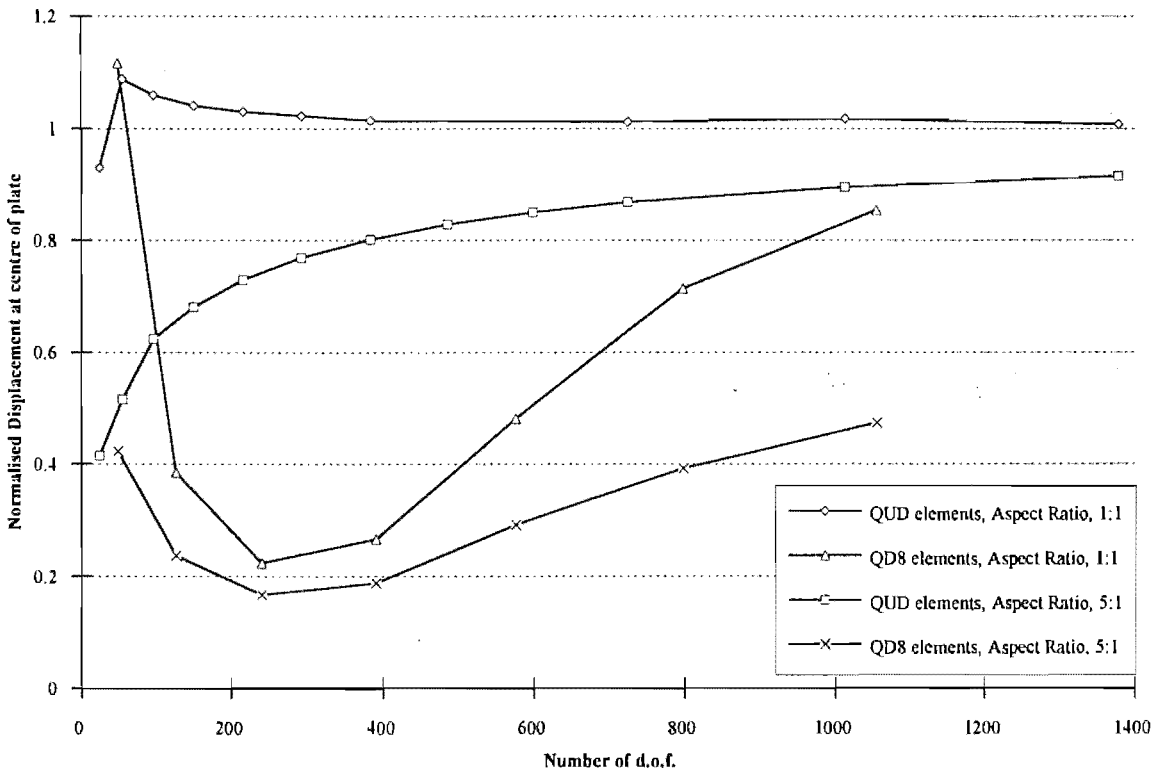

Figure 3.14: Results: Clamped plate under uniformly distributed loading.

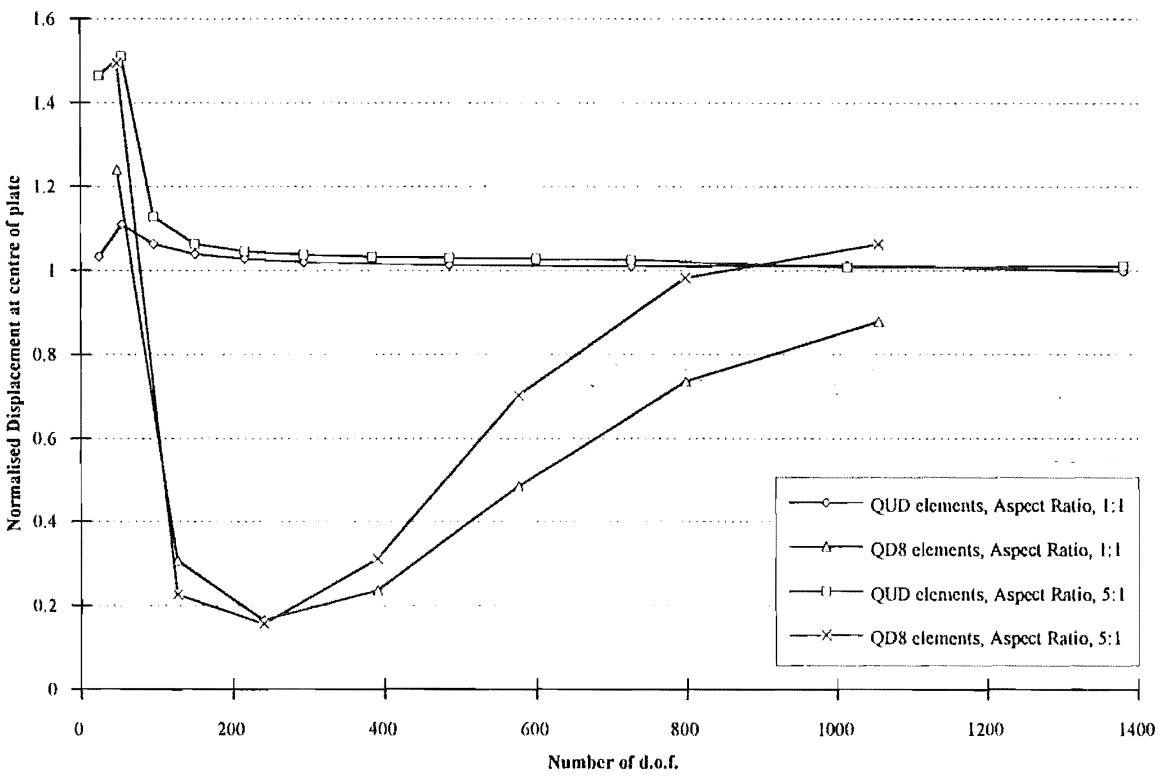

Figure 3.15: Results: Scordelis–Lo roof.

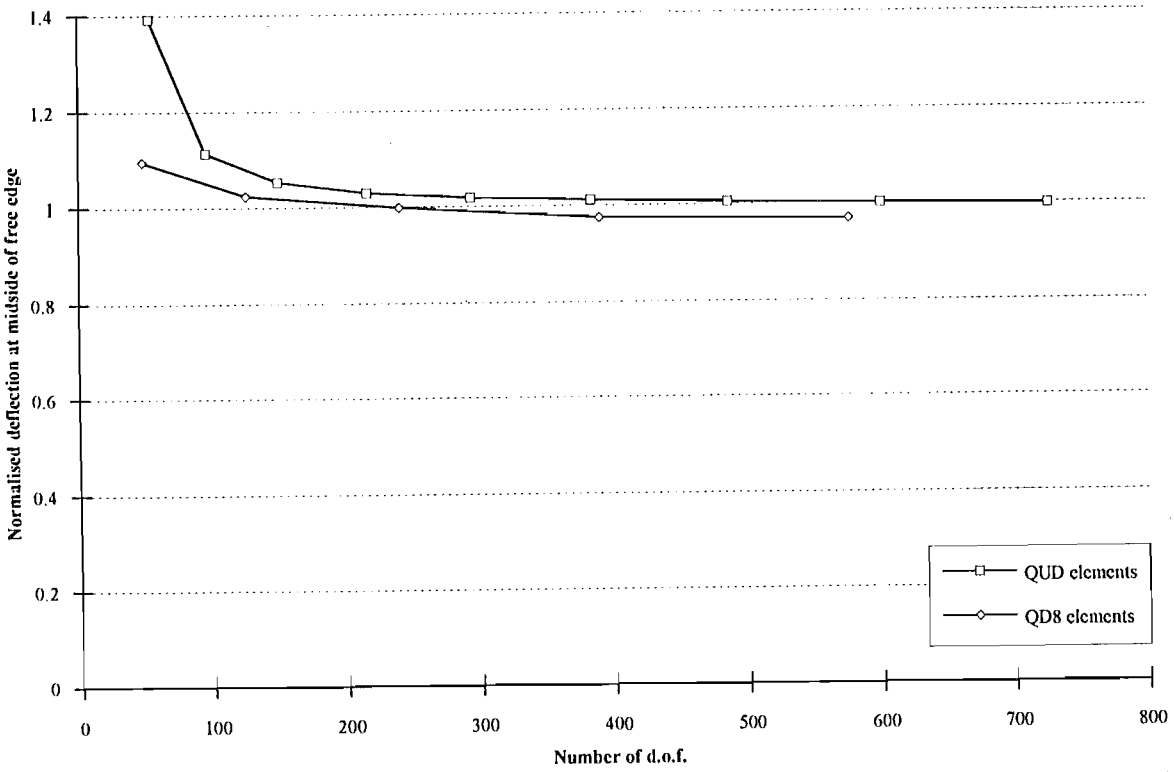

single curvature shell problem, showing the effect of membrane locking, and also the fact that a facet shell approximation requires a number of elements to effectively model a curved surface.

The QD8 element appeared to converge to a solution below the "correct" solution, however upon reading Ref. [46], it is possible that the element is converging to the shallow shell solution mentioned, in which the deflection is about 3.5% larger.

Of the two elements tested, the QUD (four–noded quadrilateral) element gives a better results trend than the QD8 (eight–noded quadrilateral) element.

3.6.7 Results for spherical shell

In this doubly-curved convergence study the QUD element again proved to be faster than the QD8 element in achieving the given solution. The convergence was monotomic in both cases[4], although the final displacement value for both elements appeared to be slightly less than that used for normalization of the results.

[4] If the first, very coarse mesh model using the QD8 elements is ignored

Figure 3.16: Results: Hemispherical shell.

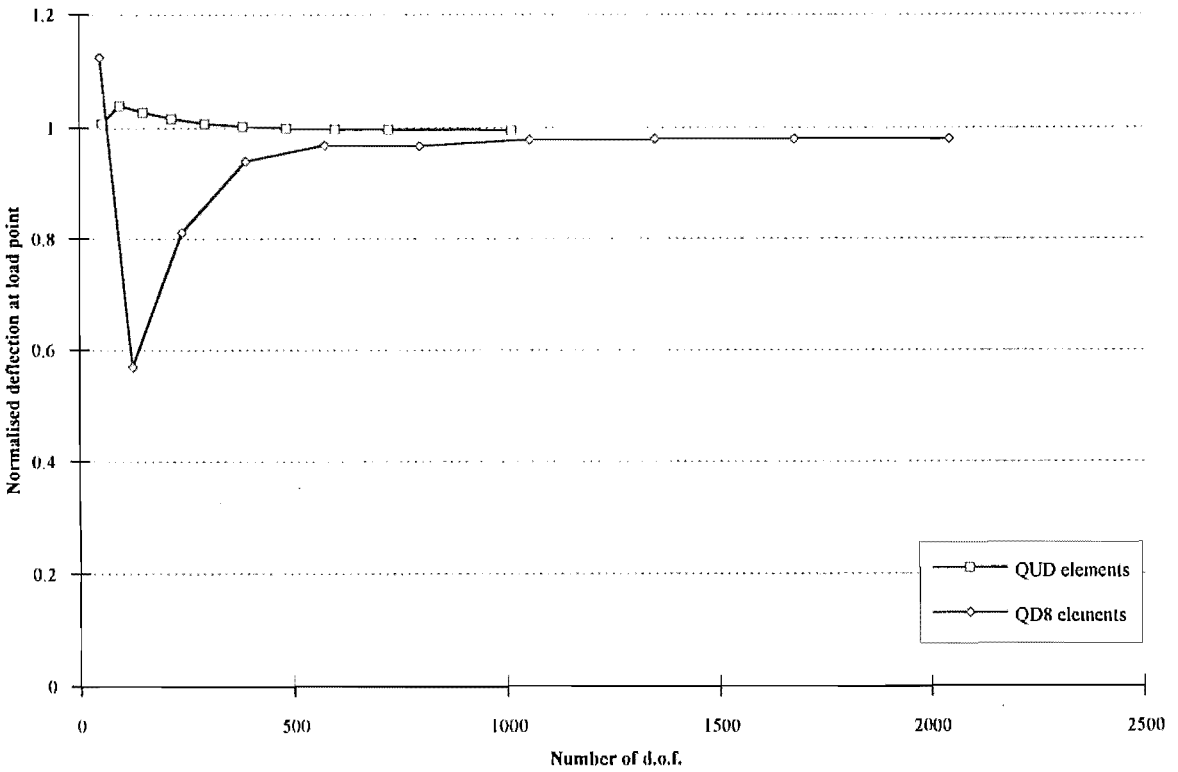

This problem is a particularly challenging test of the ability of an element to represent inextensional bending modes, since the membrane strains are small over most of the shell, [103], and in this respect it appears that the QUD element is more accurate.

3.6.8 Results for thick-walled cylinder

The results for the thick–walled cylinder testcase are good considering the extreme numerical difficulty of the problem, the QUD four–noded elements performing slightly better than the QD8 eight–noded elements.

It could be concluded, from this testcase, that the I/FEM quadrilateral shell elements perform well in near incompressible problems.

Table 3.10: Results: Thick–Walled Cylinder Testcase.

Poisson's Ratio	Normalised Radial deflection $r = R_1$	
	QUD elements	QD8 elements
0.49	1.0871	1.0951
0.499	1.0869	1.0951
0.4999	1.0868	1.0951

3.7 Element Verification Results Summary

The results for the patch test were as expected, both elements passing the constant stress (in–plane) patch test exactly, the QD8 element also passing the constant curvature (out–of–plane) patch test. The QUD element did not pass this test due to the non–conforming elements used to form the plate–bending part of the element.

The QD8 element out–performed the QUD element in all the straight cantilever beam testcases, although the performance of both elements in the twisting subcase was particularly bad. The QUD element also performed poorly in the in–plane shear subcase for trapezoidal shaped elements.

The curved beam testcase showed that both elements are sensitive to slight irregularity of element shape, and also that the QUD element again had problems with representing the twisting that occurs in the out–of–plane subcase.

Both elements performed exceedingly poorly in the twisted beam testcase, with the QUD element out–performing the QD8 element, but still failing.

The normalised deflection trends exhibited by the QUD element were in general better than those exhibited by the QD8 element in the square and rectangular plate testcases. The QUD element converged in a manner that gave some confidence in the element, wheras the trend in deflection from the QD8 element meshes, especially in the cases with clamped boundary conditions where membrane locking occured was certainly not monotomic.

The QUD element again out–performed the QD8 element in the Scordelis–Lo roof testcase, converging to the normalised solution more quickly.

The hemispherical shell testcase showed the QUD element more economical in achieving the normalised solution, the QD8 element apparently converging towards a different solution.

Both of the I/FEM quadrilateral elements gave results that were acceptable in the incompressible material – plane strain testcase, the solutions achieved being only slightly

Table 3.11: Rules for assigning results grades.

Grades	Rules
A	$2\% \geq$ error
B	$10\% \geq$ error $\geq 2\%$
C	$20\% \geq$ error $\geq 10\%$
D	$50\% \geq$ error $\geq 20\%$
F	error $\geq 50\%$

different to the theoretical solution given in Ref. [68].

Grading of the Element Accuracy. A letter grade is given for the accuracy of the element, the rules used for assigning the grades are given in table 3.11.

Where more than one case contributes to a letter grade, the absolute errors have been averaged before assigning a letter grade.

The results used for table 3.12 are, in general, given in the element verification examples in Chapter 11 of the I/FEM Reference Manual. The remainder of the tests being modifications of these, or new files created from scratch.

3.8 Element Verification Conclusions

As a result of this investigation into the plate and shell element library of the Intergraph I/FEM package, the elements have been ranked in order of accuracy for the proposed application of analysing the C. W. F. Hamilton Model 273 Reverse Duct.

The results obtained for both the QUD and QD8 elements are disapointing in view of the excellence of the rest of the Intergraph products available, but it is taken from this study that the elements will produce solutions of 'engineering' accuracy.

Of the quadrilateral elements, the four–noded QUD element produced more acceptable results, while failing the testcases in which twisting was a major component of the load. The QUD element consistently displayed a faster and more reliable trend towards the normalised displacement solution in the testcases in which single or double curvature was involved.

The eight–noded QD8 element, on the other hand while producing better results eventually in some of the testcases, displayed very poor convergence characteristics. The QD8 performed similarly to the QUD element in the twisting loadcases, very poorly indeed,

Table 3.12: Results summary.

	Test	Element Loading		Element	QUD	QD8
		In-plane	Out-of-plane	shape		
(1)	Membrane Patch Test	X		Irregular	A	A
(2)	Bending Patch Test		X	Irregular	B	A
(3)	Straight beam, extension	X		All	A	A
(4)	Straight beam, bending	X		Regular	A	A
(5)	Straight beam, bending	X		Irregular	F	A
(6)	Straight beam, bending		X	Regular	B	A
(7)	Straight beam, bending		X	Irregular	B	A
(8)	Straight beam, twist			All	F	F
(9)	Curved beam	X		Regular	B	A
(10)	Curved beam		X	Regular	D	B
(11)	Twisted beam	X	X	Regular	D	F
(12)	Rectangular plate (N=4)		X	Regular	B	D
(13)	Scordelis-Lo roof (N=4)	X	X	Regular	B	B
(14)	Spherical shell (N=8)	X	X	Regular	A	B
(15)	Thick-walled cylinder ($\nu = 0.4999$)	X		Regular	A	A
	Number of failed tests (D's & F's)				4	3

and for the increase in the computational effort required, the QD8 eight–noded elements displayed no major advantage over the simpler four–noded elements.

Therefore the QUD four–noded quadrilateral shell element was chosen over the QD8 eight–noded quadrilateral shell element for the analysis of the 273 Reverse Duct, as it should produce results of engineering or acceptable accuracy and as the model is further refined, if required, the elements will converge towards a correct solution in a more economical manner.

Chapter 4

Control Volume Theory for Analysis of the Reverse Duct.

4.1 Introduction

In 1991, a research project for study in a Masters degree was proposed between the author and C.W.F. Hamilton Ltd. The proposed course of events was that several components of a waterjet unit currently in production would be analysed using the Intergraph I/FEM finite element package, followed by experimental verification using strain gauges and similar methods. However due to difficulties, both with the software and in procuring suitable funding, this project was shortened to cover analysis of the reverse duct of a jet unit, as well as extensive work in verifying the plate and shell elements available on the I/FEM package.

The first problem in the analysis of the reversing duct is that of the determination of the loads to adequately and accurately model the in-service stresses. A theoretical analysis of the forces on the bucket was undertaken, using the concepts of conservation of momentum, control volumes, and ignoring the internal flow regimes, for example "swirling" effects.

This chapter covers the theoretical analysis used to derive the forces, and hence pressures on the reverse duct. The result of this analysis was a spreadsheet which, given a set of reverse duct design angles and the input conditions, could calculate the forces that were being transmitted through the duct.

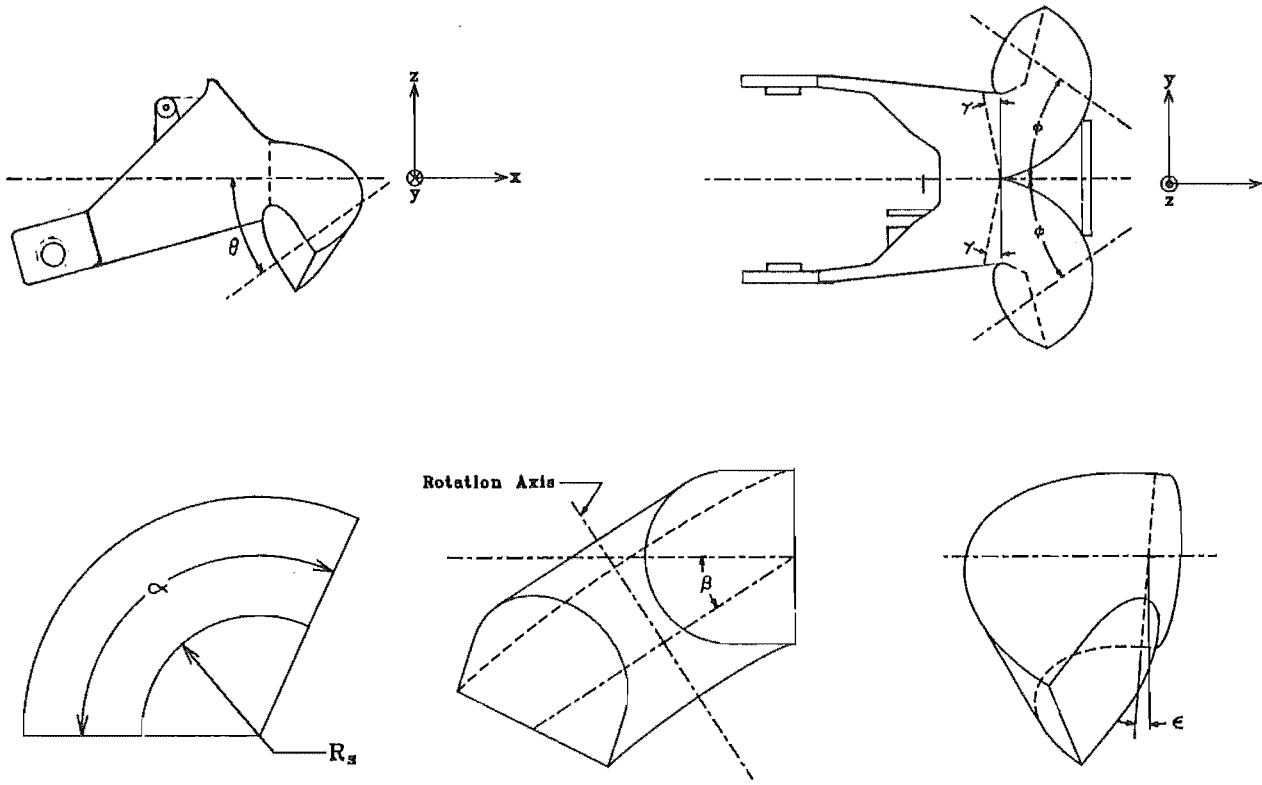

Figure 4.1: Duct Design Angles.

4.2 Initial assumptions in the force analysis

Consider the reverse duct in operation, with the fluid entering along the centerline of, and flowing down one 'runner' or side. The overall force imparted to the duct can be calculated using the principle of conservation of momentum, ie. the force applied is equal and opposite to the change in the fluid momentum.

Now at constant operating conditions, the amount of fluid flowing through the duct is the same at all times of operation, (mass continuity is maintained). In other words, the amount of water flowing into the duct is equal to the amount of fluid leaving the duct in the same time period.

In an initial simplistic case, the magnitude of the fluid velocity can be considered constant, therefore the change in the momentum of the fluid is simply due to the change in fluid velocity. Later, (as CWFH do), this change in the magnitude of the fluid velocity is accounted for by the inclusion of a duct efficiency factor, which is defined as $\eta = \| v_2 \| / \| v_1 \|$, where the initial velocity into the duct is v_1, and the velocity out of the duct is v_2.

The initial direction of the fluid velocity, along the jet centerline, is taken as being

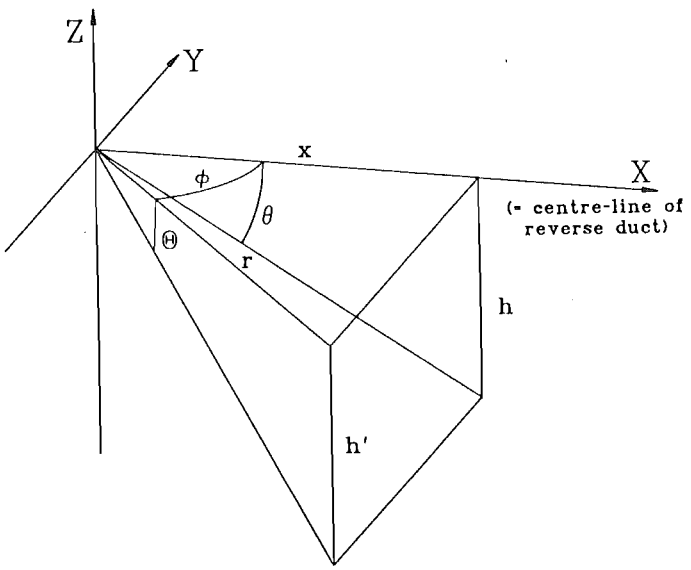

Figure 4.2: Coordinate System.

along the x-axis, parallel to the centerline of the vessel, with the y-axis being taken as parallel to the perceived fluid surface and the z-axis being taken as perpendicular to the fluid surface.

Now the fluid is turned in two directions in the runner, being deflected through an angle, θ, of approximately 40 degrees in the $x - y$ plane, and deflected downwards in the $x - z$ plane, ϕ, approximately 30 degrees from the intake end, these values varying depending on the particular jet unit being considered.

A factor to simplify this analysis is the fact that the actual angle through which the fluid is deflected downwards is not the vertical discharge direction, θ, or the duct design angle, β, but a function of θ and the horizontal discharge direction, ϕ.

Therefore to simplify the analysis of the duct forces, a new angle will be defined. This angle, the 'Modified Vertical Displacement Angle' or Θ, will simplify the analysis of the duct velocities, and hence forces, considerably by enabling the use of spherical polar coordinates. The use of this angle has the effect of slightly decreasing the angle through which the fluid is deflected in the cases we are considering. Therefore the following calculations shall use this modified vertical discharge direction, Θ.

$$\begin{aligned} \text{Now } h &= x \tan\theta \\ \text{and } h' &= r \tan\Theta \\ \text{But } h &= h' \end{aligned}$$

$$\therefore \; x \tan\theta = r \tan\Theta$$

$$\begin{aligned} \text{Also } x &= r \cos\phi \\ \therefore \; r &= x/\cos\phi \\ \therefore \; x \tan\theta &= x \tan\Theta/\cos\phi \\ \therefore \; \tan\Theta &= \tan\theta * \cos\phi \end{aligned} \tag{4.1}$$

or

$$\begin{aligned} \Theta &= \tan^{-1}(\tan\theta * \cos\phi) \\ &= \text{'Modified Vertical Displacement Angle'} \end{aligned} \tag{4.2}$$

4.3 Force Analysis

4.3.1 Derivation of concentrated forces at a point on the duct

Now consider only velocity changes in the $x - y$ plane;

$$\text{The x-velocity in} = v_{1x} \tag{4.3}$$

$$\begin{aligned} \text{The x-velocity out} &= v_{2x} \\ &= v_2 \cos(180 - \phi) \\ &= -v_2 \cos\phi \end{aligned} \tag{4.4}$$

$$\text{The y-velocity in} = v_{1y} = 0 \tag{4.5}$$

$$\begin{aligned} \text{The y-velocity out} &= v_{2y} \\ &= v_2 \sin(180 - \phi) \\ &= v_2 \sin\phi \end{aligned} \tag{4.6}$$

Now consider velocity changes only in the $x - z$ plane;

$$\text{The x-velocity in} = v_{1x} \tag{4.7}$$

$$\begin{aligned} \text{The x-velocity out} &= v_{2x} \\ &= v_2 \cos(180 - \Theta) \end{aligned}$$

$$= -v_2 \cos\Theta \tag{4.8}$$

$$\begin{aligned} \text{The z-velocity in} &= v_{1z} \\ &= 0 \end{aligned} \tag{4.9}$$

$$\begin{aligned} \text{The z-velocity out} &= v_{2z} \\ &= v_2 \sin(180 - \Theta) \\ &= v_2 \sin\Theta \end{aligned} \tag{4.10}$$

Therefore the overall 3-dimensional velocity changes are:

$$\begin{aligned} \text{The x-velocity in} &= v_{1x} \\ &= v_1 \end{aligned} \tag{4.11}$$

$$\begin{aligned} \text{The x-velocity out} &= v_{2x} \\ &= v_2 \cos(180 - \phi) \cos(180 - \Theta) \\ &= v_2 \cos\phi \cos\Theta \end{aligned} \tag{4.12}$$

$$\begin{aligned} \text{The y-velocity in} &= v_{1y} \\ &= 0 \end{aligned} \tag{4.13}$$

$$\begin{aligned} \text{The y-velocity out} &= v_{2y} \\ &= -v_2 \sin(180 - \phi) \cos(180 - \Theta) \\ &= v_2 \sin\phi \cos\Theta \end{aligned} \tag{4.14}$$

$$\begin{aligned} \text{The z-velocity in} &= v_{1z} \\ &= 0 \end{aligned} \tag{4.15}$$

$$\begin{aligned} \text{The z-velocity in} &= v_{2z} \\ &= -v_2 \sin(180 - \Theta) \\ &= -v_2 \sin\Theta \end{aligned} \tag{4.16}$$

Therefore the resultant forces on the duct can be calculated:

$$F_x = \rho Q (v_1 - v_2 \cos\phi \cos\Theta) \tag{4.17}$$

$$F_y = -\rho Q v_2 \sin\phi \cos\Theta \tag{4.18}$$

$$F_z = \rho\, Q\, v_2 \sin\Theta \tag{4.19}$$

Note: if the duct efficiency factor, η , is included, then the resultant forces will become:

$$F_x = \rho\, Q\, v_1(1 - \eta \cos\phi \cos\Theta) \tag{4.20}$$

$$F_y = -\rho\, Q\, \eta\, v_1 \sin\phi \cos\Theta \tag{4.21}$$

$$F_z = \rho\, Q\, \eta\, v_1 \sin\Theta \tag{4.22}$$

The magnitude of the total resultant force is therefore:

$$F_R = \left(F_x^2 + F_y^2 + F_z^2\right)^{\frac{1}{2}} \tag{4.23}$$

and the direction of the resultants:

$$\phi' = \tan^{-1}(F_y/F_x) \quad \text{(In } x-y \text{ plane measured clockwise around } z \text{ axis)}$$
$$\text{(from } \theta = 180^o, \phi = 180^o) \tag{4.24}$$

$$\Theta' = \tan^{-1}(F_z/F_x) \quad \text{(In } x-z \text{ plane measured clockwise around } y \text{ axis)}$$
$$\text{(from } \theta = 180^o, \phi = 180^o) \tag{4.25}$$

As a check, compare the results of these formulae with a worked example in a fluid mechanics text, Douglas, Gasiorek and Swaffield [51].

Example 5.3 - Force due to Deflection of a Jet by a Curved Vane.

In the coordinate system previously defined, the variables are as follows:

$$\rho\, Q = 0.8\ m^3/s$$
$$v_1 = 30\ m/s$$
$$\Theta = 180^o$$
$$v_2 = 25\ m/s$$
$$\phi = 120^o$$

Using eqns. (4.20) and (4.21):

$$F_x = \rho\, Q(v_1 - v_2 \cos\phi \cos\Theta)$$

$$
\begin{aligned}
&= 0.8(30 - 25\ \cos 120\ \cos 180) \\
&= 0.8(30 - 12.5) \\
&= 14\ N
\end{aligned}
$$

$$
\begin{aligned}
F_y &= -\rho\, Q\ v_2\ \sin\phi\ \cos\Theta \\
&= -0.8 * 25\ \sin 120\ \cos 180 \\
&= 0.8 * 25\ \sin 120 \\
&= 17.32\ N
\end{aligned}
$$

Both these values agree exactly with the values and directions given in D.G.S.

Rearrange the example in another plane, (the $x - z$ plane).

In the given coordinate system the variables are as follows:

$$
\begin{aligned}
\rho\, Q &= 0.8\ m^3/s \\
v_1 &= 30\ m/s \\
\Theta &= 120^o \\
v_2 &= 25\ m/s \\
\phi &= 180^o
\end{aligned}
$$

Using eqns. (4.20) and (4.22):

$$
\begin{aligned}
F_x &= \rho\, Q(v_1 - v_2\ \cos\phi\ \cos\Theta) \\
&= 0.8(30 - 25\ \cos 180\ \cos 120) \\
&= 0.8(30 - 12.5) \\
&= 14\ N
\end{aligned}
$$

$$
\begin{aligned}
F_z &= \rho\, Q\ v_2\ \sin\Theta \\
&= 0.8 * 25\ \sin 120 \\
&= 17.32\ N
\end{aligned}
$$

Both these values agree exactly with the values and directions given in D.G.S.

4.3.2 Derivation of a line of fluid force vectors around the duct

Now this simple vector representation of the forces on the duct is rather too simple for an accurate analysis of the duct, therefore the next step is to consider incremental changes in angle around the duct and the effect this has on the forces around the fluid path in the duct.

For incremental angle changes the overall 3-dimensional velocity changes are:

$$\begin{aligned} \text{The x-velocity in} &= v_{1x} \\ &= v_1 \cos\phi_1 \cos\Theta_1 \qquad (4.26) \\ \text{The x-velocity out} &= v_{2x} \\ &= v_2 \cos\phi_2 \cos\Theta_2 \qquad (4.27) \end{aligned}$$

$$\begin{aligned} \text{The y-velocity in} &= v_{1y} \\ &= v_1 \sin\phi_1 \cos\Theta_1 \qquad (4.28) \\ \text{The y-velocity out} &= v_{2y} \\ &= v_2 \sin\phi_2 \cos\Theta_2 \qquad (4.29) \end{aligned}$$

$$\begin{aligned} \text{The z-velocity in} &= v_{1z} \\ &= -v_1 \sin\Theta_1 \qquad (4.30) \\ \text{The z-velocity out} &= v_{2z} \\ &= -v_2 \sin\Theta_2 \qquad (4.31) \end{aligned}$$

Therefore the resultant forces on the duct are:

$$F_x = \rho Q(v_1 \cos\phi_1 \cos\Theta_1 - v_2 \cos\phi_2 \cos\Theta_2), \qquad (4.32)$$

$$F_y = \rho Q(v_1 \sin\phi_1 \cos\Theta_1 - v_2 \sin\phi_2 \cos\Theta_2) \qquad (4.33)$$

$$F_z = -\rho Q(v_1 \sin\Theta_1 - v_2 \sin\Theta_2) \qquad (4.34)$$

Note: if the duct efficiency factor, η , is included, then the resultant forces will become:

$$F_x = \rho\, Q\, v_1(\cos\phi_1 \cos\Theta_1 - \eta \cos\phi_2 \cos\Theta_2) \qquad (4.35)$$

$$F_y = \rho\, Q\, v_1\, (\sin\phi_1\, \cos\Theta_1 - \eta\, \sin\phi_2\, \cos\Theta_2 \tag{4.36}$$

$$F_z = -\rho\, Q\, v_1\, (\sin\Theta_1 - \eta\, \sin\Theta_2) \tag{4.37}$$

As before, the magnitude of the total resultant force is:

$$F_R = \left(F_x^2 + F_y^2 + F_z^2\right)^{\frac{1}{2}} \tag{4.38}$$

the direction of the resultants being calculated as before.

As a check on this again compare the results of these formulae with a worked example in a fluid mechanics text, Douglas, Gasiorek and Swaffield [51].

Example 5.3 - Force due to Deflection of a Jet by a Curved Vane.

In the given coordinate system the variables are as follows:

$$\begin{aligned} \rho\, Q &= 0.8\ m^3/s \\ v_1 &= 30\ m/s \\ \Theta_1 &= 180^o \\ \Theta_2 &= 180^o \\ v_2 &= 25\ m/s \\ \phi_1 &= 180^o \\ \phi_2 &= 120^o \end{aligned}$$

Using eqns (4.32) and (4.33):

$$\begin{aligned} F_x &= \rho\, Q(v_1\, \cos\phi_1\, \cos\Theta_1 - v_2\, \cos\phi_2\, \cos\Theta_2) \\ &= 0.8(30\, \cos 180\, \cos 180 - 25\, \cos 120\, \cos 180) \\ &= 0.8(30 - 12.5) \\ &= 14\ N \end{aligned}$$

$$\begin{aligned} F_y &= \rho\, Q(v_1\, \sin\phi_1\, \cos\Theta_1 - v_2\, \sin\phi_2\, \cos\Theta_2) \\ &= 0.8(30\, \sin 180\, \cos 180 - 25\, \sin 120\, \cos 180) \\ &= 0.8 * 25\, \sin 120 \\ &= 17.32\ N \end{aligned}$$

Both these values agree exactly with the values given in D.G.S.

Rearrange the example in another plane, (the $x - z$ plane).
In the given coordinate system the variables are as follows:

$$\begin{aligned} \rho Q &= 0.8\ m^3/s \\ v_1 &= 30\ m/s \\ \Theta_1 &= 180^o \\ \Theta_2 &= 120^o \\ v_2 &= 25\ m/s \\ \phi_1 &= 180^o \\ \phi_2 &= 180^o \end{aligned}$$

Using eqns (4.32) and (4.34):

$$\begin{aligned} F_x &= \rho Q(v_1 \cos\phi_1 \cos\Theta_1 - v_2 \cos\phi_2 \cos\Theta_2) \\ &= 0.8(30 \cos 180 \cos 180 - 25 \cos 120 \cos 180) \\ &= 0.8(30 - 12.5) \\ &= 14\ N \end{aligned}$$

$$\begin{aligned} F_z &= -\rho Q(v_1 \sin\Theta_1 - v_2 \sin\Theta_2) \\ &= -0.8(30 \sin 180 - 25 \sin 120) \\ &= 0.8 * 25 \sin 120 \\ &= 17.32\ N \end{aligned}$$

Both these values agree exactly with the values given in D.G.S.

4.3.3 Accuracy of the Control Volume Analysis.

Fluid Force Line.

A point which must be considered at this stage is that the fluid does not flow around a simple line in the duct, but around a complex path over the inner surface. This 'fluid force line' should be determined by careful study of the fluid paths, or by the use of some computational fluid dynamics package if possible.

The amount of fluid flowing through the duct has a major effect on the fluid force line. When the reverse duct is being lowered into the fluid stream, only a small amount of fluid is flowing through the duct, the fluid entering at the lower bottom corner of the inlet, and exiting at the upper top corner of the outlet. As the amount of fluid flowing through the duct increases, the duct fills up from these two corners respectively. This means that the fluid force line is a path somewhere across the flat of the duct. A simple curve between these two corners would do for a first approximation, but this is inaccurate, and would be better approximated by a line which follows a horizontal plane around the duct, until this plane contacts the edge of the back, (flat) surface, and then follows this join line around to the exit corner. For this analysis, using maximum forces, only the maximum amount of fluid flowing in the duct needs to be considered.

Another point to consider is that the fluid doesn't actually enter the reverse duct along the centerline of the unit if a turn is being undertaken, (for example in the worst full reverse, full steering loadcase), due to the effect of the steering nozzle/deflector. This can be taken account of if the spatial positions of the nozzle and the duct are known, and was included in the calculations by the addition of a "Fluid entry angle", Y_f, calculated from the documentation that is supplied with the Model 273 jet unit.

To more exactly model the flow, it is likely that the fluid deflected by the nozzle doesn't follow the centerline of the nozzle, and this must be investigated if a more exact solution is desired, however time constraints, among others, dictated that this consideration be ignored.

Other Avenues for Force Analysis.

Several other methods of calculating the forces and pressures on the duct are available, and given more time and funding these could be investigated further.

CFD Packages. A computational fluid dynamics package currently available in the Mechanical Engineering Department, Fluent 3-D, does appear to be useful for determining this fluid force distribution over the duct surface. Although the program does not accept free surfaces on the fluid, which are present in the reverse duct, some approximation could be made in order to determine the position and relative magnitude of the forces/pressures on the duct surfaces.

Other computer packages are available which accept free surfaces on the fluid and these would be useful for determining the fluid force distribution over the inner surface of the duct, although, similar to the finite element method, the simplifying assumptions made

to enable a reasonable model will decrease the solution accuracy.

Measurement of Reverse Duct Pressures. The other alternative to some form of model of the fluid flow in the duct is to simply place pressure taps around the ducts and to measure the pressures at points around the duct to build up an overall picture of the distribution. The advantage of this method is that it is accurate (within experimental errors) and the results may give a general picture which could be used as a guide for other sizes of reverse duct. However the results may only be valid for one particular size of reverse duct, and the process of instrumentation and testing may have to be repeated for the other sizes of duct, and certainly if any change in duct shape is to be modelled, the forces on any modified shape duct will not be accurately known until a casting or fabrication has been made and tested.

4.3.4 Derivation of Pressure Loads.

While concentrated forces will give a general representation of the stresses in the duct, at a distance from the point at which the forces are applied, (Saint Venant's theorem), it would be more desirable to apply pressures across the inner surface of the duct.

In the absence of pressure distribution data, or computer models of the reverse duct fluid flows, a simple approximation was made about the pressure distribution in the duct. It was assumed that a uniform pressures acted over the rear and upper surfaces of the duct.

The method employed in this analysis for derivation of the pressure values was to calculate a pressure load based on the approximate projected areas and force values in the $x-$ and $y-$directions. These values were then applied to the appropriate surfaces of the model and the model solved. The resultant forces were then checked from the program output, compared to the values from the concentrated force loadcases and the pressures adjusted to correct values using simultaneous equations.

Upon re-analysis the corrected pressure values were found to provide the correct resultant forces, and were used in the ensuing analysis.

4.4 Conclusions–Control Volume Force Analysis

Two main loadcases are expected to be analysed, these being "crash" stops from 25 knots with no–steering and full–steering. In comparing the formulae that have been derived in this chapter, and the formulae from the C.W.F. Hamilton Reverse Duct Standard, [63],

the formulae described herein predict the resultant force to be about 2 % less for the former loadcase, and 12 % less for the latter. This discrepancy is due to the fact that the formulae derived here account for the vertical force applied to the duct, and also account for the angle that the fluid from the jet unit nozzle impinges on the reverse duct.

The formulae derived in this chapter have been used for the calculation of the forces and pressure loads to be applied to the finite element model which is described in the following chapter, as the author understands the derivations, and has confidence in the formulae.

Chapter 5

Finite Element Modelling and Analysis of the 273 Reverse Duct

5.1 Introduction

This chapter covers the finite element modelling and subsequent analysis results of the C.W.F. Hamilton Ltd. Model 273 reverse duct. The generation of a shell element model is briefly described herein, followed by the analysis, results and conclusions.

5.2 Modelling

The analysis was undertaken in the following manner:

1. A brief study of the existing design methods for CWFH reverse ducts.
2. The generation of a shell element model of the 273 reverse duct.
3. The derivation of correct appropriate loads to be applied to the model for the load-cases.
4. The finite element analysis.

5.3 Steps in the Analysis

5.3.1 Existing design methods for waterjet reverse ducts.

The current method of designing a reverse duct for a jet unit involves empirical formulae for determining stress in small sections of the duct. As the complex shape does not easily lend

itself to simple approximations, experience and an intuitive 'feel' for the expected stresses and highly stressed regions in the duct has been utilised in the past. The forces applied to the duct are calculated with reasonable accuracy using the control volume theory covered in the previous chapter, and the path of these forces can be visualised in the simpler ducts. As the ducts become more complex, due to increasing power throughputs, and the need for better power–to–weight ratios, these force paths are becoming more and more convoluted and harder to visualise.

The current criteria for determining whether or not a reverse duct will be adequate in service is based upon the calculation of the normal stress in the reverse duct arms. This normal stress is calculated by dividing the force applied to the reverse duct by the cross–sectional area of the arm, a value of about 15 MPa being taken as being acceptable. Considering the material properties of the aluminium alloy used to construct the reverse duct, (Appendix C), and the limited portion of the reverse duct about which the magnitude of the stresses are known, a finite element analysis, or testing program is desirable.

C.W.F. Hamilton Ltd. have produced an internal design standard to aid with the design of the reverse ducts, and a simple program for calculation of expected forces is also available to aid the designer. Finite element analysis, using a reliable package, has the ability to model very complex shapes with a reasonable degree of accuracy, and this has been utilised in the redesign of parts of their jet units, in an effort to minimise wastage in castings and reduce weight while maintaining an acceptable factor of safety for operation.

5.3.2 The I/FEM Finite Element Program.

The Intergraph I/FEM finite element program is part of the Intergraph I/EMS modelling system, which is an integrated suite of programs covering basic draughting through to milling, casting and a finite element program. This set of programs is running on an Intergraph Unix workstation in the Mechanical Engineering Department of the Engineering School at the Unversity of Canterbury.

The I/FEM finite element package can be used in several ways. As a finite element package in its own right, running on top of the I/EMS environment, or as a pre– and post–processor, with the analysis being done by an appropriate third party solver, such as MSC/NASTRAN or ANSYS.

In this project I/FEM was used as the solver, the shortcomings of the shell element library being overlooked[1], as no other comprehensive solver was readily available with the

[1]The shell elements selected are expected to provide results of 'engineering accuracy' for the complex geometry, based upon the element verification detailed in Chapter Three.

ability to solve the complicated model of the reverse duct.

5.3.3 Generation of a shell element model.

Initially a solid model of the reverse duct was constructed from the supplied drawings, [62], but as the reverse duct had geometry which would lend itself to a simpler shell element model, a separate shell element model was constructed, and analysed.

Other advantages which can be cited for using a shell element model in preference over a solid model include economy, both in creation time, solver time and storage requirements.

The same drawings, supplied by C.W.F. Hamilton Ltd. were used to generate the shell element model of the reverse duct, which can be seen in figure 5.1. Problems were found in the creation of an accurate model, as the drawings could not adequately convey the three–dimensional compound curves and junctions that are employed in the construction of the duct. As close an approximation as was possible, within reasonable bounds, was drawn on the Intergraph Engineering Modelling System, I/EMS. The powerful geometry manipulation commands that are built into the package, such as the ability to perform Boolean operations on solids and surfaces proved to be a lifesaver for this project.

5.3.4 Derivation of Forces

The derivation of the forces to be applied to the CWFH Model 273 reverse duct used information supplied by Mr M. Hamilton in his visit to The University of Canterbury on Thursday, November 26, 1992.

These figures were checked in a spreadsheet, using the formulae of the previous chapter as a basis for the calculations. See Appendix B.1 for a printout of this spreadsheet. These forces values were subsequently applied to a shell element model generated from drawings supplied by CWFH.

Derivation of point loads

Given α, β, ϵ *and* γ from drawings supplied by C.W.F. Hamilton Ltd [62].

1. Calculate ϕ, θ *and* Θ

$$\begin{aligned} \phi &= \tan^{-1}(\tan(180-\alpha)\cos\beta) \\ \theta &= \tan^{-1}(\tan\beta\tan\phi) \\ \Theta &= \tan^{-1}(\tan\beta\sin\phi) \end{aligned}$$

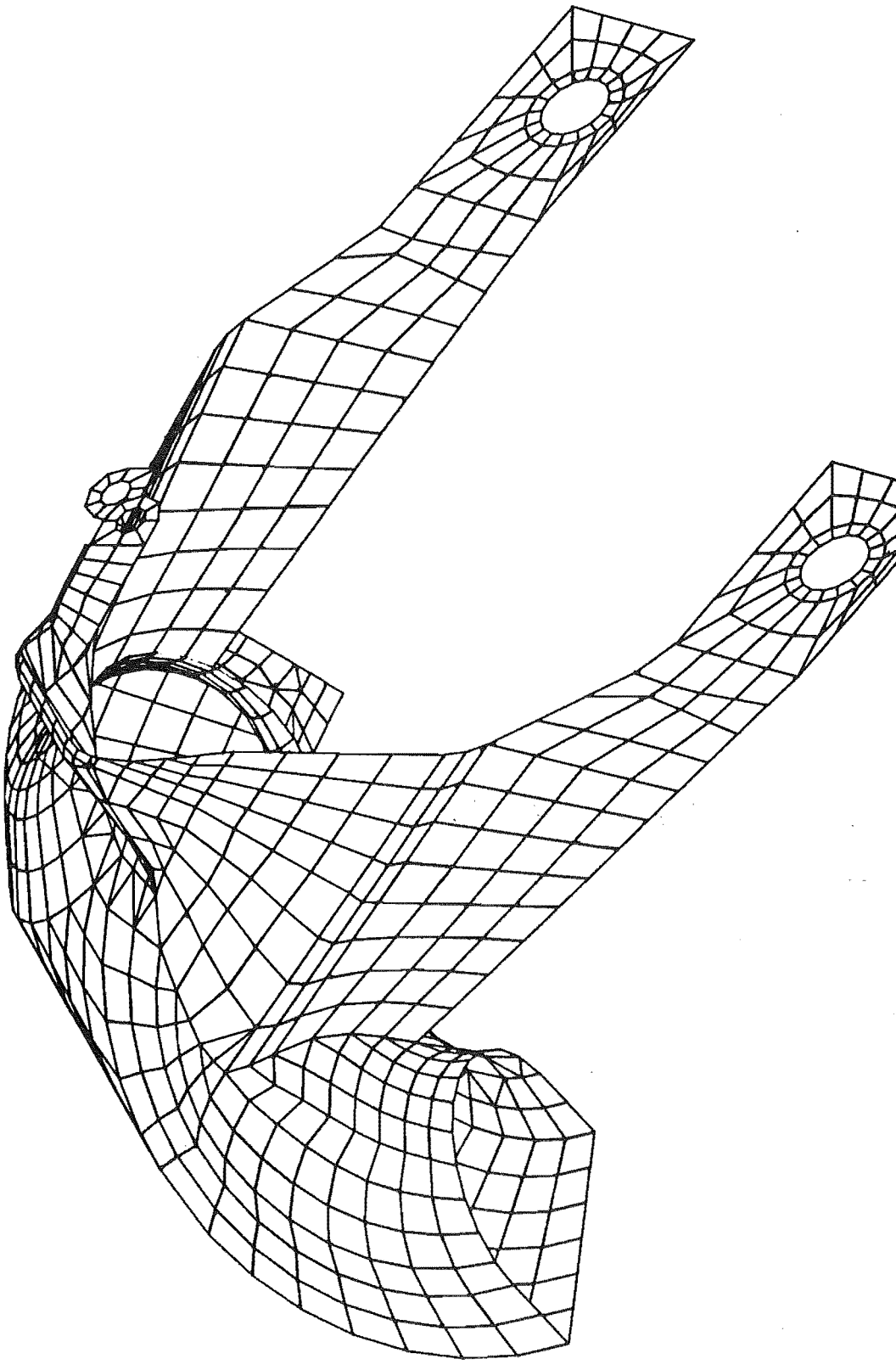

Figure 5.1: Shell element model of the 273 Reverse Duct.

2. Calculate $F_x, F_y, F_z, F_R, \Theta', \phi'$ using eqns (4.32–4.34) and (4.38):

$$\begin{aligned} F_x &= \rho Q(v_1 \cos\phi_1 \cos\Theta_1 - v_2 \cos\phi_2 \cos\Theta_2), \\ F_y &= \rho Q(v_1 \sin\phi_1 \cos\Theta_1 - v_2 \sin\phi_2 \cos\Theta_2) \\ F_z &= -\rho Q(v_1 \sin\Theta_1 - v_2 \sin\Theta_2) \\ F_R &= \left(F_x^2 + F_y^2 + F_z^2\right)^{\frac{1}{2}} \end{aligned}$$

and the direction of the resultants, from eqns (4.24) and (4.25):

$$\begin{aligned} \phi' &= \tan^{-1}(F_y/F_x) \quad (\text{In } x-y \text{ plane measured clockwise around } z \text{ axis}) \\ &\qquad\qquad (\text{from } \theta = 180^o, \phi = 180^o) \\ \Theta' &= \tan^{-1}(F_z/F_x) \quad (\text{In } x-z \text{ plane measured clockwise around } y \text{ axis}) \\ &\qquad\qquad (\text{from } \theta = 180^o, \phi = 180^o) \end{aligned}$$

Derivation of pressure loads

To generate the pressure loadings, approximate projected areas in the $x-$ and $y-$directions were calculated, using the Intergraph Engineering Modelling System or I/EMS. These pressures were then applied to the model, an analysis run and then the resultant reactions checked against the required forces.

These pressures were then recalculated on the basis of this analysis, new pressures applied and the analysis rerun. The recalculated pressures gave acceptable reaction results, and were then used for the complete analysis.

5.3.5 Summary of Loadcases.

The boundary conditions applied in all the loadcases were to simulate a bearing surface at the reverse duct pivots. This was done by constraining all displacements, (Tx, Ty and Tz), in the forward side of the pivot hole.

Two models were run for each loadcase, a pressure loadcase and a concentrated force loadcase, as a check on the accuracy of the pressure loads that were applied to the model.

1. A full reverse load evenly split between the ducts, ie. no steering. This load is applied as a 0.21959 MPa pressure load on the rear flat surface of the ducts, and a 0.34136 MPa pressure load over the upper flat surface of both ducts.

2. A full reverse load evenly split between the ducts, ie. no steering. This load is applied as two 12447 N vector forces acting at a point half way around each duct.

3. A full reverse, full steering load, ie applied to one duct only. This load is applied as a 0.43992 MPa pressure load over the rear flat surface of one duct, and a 0.66951 MPa pressure load over the upper flat surface of the same duct.

4. A full reverse load applied to one duct, ie full steering. This load is applied as a 21883 N vector force acting at a point half way around the starboard duct.

5.4 Analysis results

The discussion of the analysis results can be best understood when read in conjunction with the plates in Appendix D. The stress types mentioned refer to Hencky–Von–Mises stresses, with the TOP, MID or BOT referring to the top, middle or bottom surfaces of the shell element model, for example HVMTOP refers to the Hencky–Von–Mises stress on the top surface of the shell element.

The results for each main loadcase are briefly discussed in two parts, stresses and displacements. The stress values are computed at the center of each element, and then averaged to the node points, as is discussed in Section 2.5.1.

5.4.1 Loadcase One: Full Reverse, no steering

Maximum Stress Values. The maximum HVMTOP stress was 152 MPa, the HVMMID stress 44 MPa, and the HVMBOT stress 111 MPa.

Stresses

The stresses calculated in the analysis initially seemed rather high, the maximum Von Mises stress being 152 MPa. However the maximum stress is concentrated in two small areas, where the arms of the reverse duct connect to the ducts, (see Figures D.1 to D.3). This is an area where the model geometry is not very representative of the actual geometry, (see Section 5.5.1), due to the fact that this is a shell element model, attempting to model complex three-dimensional solid intersections.

Overall the stresses in the model ducts are within a reasonable range, 1E-4 to 45 MPa, the arms of the duct, and the splashguard having stresses in the range 1E-4 to 15 MPa, the average stress across the arm where the pivot 'block' connects to the arm being 15.8 MPa.

Displacements

The displacement mode of this model was as the author expected. As the pressure was applied to the rear- and upper flat surfaces of the duct, the arms lengthened slightly, and the outer ends of the ducts tended to move rearward relative to the rest of the reverse duct. This is to be expected, as the water pressure acts upon the duct it will tend to straighten the ducts.

The influence of the water pressure on the reverse duct itself, is to tend to distort the 'D' cross–sectional shape of the duct to a more elliptic shape. This can be seen in the deflected shape figure, (Figure D.13), where the rear flat surface of the duct has been distorted into a curved shape, and the upper flat surface of the duct has attempted to take on a smoother curve from the junction of the arms to the rear of the duct.

5.4.2 Loadcase Two

The results from this loadcase were very close to those results generated from loadcase one, with a pressure load. The major difference is that a high stress area, (45–55 MPa), can be seen around the area where the concentrated vector forces were applied to the model. This is expected behaviour, and should be ignored for the purposes of this analysis.

The displacement mode was also very similar to those in loadcase one, with the exception again being in the vicinity of the point load, where a localised 'dimple' can be observed.

5.4.3 Loadcase Three: Full Reverse, full steering

Maximum Stress Values. The maximum HVMTOP stress was 127 MPa, the HVMMID stress 63 MPa, and the HVMBOT stress 168 MPa.

Stresses

The full reverse - full steering loadcase was expected to generate the highest stresses, and this was confirmed by the following two loadcases.

For this loadcase it was assumed that the fluid was being deflected through the side of the reverse duct which did not have the actuator lug and associated reinforcment, and was therefore the weakest side.

The side, and arms of the reverse duct through which the fluid is being deflected are much more highly stressed than the other side of the reverse duct. The maximum Von

Mises stress of 150 MPa was again in the vicinity of the junction of the reverse duct arms and the duct on that particular side. This is expected as the force path travels directly from the duct through the arm to the pivot.

The stresses in the high–stressed arm of the reverse duct were in the range of 1E-4 to 29 MPa, the average stress across the arm where the pivot 'block' connects to the arms being 26.1 MPa.

The stresses in the duct, through which all the fluid is being deflected, are in the range of 15-73 MPa. The high stresses being in areas where the duct is being deformed by the water pressure.

Displacements

The displacement mode for this duct was again as expected. The deformation mode itself can be split into two main parts:

1. A torsional effect due to the reaction from the fluid being turned downwards on one side of the duct,

2. A straightening of the duct through which the fluid is being turned.

5.4.4 Loadcase Four

Again both the stresses and deformation modes were very similar to loadcase three, with small perturbations where the concentrated vector force was applied to the model to simulate the pressure loading.

The maximum stress of 149 MPa was again found at the junction of the ducts and arms of the reverse duct.

5.5 Limitations of the shell finite element model

5.5.1 Geometric Limitations of the Model

The shell element model of the reverse duct is as accurate as can be derived from the CWFH Drawings, [62], however because of the nature of a shell element model, several approximations arise. The main approximation is that the complex solid geometry of the reverse duct is being modelled using surfaces, which are positioned at the mid-plane of the the solid geometry. This gives rise to problems in this model where the arms of the

reverse duct connect to the actual ducts or deflectors - this can be seen in the figures in Appendix D.

5.5.2 Solution Accuracy

A fact which must be stressed when the results of this analysis is that the finite element method is not an exact method, but a numerical approximation of the solution.

Accuracy can be gauged by considering areas in which stresses and/or displacements are known, and comparing the actual results with those given in the finite element method. Another method of gauging accuracy is to test the elements/finite element package with a series of testcases, and through this build some confidence in the results of an analysis.

A possible measure of the accuracy of this analysis can be gauged from a calculation of the stresses across the arms of the reverse duct. In the CWFH Reverse Duct Standard, [63], the arms are designed for a maximum tensile stress of 15 MPa. In loadcase one of this analysis, the average stress across the arm was 16 MPa.

5.6 Conclusions

The 273 reverse duct has adequate strength, as evidenced by it's success in service, however, several points of interest were raised by this analysis.

The loadcases as tested rarely occur in service.

The pivot 'blocks' and the arms of the reverse duct are, as a whole, under moderate stress - under 30 MPa for both the loadcases tested. The ducts themselves are, for the worst loadcase, stressed up to a level of about 50 MPa.

LM-6M aluminium alloy has a yield stress of about 70 MPa, therefore these stresses are about as high as can safely be designed for.

It appears that the region where the arms of the reverse duct connect to the actual ducts is under quite high stresses when loaded as highly as in both the symmetric and asymmetric loadcases. If any re-design is being contemplated, then this area should be carefully changed. A thickness increase in the duct close to the arm may be required to lower the stresses in this area, or fillets may be required to further reinforce this connection to the ducts.

Chapter 6

Additional Analysis of the Reverse Duct

6.1 Introduction

As a result of the analysis covered in the previous chapter, C.W.F. Hamilton Ltd. requested that some modifications be made to the model of the reverse duct, to try and reduce the magnitude of the stresses obtained. The modifications proposed were to double the thickness of the reverse duct around the junction of the arms of the reverse duct and the front curved surface of the duct.

This chapter briefly comments upon the effect of changing the duct thickness in the high stress regions of the duct, and the effect that this change in thickness had upon the stresses in the duct under the two main (pressure) loadcases for the 273 reverse duct.

6.2 Steps in the Analysis

Only two loadcases have been used in this analysis, in an effort to reduce computing time, and unnecessary data/results.

The elements adjacent to the intersection of the reverse duct arms and the reverse ducts have been thickened by a factor of two, by modification of the elements, and individual element properties in the Intergraph finite element package, I/FEM. The model was then re–run through the processor and the results analysed.

The modified finite element model can be seen in figure 6.1, the area of modification visible at the junction of the reverse duct and the reverse duct arms.

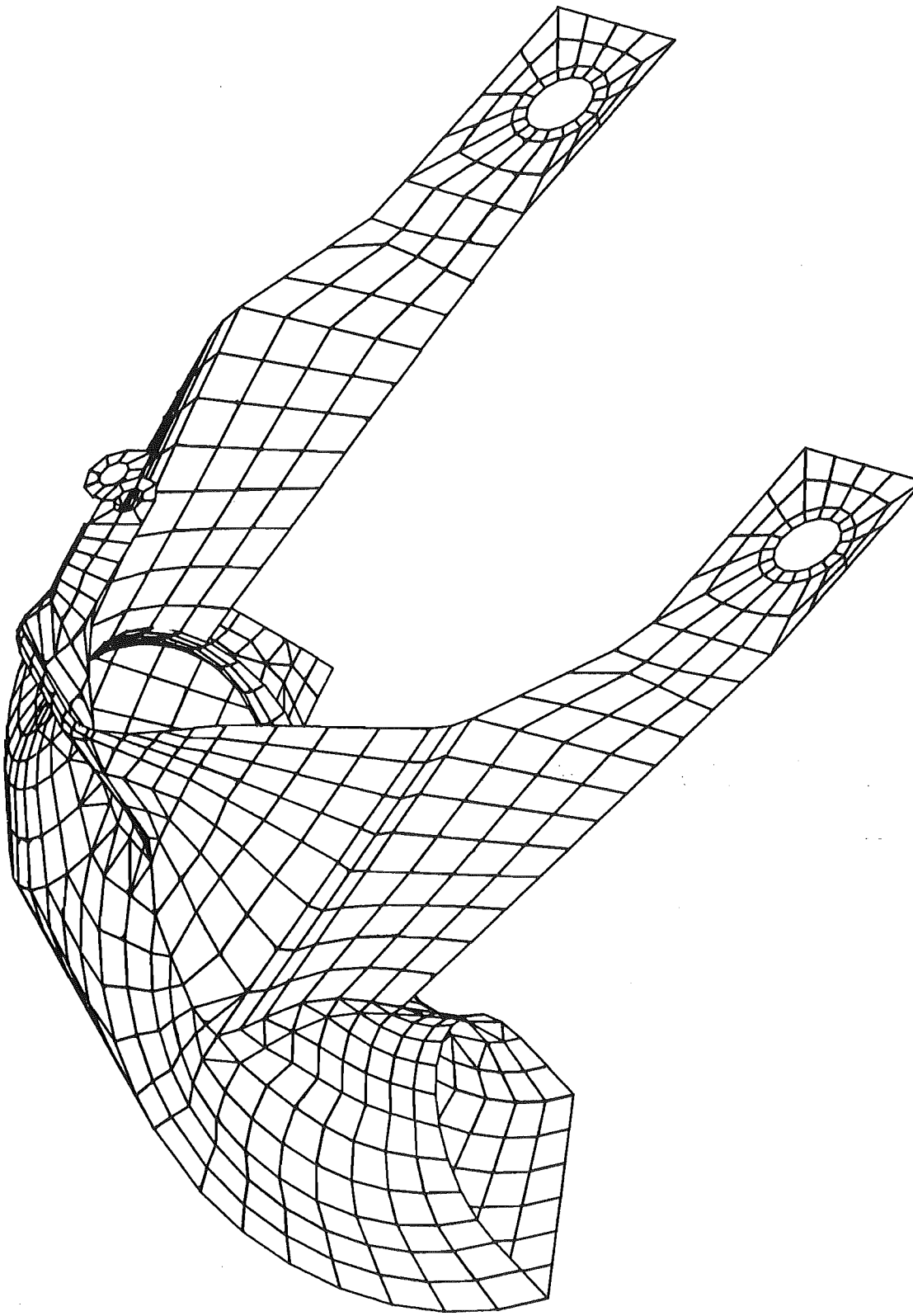

Figure 6.1: Modified Shell element model of the 273 Reverse Duct.

6.3 Results.

The results discussion in this section is best understood when considered in conjunction with figure 6.1 and the plates in Appendix E.

Increasing the thickness of the elements adjacent to the intersection of the reverse duct arms and the ducts had the effect of decreasing the stresses obtained in the analysis, 36 % being the average reduction in the Hencky–Von–Mises stresses for the two loadcases.

6.3.1 Loadcase One: Full reverse, no steering

Stresses

The maximum Hencky–Von–Mises stresses in general decreased by 36 % when the highest stress area, (where the shell element geometric representation is erroneous), was locally reinforced, or doubled in thickness.

For example the maximum HVMTOP stress, which is found at the junction of the reverse duct arms and the duct, decreased from 152 to 75 MPa, the maximum HVMMID stress, which is found in the middle of the front curved edges, decreased from 44 to 40 MPa and the maximum HVMBOT stress, found in the same area as the maximum HVMTOP stress decreased from 111 to 56 MPa.

Displacements

The displaced shape remained similar to that which was obtained for the un–reinforced duct.

6.3.2 Loadcase Two: Full reverse, full steering

Stresses

The stresses obtained in the analysis of the duct with local reinforcing were in general substantially less than those obtained for the un–reinforced duct, the average reduction in Hencky–Von–Mises stress being 37 %.

For example, the maximum HVMTOP stress, which is found at the lower point of the reverse duct arm where it connects to the duct decreased from 127 to 97 MPa, the maximum HVMMID stress, which is found on the outer front curved edge of the duct decreased from 63 to 60 MPa and the HVMBOT stress, which is found on the front upper–curved surface of the duct decreased from 168 to 78 MPa.

Displacements

The displaced shape was much the same as that mentioned in the previous chapter, with the reverse duct being twisted in reaction to the fluid. This is due to the contribution of the vertical force on the upper flat surface of the duct. The duct is therefore pushed away from the centerline of the duct, in the direction of the jet, and is twisted about the centerline by the vertical force imparted to the duct by the jet.

6.4 Conclusions

6.4.1 Effect of locally reinforcing the reverse duct

Doubling the thickness of the duct in the region adjacent to the junction of the reverse duct arms and the duct was most beneficial in decreasing the maximum stresses, a general reduction of 36 % being typical.

The displaced shapes remained very similar to those obtained for the un–reinforced reverse duct.

Chapter 7

Summary

7.1 I/FEM Quadrilateral Shell Elements.

The accuracy of the Intergraph I/FEM quadrilateral shell element library is disappointing, in view of the excellence of the user interface and the geometric modelling capabilities. An upgraded version of the finite element package has been released, however the shell element library has not been improved at all – the supplied element verification examples giving the same results.

While the accuracy of the shell elements is not of the highest order, on the basis of the element verification exercise detailed in Chapter Three it can be assumed that the results of a general analysis will provide results of 'engineering accuracy'.

7.2 The Finite Element Analysis.

The shell element analysis of the Model 273 Reverse Duct was a most interesting project, and has produced results which seem acceptable to both the analyst, and the company involved, C.W.F. Hamilton Ltd.

The Model 273 Reverse Duct, when used for a 'crash–stop' from 25 knots, is stressed to the limits of the design, and the material. However, as this extreme loading occurs only rarely in service, the reverse duct is generally operating with a reasonable degree of safety, as evidenced by the successful service record thus far.

The re–analysis of the reverse duct, with the thickness increased in the highest stress areas succeeded in decreasing these stresses by up to 50 % for individual cases, an average reduction in the Hencky–Von–Mises stress being 36 %.

If any re–design of the duct is being contemplated, areas of interest, (or highest stress), are around the junction of the reverse duct arms and the actual ducts. The other main region of high stress was on the upper curved surface of the ducting, (not the splashguard).

7.3 Further Research Directions.

Further avenues of research that could be continued on from this project can be divided into two main areas.

1. Improving the accuracy of the finite element analysis, and

2. Verifying the results obtained by the analysis.

7.3.1 Improving the Accuracy of the Finite Element Model.

Probably the simplest method to improve the accuracy of the finite element analysis would be to re–analyse the shell element model using another finite element processor or solver, such as ANSYS, or MSC/NASTRAN. This can be simply done if these "third–party" solvers are loaded onto the Intergraph workstation in conjunction with the I/FEM program, or a "neutral" file in the PATRAN format can be exported from I/FEM, and imported into these programs to be analysed. These processors have more sophisticated shell elements available, and will give more accurate results than the Intergraph I/FEM processor.

More accurate representation of the reverse duct geometry is another area in which improvements in accuracy can be made. A solid model of the reverse duct, in which the geometry should be exact, could be analysed or else 'substructuring' could be utilised. Two options are available for substructuring, a small part of the model can be refined using shell elements (higher order elements if required), have appropriate boundary conditions, displacements and rotations applied to simulate the rest of the model, and be re–analysed, or else solid elements could be used, if again the appropriate boundary conditions, displacements and rotations are calculated and applied.

Other measures that could be taken in an effort to model the reverse duct more accurately involve modelling, or measuring the pressure distribution and fluid flow over the inner surface of the reverse duct, and using the results from the analysis in the application of the pressures in the finite element analysis.

7.3.2 Verifying the Finite Element Analysis Results.

The easiest method of verifying the accuracy of the finite element analysis, would be to strain–gauge the reverse duct under the given test conditions. C.W.F. Hamilton Ltd. would have liked to have seen some strain–gauging results, but as funding was not forthcoming, no further research was able to be undertaken.

A simpler method of verification, apart from actual strain–gauge testing of the reverse duct on the test boat, would be to apply a specified load to the reverse duct in a test rig, and then to model this load on the shell element model of the reverse duct. The advantage of this method, apart from the conveience aspects, are that the strain gauges will be tested in a more controlled environment, possibly giving more reliable results.

References

[1] J. Archer. Consistent mass matrix for distributed mass systems. *Journal of the Structural Division, ASCE*, 89(ST4):161–178, 1963.

[2] J. H. Argyris. *Energy Theorems and Structural Analysis.* Butterworths, 1960.

[3] J.H. Argyris and D.W. Scharpf. The SHEBA family of shell elements for the matrix displacement method. *Journal of the Royal Aeronautical Society*, 72:873–883, 1968.

[4] D. G. Ashwell and R. H. Gallagher, editors. *Finite Element Analysis for Thin Shells and Curved Members.*, University College, Cardiff, Wales, 1974, 1976. John Wiley and Sons; London.

[5] R. J. Astley. *Finite Elements in Solids and Structures : An Introduction.* Chapman and Hall., London, 1992.

[6] R.J. Astley and W. Eversman. A note on the utility of a wave envelope approach in finite element duct transmission studies. *Journal of Sound and Vibration*, 76:595–601, 1981.

[7] J. Barlow. Optimal stress locations in finite element models. *International Journal for Numerical Methods in Engineering*, 10(2):243–251, 1974.

[8] J.-L. Batoz. An explicit formulation for an efficient triangular plate–bending element. *International Journal for Numerical Methods in Engineering*, 18:1077–1089, 1982.

[9] J.-L. Batoz and G. Dhatt. Development of two simple shell elements. *Journal A.I.A.A.*, 10(2):237–238, February 1972.

[10] J.-L. Batoz and M. B. Tahar. Evaluation of a new quadrilateral thin plate bending element. *International Journal for Numerical Methods in Engineering*, 18:1655–1677, 1982.

[11] P.G. Bergan and M.K. Nygard. Finite elements with increased freedom in choosing shape functions. *International Journal for Numerical Methods in Engineering*, 20:643–663, 1984.

[12] P.G. Bergan and X. Wang. Quadrilateral plate bending elements with shear deformation. *Computers and Structures*, 19(1/2):25–34, 1984.

[13] P. Bettess and O.C. Zienkiewicz. Diffraction and refraction of surface waves using finite and infinite elements. *International Journal for Numerical Methods in Engineering*, 11:1271–1290, 1977.

[14] N. Bicanic and E. Hinton. Spurious modes in two–dimensional isoparametric elements. *International Journal for Numerical Methods in Engineering*, 14:1545–1557, 1979.

[15] D. S. Burnett. *Finite Element Analysis: From Concepts to Applications.* Addison Wesley Publishing Co., Reading, Mass., 1988.

[16] D. Bushnell. Computerized analysis of shells–Governing equations. *Computers and Structures*, 18(3):471–536, 1984.

[17] A. Carr. ENCI 622 – finite element analysis lecture notes., 1992.

[18] R. W. Clough and C. A. Felippa. A refined quadrilateral for the analysis of plate bending. In *Proc. (Second) Conf. on Matrix Methods in Struct. Mech.*, pages 399–440, Wright–Patterson Air Force Base, Dayton, Ohio, October 1968.

[19] R. W. Clough and C. P. Johnson. A finite element approximation for the analysis of thin shells. *International Journal of Solids and Sructures*, 4:43–60, 1968.

[20] R. W. Clough and J. Tocher. Finite element stiffness matrices for the analysis of plate bending. In *Proc. (First) Conf. on Matrix Methods in Struct. Mech.*, pages 66–80, Wright–Patterson Air Force Base, Dayton, Ohio, 1965.

[21] R.W. Clough. The finite element in plane stress analysis. In *Proc. 2nd ASCE Conf. on Electronic Computation*, pages 345–378, Pittsburgh, Pa., 1960.

[22] R. D. Cook. *Concepts and Applications of Finite Element Analysis.* John Wiley and Sons, New York, third edition, 1989.

[23] R. Courant. Variational methods for the solution of problems of equilibrium and vibration. *Bulletin of the American Mathematics Society*, 49:1–23, 1943.

[24] G. S. Dhatt. Numerical analysis of thin shells by curved triangular elements based on Discrete–Kirchoff hypothesis. In W. H. Rowan Jr. and R. M. Hackett, editors, *Symposium on Application of Finite Element Methods in Civil Engineering*, pages 255–278, Vanderbilt University, Nashville, Tennessee, November 1969.

[25] G. S. Dhatt. An efficient triangular shell element. *Journal A.I.A.A.*, 8(11):2100–2102, November 1970.

[26] E.M. Salonen E. Hinton and N. Bicanic. A study of locking phenomena in isoparametric elements. In *Third MAFELAP Conference*, number 37, Brunel University, Uxbridge, 1978.

[27] R.L. Fox F.K. Bogner and L.A. Schmit. The generation of interelement, compatible stiffness and mass matrices by the use of interpolation formulas. In J. S. Przemieniecki et.al, editor, *Conference on Matrix Methods in Structural Mechanics.*, Wright Patterson Air Force Base, Dayton, Ohio, November 1965. NTIS, Springfield, Virginia.

[28] W. Flugge. *Stresses in Shells.* Springer-Verlag, Berlin, second edition, 1973.

[29] B. Fraejis de Veubeke. A conforming finite element for plate bending. *International Journal of Solids and Sructures*, 4(1):95–108, 1968.

[30] B. Fraejis de Veubeke. An equilibrium model finite element for plate bending. *International Journal of Solids and Sructures*, 4(3):447–468, 1968.

[31] D. T. Oden G. A. Wempner and D. A. Kross. Finite element analysis of thin shells. *Journal of the Structural Division, ASCE*, EM6:1273–1294, December 1968.

[32] M. H. Schultz G. Birkhoff and R.S. Varga. Piecewise hermite interpolation in one and two variables with applications to partial differential equations. *Numer. Math.*, 11:232–256, 1968.

[33] R. H. Gallagher. *Finite Element Analysis : Fundamentals.* Prentice–Hall, Inc., Englewood Cliffs, New Jersey, 1975.

[34] R.H. Gallagher. Analysis of plate and shell structures. In W. H. Rowan Jr and R. M. Hackett, editors, *Symposium on Application of Finite Element Methods in Civil Engineering*, pages 155–205, Vanderbilt University, Nashville, Tennessee, November 1969.

[35] B. M. Irons G.P. Bazeley, Y. K. Cheung and O. C. Zienkiewicz. Triangular elements in bending-conforming and non-conforming solutions. In *Proceedings of the Conference on Matrix Methods in Structural Mechanics*, pages 547–576, Wright Patterson Air Force Base, Dayton, Ohio, 1965.

[36] P. E. Grafton and D. R. Strome. Analysis of axisymmetrical shells by the direct stiffness method. *Journal A.I.A.A.*, 1:2342–2347, 1963.

[37] J. G. Greenstadt. On the reduction of continuous problems to discrete form. *IBM Journal Res. Develop.*, 3:355–368, 1959.

[38] R.T. Haftka and J.C. Robinson. Effect of out-of-planeness of membrane quadrilateral finite elements. *Journal A.I.A.A.*, 11(4):742–744, May 1973.

[39] E. Hinton and N. Bicanic. A comparison of Lagrange and Serendipity Mindlin plate elements for free vibration analysis. *Computers and Structures*, 10:483–493, 1979.

[40] E. Hinton and J.S. Campbell. Local and global smoothing of discontinuous finite element functions using a least squares method. *International Journal for Numerical Methods in Engineering*, 8(3):461–480, 1974.

[41] E. Hinton and H.C. Huang. A family of quadrilateral Mindlin plate elements with substitute shear strain fields. *Computers and Structures*, 23(3):409–431, 1986.

[42] M. M. Hrabok and T. M. Hrudey. A review and catalogue of plate bending finite elements. *Computers and Structures*, 19(3):479–495, 1984.

[43] A. Hrennikoff. Solution to problems in elasticity by the framework method. *ASME Journal of Applied Mechanics*, 8(4):A169–A175, 1941.

[44] T. J. R. Hughes and M. Cohen. The 'heterosis' finite element for plate bending. *Computers and Structures*, 9:445–450, 1978.

[45] T. J. R. Hughes and T. E. Tezduyar. Finite elements based upon Mindlin plate theory with particular reference to the four–node bilinear isoparametric element. *ASME Journal of Applied Mechanics*, 48:587–596, September 1981.

[46] S. Idelsohn. On the use of deep, shallow or flat shell finite elements for the analysis of thin shell structures. *Computer Methods in Applied Mechanics and Engineering*, 26:321–330, 1981.

[47] B. M. Irons. The Semi–Loof shell element. In D. G. Ashwell and R. H. Gallagher, editors, *Finite Element Analysis for Thin Shells and Curved Members.*, pages 197–222, London, 1976. John Wiley and Sons; London.

[48] B. M. Irons and S. H. Ahmad. *Techniques of Finite elements.* Wiley, New York, 1980.

[49] B. M. Irons and K. J. Draper. Inadequacy of nodal connections in a stiffness solution for plate bending. *Journal A.I.A.A.*, 3(5):961, May 1965.

[50] P. R. Tisdale J. A. Stricklin, W. E. Haisler and R. Gunderson. A rapidly converging triangular plate element. *Journal A.I.A.A.*, 7(1):180–181, January 1970.

[51] J. M. Gasiorek J. F. Douglas and J. A. Swaffield. *Fluid Mechanics.* Longman Scientific and Technical, England, second edition, 1985.

[52] K-J. Bathe J-L. Batoz and W. L. Ho. A study of three-noded triangular plate bending elements. *International Journal for Numerical Methods in Engineering*, 15:1771–1812, September 1980.

[53] R.E. Fulton J.E. Walz and N.J. Cyrus. Accuracy and convergence of finite element approximations. In J. S. Przemieniecki et.al, editor, *Conference on Matrix Methods in Structural Mechanics.*, pages 995–1027, Wright Patterson Air Force Base, Dayton, Ohio, October 1968. NTIS, Springfield, Virginia.

[54] C. Jeyachandrabose and C. Ramesh Babu. An alternative explicit formulation for the DKT plate-bending element. *International Journal for Numerical Methods in Engineering*, 21:1289–1293, 1985.

[55] C. Jeyachandrabose and C. Ramesh Babu. Short communication: Least squares strain smoothing for the eight-node Serendipity plane stress element. *International Journal for Numerical Methods in Engineering*, 21:1164–1166, 1985.

[56] B.M. Irons J.G. Ergatoudis and O.C. Zienkiewicz. Curved isoparametric, quadrilateral elements for finite element analysis. *International Journal of Solids and Sructures*, 4:31–43, 1968.

[57] J. Jirousek and A. Bouberguig. A contribution to evaluation of shear forces and reactions of Mindlin plates by using isoparametric elements. *Computers and Structures*, 19(5/6):793–800, 1984.

[58] R. E. Jones. A generalization of the direct stiffness method of structural analysis. *Journal A.I.A.A.*, 2:821–826, 1964.

[59] H. Kardestuncer and D. H. Norrie, editors. *Finite Element Handbook.* McGraw-Hill Book Co., 1987.

[60] H. A. Koenig and N. Davids. The damped transient behaviour of finite beams and plates. *International Journal for Numerical Methods in Engineering*, 1:151–162, 1969.

[61] H. Kraus. *Thin Elastic Shells.* John Wiley and Sons Inc., New York, London, Sydney, 1967.

[62] C.W.F. Hamilton Ltd. 273 reverse duct drawings, 1991.

[63] C.W.F. Hamilton Ltd. Draft reverse duct standard, 1992.

[64] H. C. Martin M. J. Turner, E. H. Dill and R. J. Melosh. Large deflections of structures subjected to heating and external loads. *Journal of Aeronautical Science*, 23:97–107, 1960.

[65] H. C. Martin M. J. Turner, R.W. Clough and L. J. Topp. Stiffness and deflection analysis of complex structures. *Journal of the Aeronautical Sciences.*, 23:805–823, 1956.

[66] R. H. MacNeal. Derivation of element stress matrices by assumed strain distributions. *Nuclear Engineering and Design*, 70:3–12, 1982.

[67] R. H MacNeal. A theorem regarding the locking of four–noded membrane elements. *International Journal for Numerical Methods in Engineering*, 24:1793–1799, 1987.

[68] R. H MacNeal and R. L. Harder. A proposed standard set of problems to test finite element accuracy. *Finite Elements in Analysis and Design*, 1:3–20, 1985.

[69] R. H MacNeal and R. L. Harder. Eight nodes or nine? *International Journal for Numerical Methods in Engineering*, 33:1049–1058, 1992.

[70] D. McHenry. A lattice analogy for the solution of plane stress problems. *Journal of the Institute of Civil Engineering*, 21:59–83, 1943.

[71] R. J. Melosh. Basis for derivation of matrices for the direct stiffness method. *Journal A.I.A.A.*, 1:1631–1637, 1963.

[72] L. S. D. Morley and A. J. Morris. Conflict between finite elements and shell theory. In J. Robinson, editor, *Finite Element Methods in the Commercial Environment*, volume 2, pages 531–562, Bournemouth, U.K., 1978.

[73] A. J. Morris. A deficiency in current finite elements for thin shell applications. *International Journal of Solids and Sructures*, 9:331–346, 1973.

[74] S. S. Murthy and R. H. Gallagher. Patch test verification of a triangular thin shell element based on Discrete Kirchoff theory. *Communications in Applied Numerical Methods*, 3:83–88, 1987.

[75] H. Stolarski N. Carpenter and T. Belytschko. A flat triangular shell element with improved membrane interpolation. *Communications in Applied Numerical Methods*, 1:161–168, 1986.

[76] H. Stolarski N. Carpenter and T. Belytschko. Improvements in 3-node triangular shell elements. *International Journal for Numerical Methods in Engineering*, 23:1643–1667, 1986.

[77] N.M. Newmark. Numerical methods of analysis in bars, plates and elastic bodies. In L.E. Grinter, editor, *Numerical Methods in Analysis in Engineering*. Macmillan, 1949.

[78] B. M. Irons O. C. Zienkiewicz and B. Nath. Natural frequencies of complex, free or submerged structures by the finite element method. In *Proc. Symp. Vibration in Civil Engineering*, pages 83–93, 1966.

[79] J. Lyness O. C. Zienkiewicz and D. R. J. Owen. A numerical method of visco-elastic stress analysis. *International Journal of Mechanical Science*, 10:807–827, 1968.

[80] R. L. Taylor O. C. Zienkiewicz and J. M. Too. Reduced integration technique in general analysis of plates and shells. *International Journal for Numerical Methods in Engineering*, 3:275–290, 1971.

[81] J.T. Oden. The finite element in fluid mechanics. In J.T. Oden and E.R.A. Olivera, editors, *Lectures on Finite Element Method in Continuum Mechanics, 1970, Lisbon.*, pages 151–186, Huntsville, Alabama, 1973. University of Alabama Press.

[82] K.C. Park and D.L. Flaggs. A Fourier analysis of spurious mechanisms and locking in the finite element method. *Computer Methods in Applied Mechanics and Engineering*, 46:65–81, 1984.

[83] K.C. Park and D.L. Flaggs. An operational procedure for the symbolic analysis of the finite element method. *Computer Methods in Applied Mechanics and Engineering*, 42:37–46, 1984.

[84] K.C. Park and D.L. Flaggs. A symbolic Fourier synthesis of a one–point integrated quadrilateral plate element. *Computer Methods in Applied Mechanics and Engineering*, 46:203–236, 1985.

[85] S. F. Pawsey and R. W. Clough. Improved numerical integration of thick shell finite elements. *International Journal for Numerical Methods in Engineering*, 3:575–586, 1971.

[86] A. Peano. Conforming approximations for Kirchoff plates and shells. *International Journal for Numerical Methods in Engineering*, 14:1273–1291, 1979.

[87] G. Prathap and G.R. Bhashyam. Reduced integration and the shear flexible beam element. *International Journal for Numerical Methods in Engineering*, 18:195–210, 1982.

[88] P. J. Beresford R. L. Taylor and E. L. Wilson. A non-conforming element for stress analysis. *International Journal for Numerical Methods in Engineering*, 10:1211–1219, 1976.

[89] A. Razzaque and B.M. Irons. Program for triangular bending elements with derivative smoothing. *International Journal for Numerical Methods in Engineering*, 6(3):333–343, 1973.

[90] J. Padlog R.H. Gallagher and P. P. Bijlaard. Stress ananlysis of heated complex shapes. *Journal of the American Rocket Society*, 32:700–707, 1962.

[91] B.M. Irons S. Ahmad and O.C. Zienkiewicz. Analysis of thick and thin shell structures by curved finite elements. *International Journal for Numerical Methods in Engineering*, 2:419–451, 1970.

[92] A. C. Scordelis and K. S. Lo. Computer analysis of cylindrical shells. *Journal of the American Concrete Institute*, 61:539–561, 1964.

[93] P. Seide. *Small Elastic Deformations of Thin Shells.* Noordhoff International Publishing ; NL, 1975.

[94] I. M. Smith and W. Duncan. The effectiveness of excessive nodal continuities in the finite element analysis of thin rectangular and skew plates in bending. *International Journal for Numerical Methods in Engineering*, 2:253–257, 1970.

[95] B. Specht. Modified shape functions for the three-node plate bending element passing the patch test. *International Journal for Numerical Methods in Engineering*, 26:705–715, 1988.

[96] B. A. Szabo and G. C. Lee. Derivation of stiffness matrices for problems in plane elasticity by Galerkin's method. *International Journal for Numerical Methods in Engineering*, 1:301–310, 1969.

[97] J. S.-J. Ong T. Belytschko, W.-K. Lau and D. Lam. Implementation and application of a 9–node Lagrange shell element with spurious mode control. *International Journal of Solids and Sructures*, 20:121–128, 1985.

[98] M. Cohen T. J. R. Hughes and M. Haroun. Reduced and selective integration techniques in the finite element analysis of plates. *Nuclear Engineering and Design*, 46:203–222, 1978.

[99] W. Kanoknukulchai T. J. R. Hughes, R. L. Taylor. A simple and efficient finite element for plate bending. *International Journal for Numerical Methods in Engineering*, 11:1529–1543, 1977.

[100] S. Timoshenko and S. Woinowsky-Krieger. *Theory of Plates and Shells.* McGraw-Hill Book Co., New York, second edition, 1959.

[101] H.F. Weinberger. Upper and lower bounds for eigenvalues by finite difference methods. *Communications in Pure and Applied Mathematics*, 9:613–623, 1956.

[102] G. Wempner. Finite elements, finite rotations and small strains of flexible shells. *International Journal of Solids and Sructures*, 5:117–153, 1969.

[103] D. W. White and J. F. Abel. Testing of shell finite element accuracy and robustness. *Finite Elements in Analysis and Design*, 6:129–151, 1989.

[104] O. C. Zienkiewicz. *The Finite Element Method*, volume 1. McGraw-Hill Book Company; London, fourth edition, 1988.

[105] O. C. Zienkiewicz. *The Finite Element Method*, volume 2. McGraw-Hill Book Company; London, fourth edition, 1991.

[106] O. C. Zienkiewicz and P. Bettess. Fluid structure dynamic interaction and wave forces. An introduction to numerical treatment. *International Journal for Numerical Methods in Engineering*, 13:1–16, 1978.

[107] M. Zlamal. On the finite element method. *Numer. Math.*, 12:395–409, 1968.

Appendix A

Element verification results

A.1 Results for rectangular plate

Table A.1: Results - Simply supported rectangular plate: uniform load.

(a) *Aspect Ratio = 1.0*

Number of node spaces per edge of model	Normalised lateral deflection at center	
	QUD	QD8
1	0.856	
2	0.984	0.894
3	0.996	
4	0.998	0.880
5	0.999	
6	1.000	0.888
7		
8	1.000	0.924
9		
10	1.000	0.965
11		
12	0.993	0.986
13		
14	0.995	0.994

(b) *Aspect Ratio = 5.0*

Number of node spaces per edge of model	Normalised lateral deflection at center	
	QUD	QD8
1	1.070	
2	1.096	1.372
3	1.048	
4	1.026	0.825
5	1.015	
6	1.078	0.868
7	1.007	
8	1.005	0.986
9	1.004	
10	1.003	1.050
11		
12	0.994	1.066
13		
14	0.995	1.059

Table A.2: Results - Simply supported rectangular plate: concentrated load.

(a) *Aspect Ratio = 1.0*

Number of node spaces per edge of model	Normalised lateral deflection at center	
	QUD	QD8
1	1.199	
2	1.077	0.998
3	1.040	
4	1.025	0.845
5	1.017	
6	1.013	0.795
7		
8	1.008	0.842
9		
10	1.006	0.918
11		
12	1.004	0.959
13		
14	1.003	0.976

(b) *Aspect Ratio = 5.0*

Number of node spaces per edge of model	Normalised lateral deflection at center	
	QUD	QD8
1	0.655	
2	0.676	1.013
3	0.709	
4	0.761	0.843
5	0.804	
6	0.838	0.820
7	0.864	
8	0.884	0.792
9	0.901	
10	0.914	0.749
11		
12	0.934	0.718
13		
14	0.947	0.718

Table A.3: Results - Clamped supported rectangular plate: uniform load.

(a) *Aspect Ratio = 1.0*

Number of node spaces per edge of model	Normalised lateral deflection at center	
	QUD	QD8
1	1.033	
2	1.109	1.240
3	1.061	
4	1.038	0.307
5	1.026	
6	1.020	0.164
7		
8	1.013	0.236
9		
10	1.010	0.484
11		
12	1.012	0.735
13		
14	0.998	0.878

(b) *Aspect Ratio = 5.0*

Number of node spaces per edge of model	Normalised lateral deflection at center	
	QUD	QD8
1	1.465	
2	1.511	1.494
3	1.127	
4	1.063	0.226
5	1.045	
6	1.037	0.156
7	1.032	
8	1.029	0.311
9	1.027	
10	1.025	0.702
11		
12	1.008	0.982
13		
14	1.011	1.063

Table A.4: Results - Clamped support rectangular plate: concentrated load.

(a) *Aspect Ratio = 1.0*

Number of node spaces per edge of model	Normalised lateral deflection at center	
	QUD	QD8
1	0.930	
2	1.088	1.116
3	1.059	
4	1.040	0.385
5	1.029	
6	1.022	0.223
7		
8	1.014	0.265
9		
10	1.011	0.481
11		
12	1.017	0.714
13		
14	1.007	0.854

(b) *Aspect Ratio = 5.0*

Number of node spaces per edge of model	Normalised lateral deflection at center	
	QUD	QD8
1	0.415	
2	0.516	0.423
3	0.624	
4	0.681	0.236
5	0.729	
6	0.769	0.167
7	0.801	
8	0.828	0.188
9	0.850	
10	0.868	0.291
11		
12	0.895	0.392
13		
14	0.915	0.474

A.2 Results for Scordelis-Lo roof

Table A.5: Results - Scordelis-Lo roof testcase.

Number of node spaces per edge of model	Normalised vertical deflection at midpoint of free edge	
	QUD	QD8
2	1.391	1.094
3	1.112	
4	1.052	1.023
5	1.029	
6	1.017	0.998
7	1.010	
8	1.005	0.974
9	1.001	
10	0.997	0.969

A.3 Results for spherical shell

Table A.6: Results - Hemisphere testcase.

Number of node spaces per edge of model	Normalised radial deflection at load point	
	QUD	QD8
2		1.124
3	1.007	
4	1.039	0.569
6	1.028	0.811
8	1.016	0.939
10	1.007	0.968
12	1.002	0.967
14	0.999	0.978
16	0.997	0.979
18	0.996	0.979
20	0.995	0.979

Appendix B

Force Calculation Spreadsheet Printout

Table B.1: Spreadsheet printout - Loadcase One.

JET UNIT AND FLUID DATA			
Jet Nozzle Diameter,	d =	0.145	(m)
Duct Efficiency Factor,	η =	0.80	
Fluid Density,	ρ =	1024.00	(kg/m^3)
Volumetric Flowrate,	Q =	0.489	(m^3/s)
DERIVED JET UNIT AND FLUID DATA			
Change(Duct Eff. Ftr)/step	=	0.20	
1 - (Change(D.E.F.) /step)	=	0.80	
Initial Fluid Velocity,	v_1 =	29.61	(m/s)
Outlet Velocity,	v_2 =	23.69	(m/s)
Mass Flowrate/side	m =	204.80	(kg/s)
FLUID ANGLE DATA			
Fluid Entry Angle,	Y_f =	0.00	$(^o)$
Duct Sweep Angle,	α =	135.00	$(^o)$
Duct Axis Angle,	β =	35.00	$(^o)$
Vert. Angle of Entry,	ϵ =	0.00	$(^o)$
Horiz. Angle of Entry,	γ =	12.00	$(^o)$
	ϕ_1 =	39.32	$(^o)$
	θ_1 =	29.84	$(^o)$
	ϕ_2 =	27.32	$(^o)$
	θ_2 =	26.54	$(^o)$
Vertical Discharge Angle,	θ =	26.54	$(^o)$
Horiz. Discharge Angle,	ϕ =	27.32	$(^o)$
Vertical Start Angle,	θ_{st} =	180.00	$(^o)$
True Vert. Discharge Angle,	θ_T =	17.82	$(^o)$
Vertical Angle Increment,	θ_{inc} =	17.82	$(^o)$
Horiz. Start Angle,	ϕ_{st} =	168.00	$(^o)$
Horiz. Angle Increment,	ϕ_{inc} =	140.68	$(^o)$

FORCE, VELOCITY AND ANGLE RESULTS

	Incremental Angle Changes				Velocity	
	θ_{m1}	ϕ_1	θ_{m2}	ϕ_2	V_1	V_2
CAA	180.0	168.00	162.2	27.30	29.61	23.69
CWFH	180.0	168.00	153.5	27.30	29.61	23.69

	Port Half Forces					Angles	
	Fx	Fy	Fz	Fr	θ_T '	θ'	ϕ'
CAA	12269	1050	1815	12447	8.4	9.5	-4.9
CWFH	12129	2354	-	12355	-	11.0	-

	Starboard Half Forces					Angles	
	Fx	Fy	Fz	Fr	θ_T '	θ'	ϕ'
CAA	12269	-1050	1815	12447	8.4	-9.5	-4.9
CWFH	12129	-2354	-	12355	-	-11.0	-

	Total Forces					Angles	
	Fx	Fy	Fz	Fr	θ_T '	θ'	ϕ'
CAA	24538	0	3630	24894	8.4	9.5	0
CWFH	24257	0	-	24710	-	0	-

Table B.2: Spreadsheet printout - Loadcase Three

JET UNIT AND FLUID DATA			
Jet Nozzle Diameter,	d =	0.145	(m)
Duct Efficiency Factor,	η =	0.80	
Fluid Density,	ρ =	1024.00	(kg/m^3)
Volumetric Flowrate,	Q =	0.489	(m^3/s)
DERIVED JET UNIT AND FLUID DATA			
Change(Duct Eff. Ftr)/step	=	0.20	
1 - (Change(D.E.F.) /step)	=	0.80	
Initial Fluid Velocity,	v_1 =	29.61	(m/s)
Outlet Velocity,	v_2 =	23.69	(m/s)
Mass Flowrate/side	m =	204.80	(kg/s)
FLUID ANGLE DATA			
Fluid Entry Angle,	Y_f =	30.00	$(^o)$
Duct Sweep Angle,	α =	135.00	$(^o)$
Duct Axis Angle,	β =	35.00	$(^o)$
Vert. Angle of Entry,	ϵ =	0.00	$(^o)$
Horiz. Angle of Entry,	γ =	12.00	$(^o)$
	ϕ_1 =	39.32	$(^o)$
	θ_1 =	29.84	$(^o)$
	ϕ_2 =	27.32	$(^o)$
	θ_2 =	26.54	$(^o)$
Vertical Discharge Angle,	θ =	26.54	$(^o)$
Horiz. Discharge Angle,	ϕ =	27.32	$(^o)$
Vertical Start Angle,	θ_{st} =	180.00	$(^o)$
True Vert. Discharge Angle,	θ_T =	17.82	$(^o)$
Vertical Angle Increment,	θ_{inc} =	17.82	$(^o)$
Horiz. Start Angle,	ϕ_{st} =	138.00	$(^o)$
Horiz. Angle Increment,	ϕ_{inc} =	110.68	$(^o)$

FORCE, VELOCITY AND ANGLE RESULTS

	Incremental Angle Changes				Velocity	
	θ_{m1}	ϕ_1	θ_{m2}	ϕ_2	V_1	V_2
CAA	180.0	168.00	162.2	27.30	29.61	23.69
CWFH	180.0	168.00	153.5	27.30	29.61	23.69

	Port Half Forces				Angles		
	Fx	Fy	Fz	Fr	θ_T '	θ'	ϕ'
CAA	21053	-4738	3630	21883	9.8	11.0	-12.7
CWFH	24257	4709	-	24710	-	11.0	-

Appendix C

LM-6M Aluminium Properties

The following are the aluminium properties assumed for this analysis of the 273 reverse duct.

Property	Value	Unit
Ultimate Stress, R_m	170	MPa
Thermal Coeff. of Linear Expansion	$20 * 10^6$	K^{-1}
Density @ 20°C	2.6898	g/cm^3
Modulus of Elasticity @ 20°C	71	GPa
Modulus of Torsion @ 20°C	25.5	GPa
Poissons Ratio	0.34	
Specific Gravity	2.65	
Fatigue Strength	51	MPa

Note: Fatigue Strength is for sand cast LM-6M alloy, under rotating cantilever beam test, $500 * 10^6$ cycles.

Appendix D

Plates from Initial Analysis of the Reverse Duct

The plates shown in this section are from the initial analysis of the reverse duct, as described in Chapter Five.

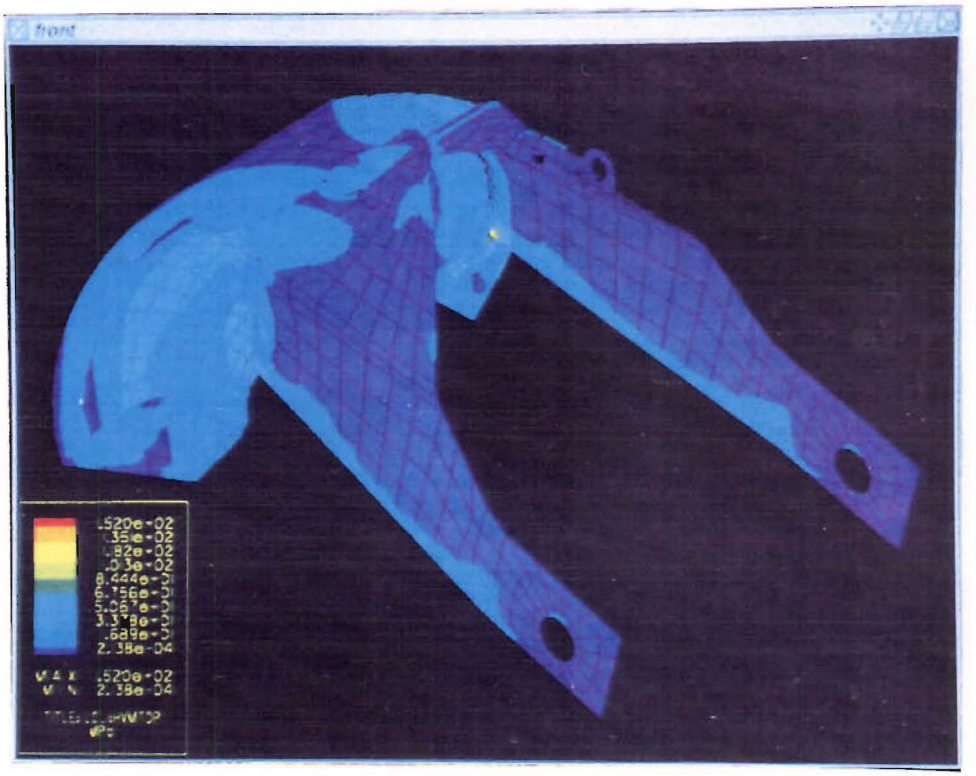

Figure D.1: 273 Reverse Duct; Isometric view–Loadcase One: HVMTOP stresses

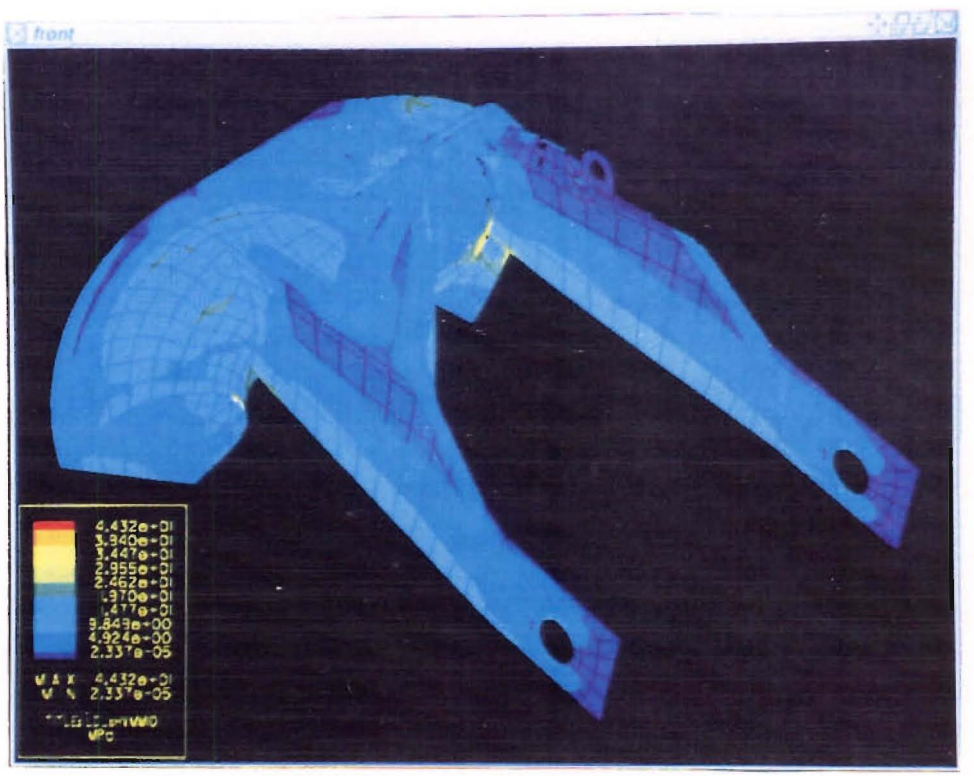

Figure D.2: 273 Reverse Duct; Isometric view–Loadcase One: HVMMID stresses

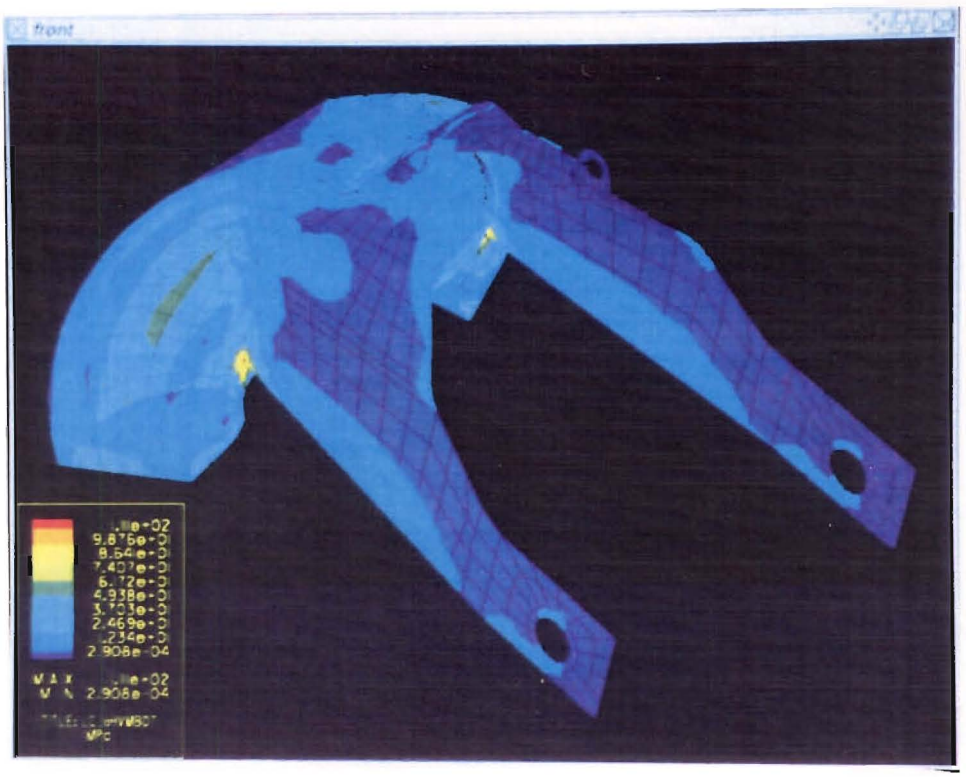

Figure D.3: 273 Reverse Duct; Isometric view–Loadcase One: HVMBOT stresses

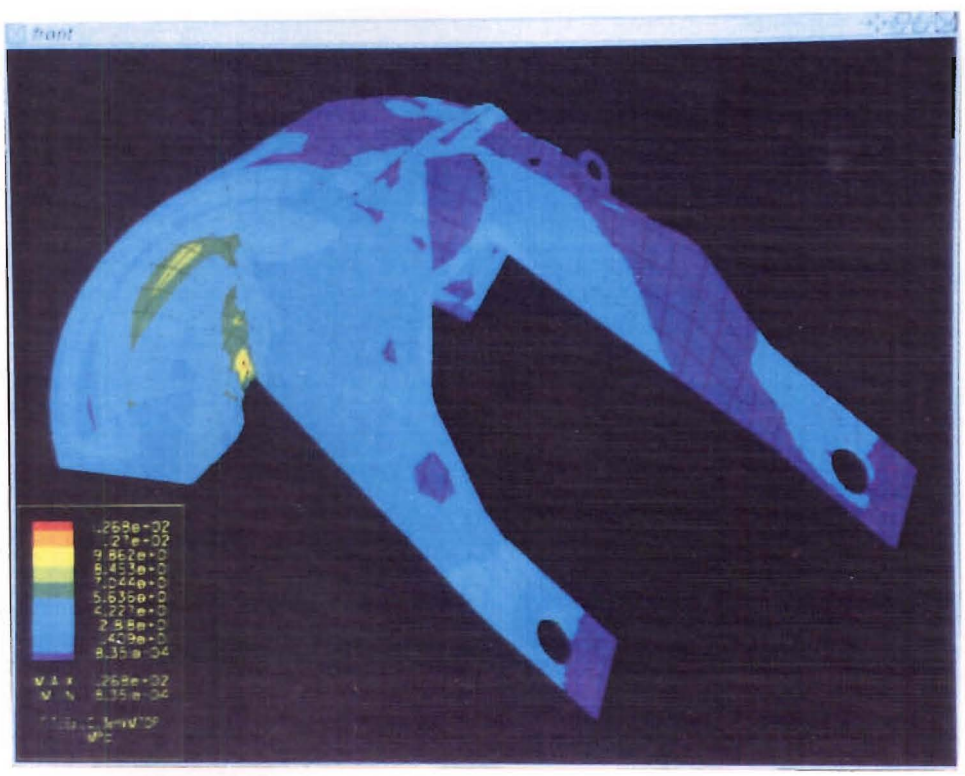

Figure D.4: 273 Reverse Duct; Isometric view–Loadcase Three: HVMTOP stresses

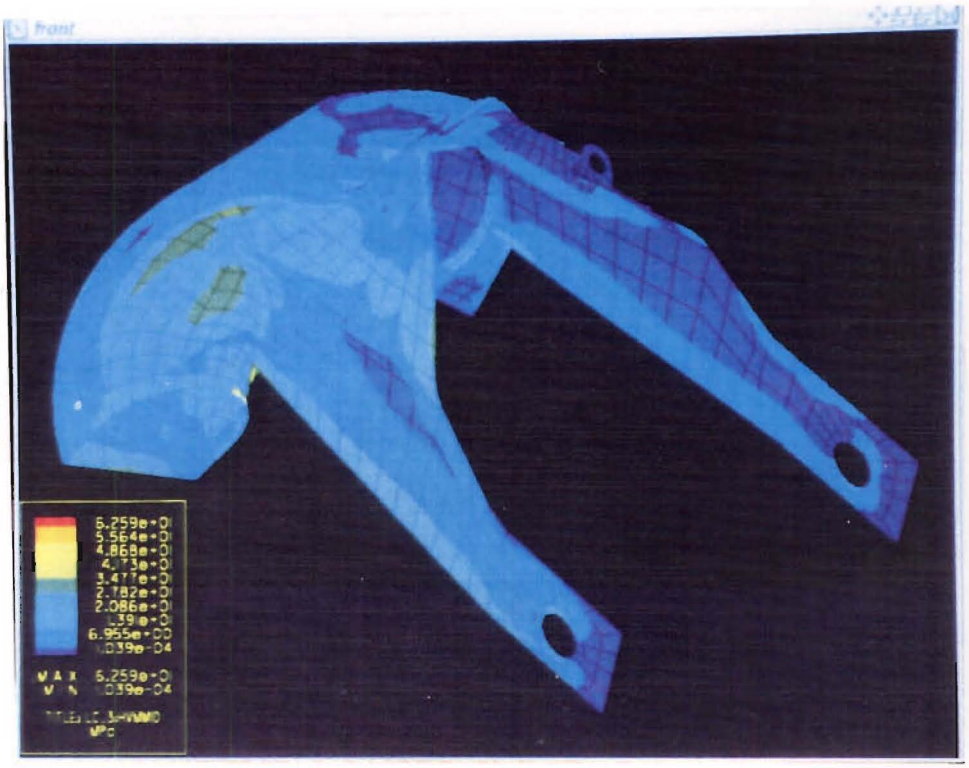

Figure D.5: 273 Reverse Duct; Isometric view–Loadcase Three: HVMMID stresses

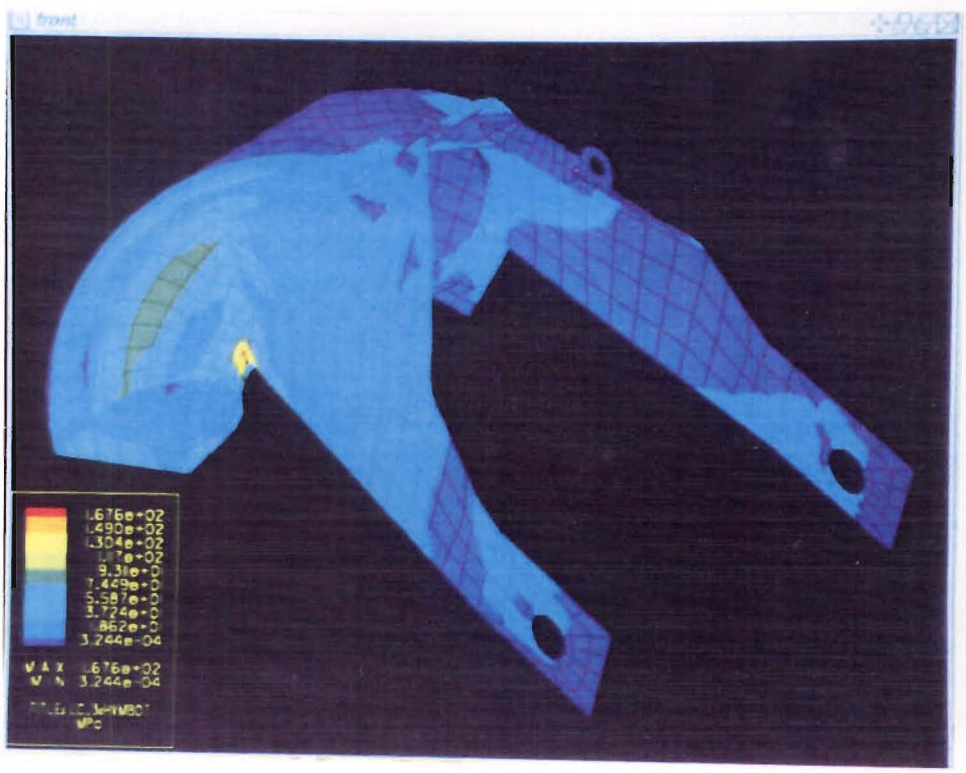

Figure D.6: 273 Reverse Duct; Isometric view–Loadcase Three: HVMBOT stresses

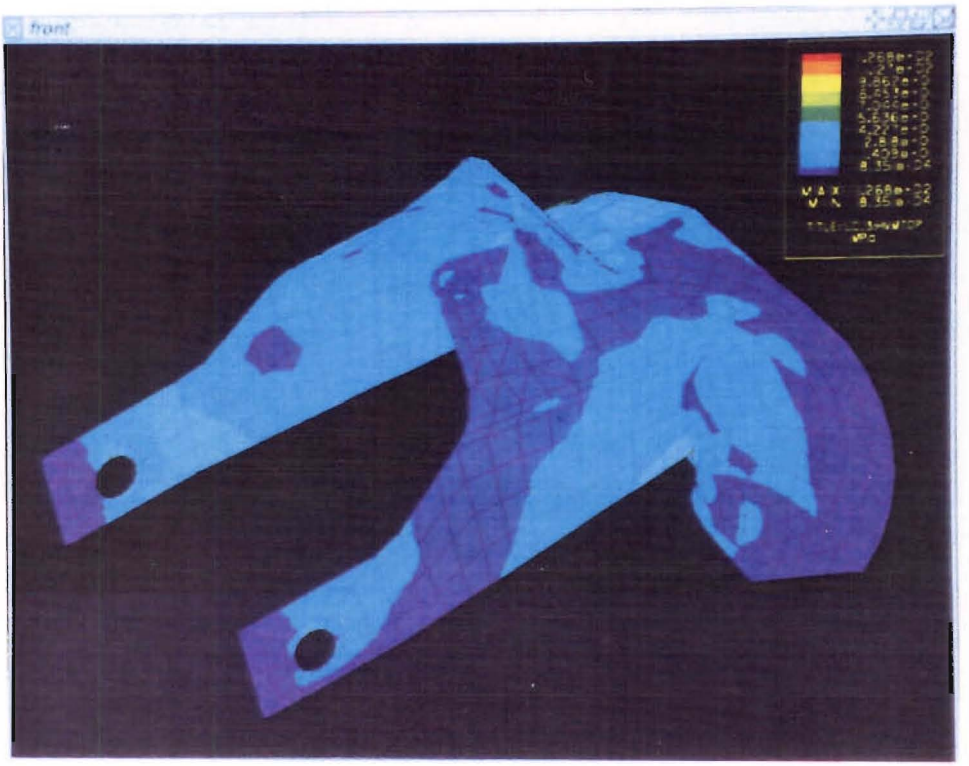

Figure D.7: 273 Reverse Duct; Alternate Isometric view–Loadcase Three: HVMTOP stresses

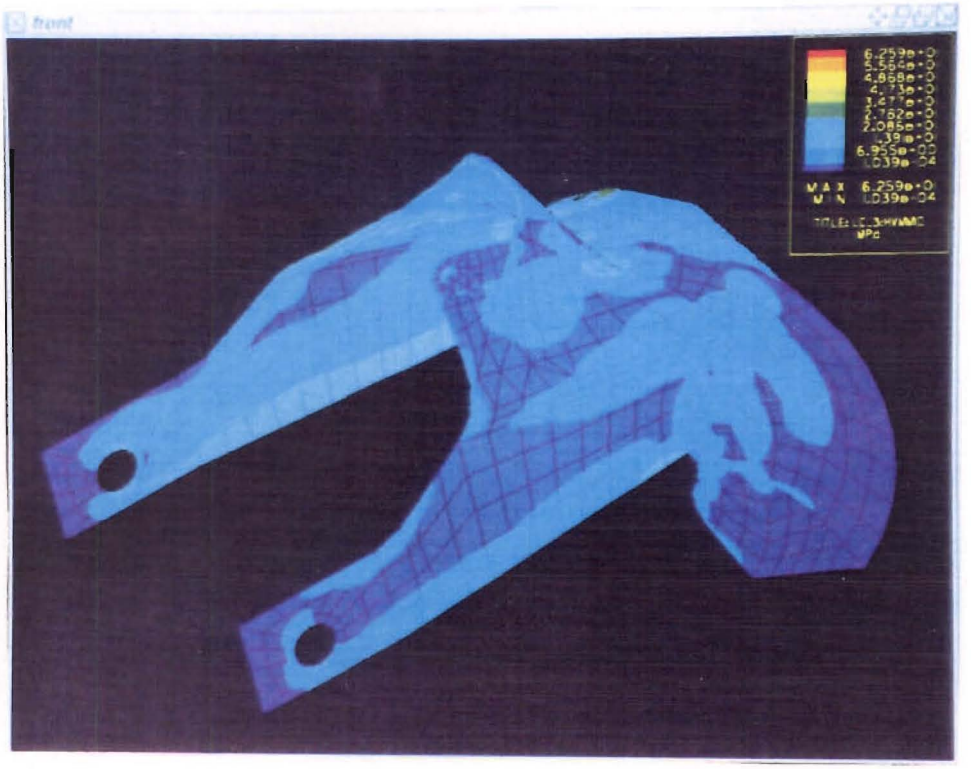

Figure D.8: 273 Reverse Duct; Alternate Isometric view–Loadcase Three: HVMMID stresses

Figure D.9: 273 Reverse Duct; Alternate Isometric view–Loadcase Three: HVMBOT stresses

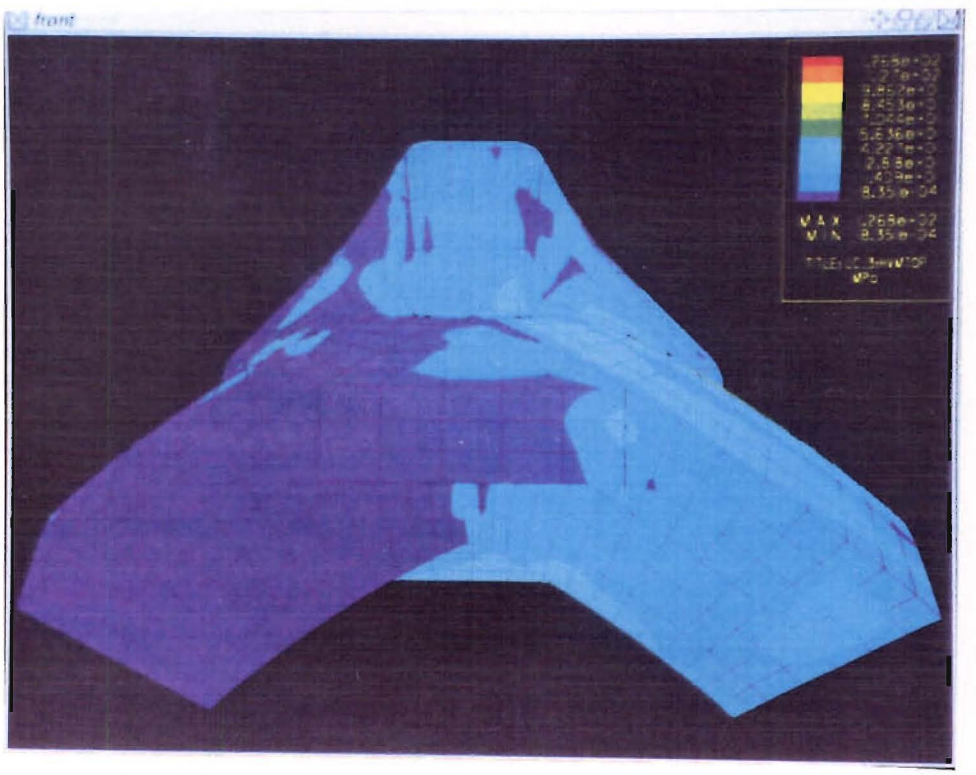

Figure D.10: 273 Reverse Duct; Rear View–Loadcase Three: HVMTOP stresses

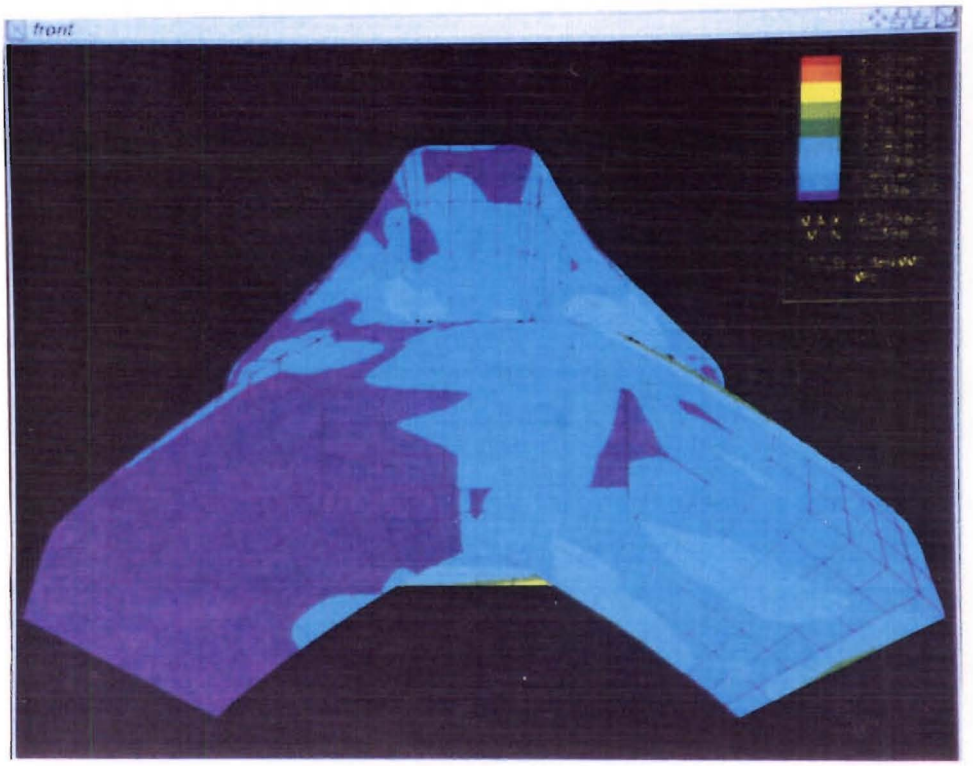

Figure D.11: 273 Reverse Duct; Rear View–Loadcase Three: HVMMID stresses

Figure D.12: 273 Reverse Duct; Rear View–Loadcase Three: HVMBOT stresses

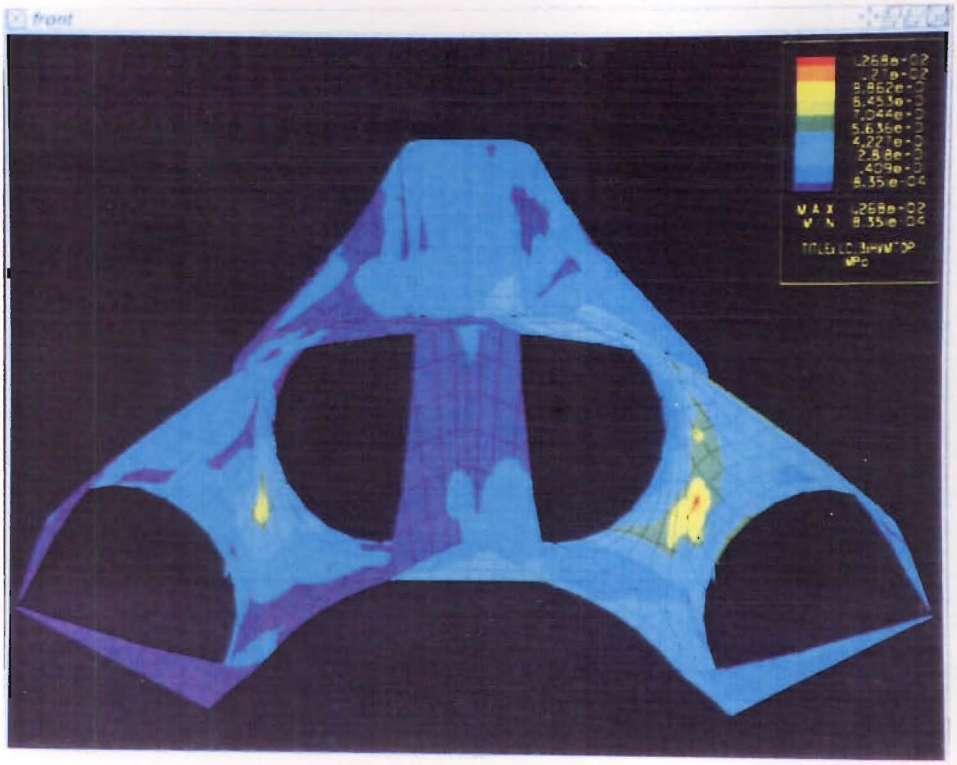

Figure D.13: 273 Reverse Duct; Cutaway rear view–Loadcase Three: HVMTOP stresses

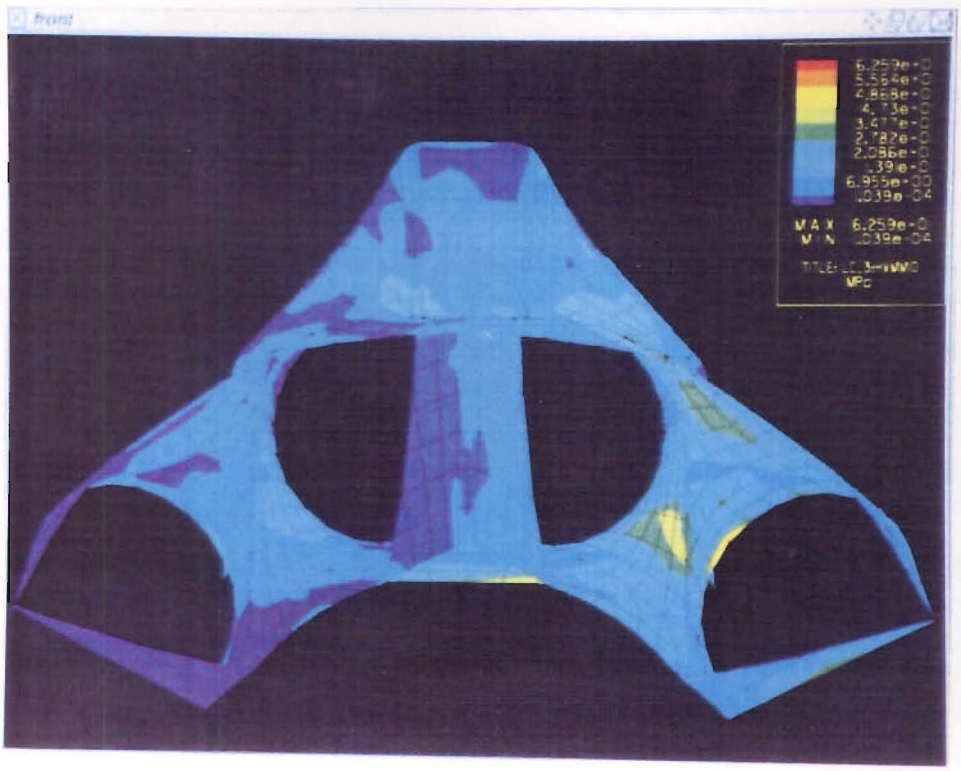

Figure D.14: 273 Reverse Duct; Cutaway rear view–Loadcase Three: HVMMID stresses

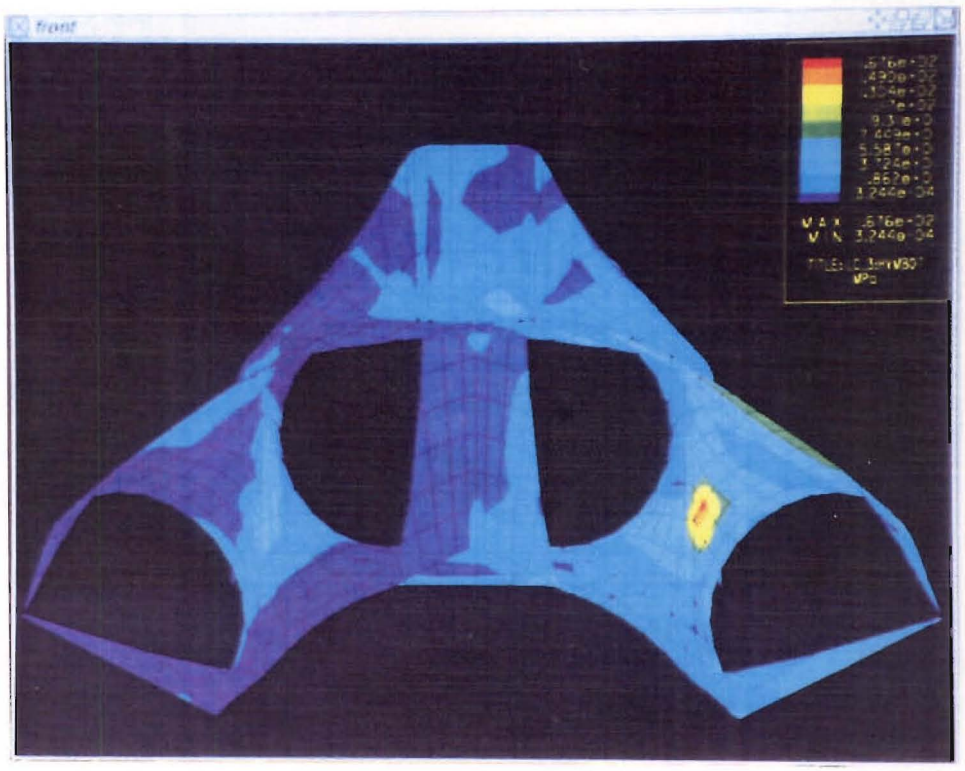

Figure D.15: 273 Reverse Duct; Cutaway rear view–Loadcase Three: HVMBOT stresses

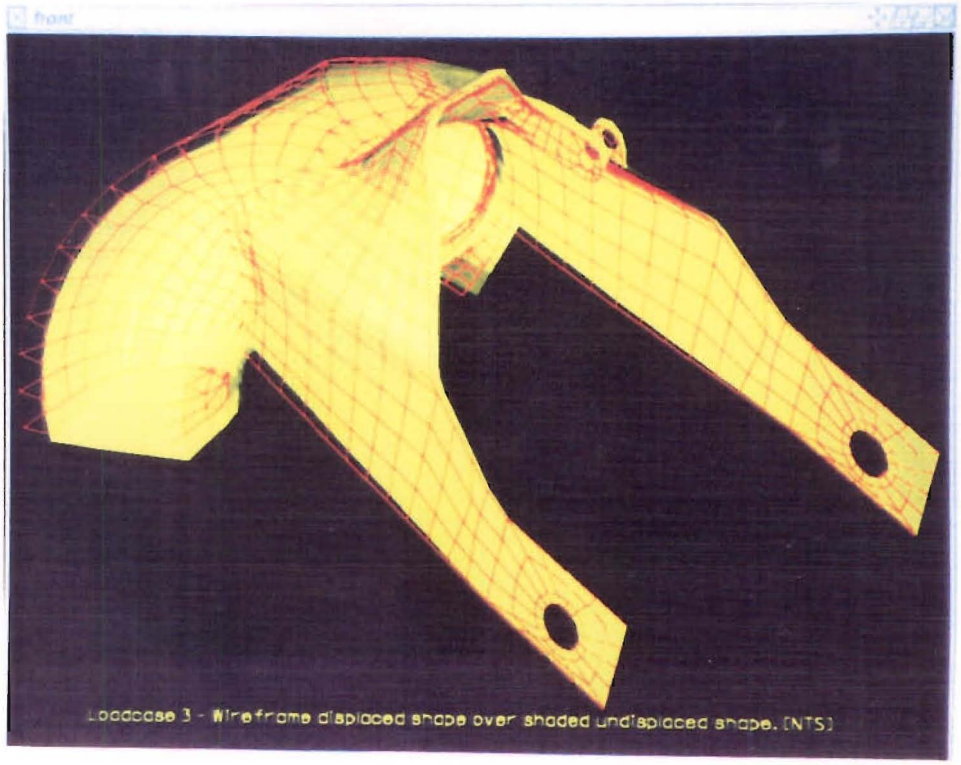

Figure D.16: Displaced shape of the 273 reverse duct–Loadcase Three

Appendix E

Plates from Analysis of the Modified Reverse Duct

The plates shown in this section are from the second analysis run of the reverse duct, that is the analysis of the reverse duct in which the thickness of the duct adjacent to the pivot arms had been doubled.

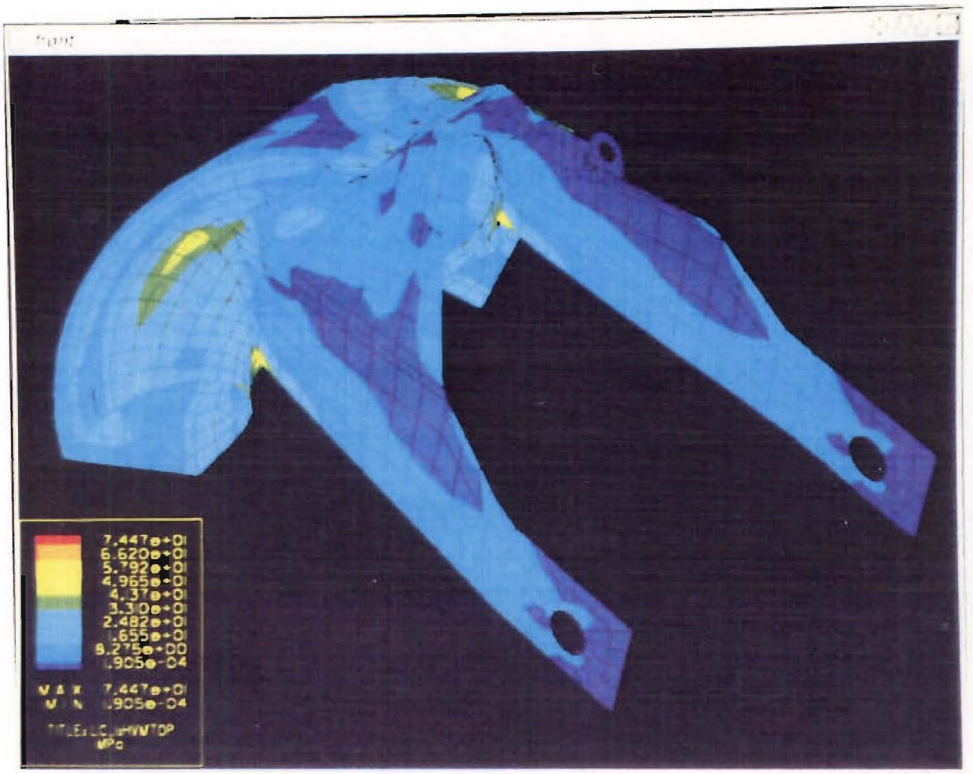

Figure E.1: 273 Reverse Duct; Isometric view–Loadcase One: HVMTOP stresses

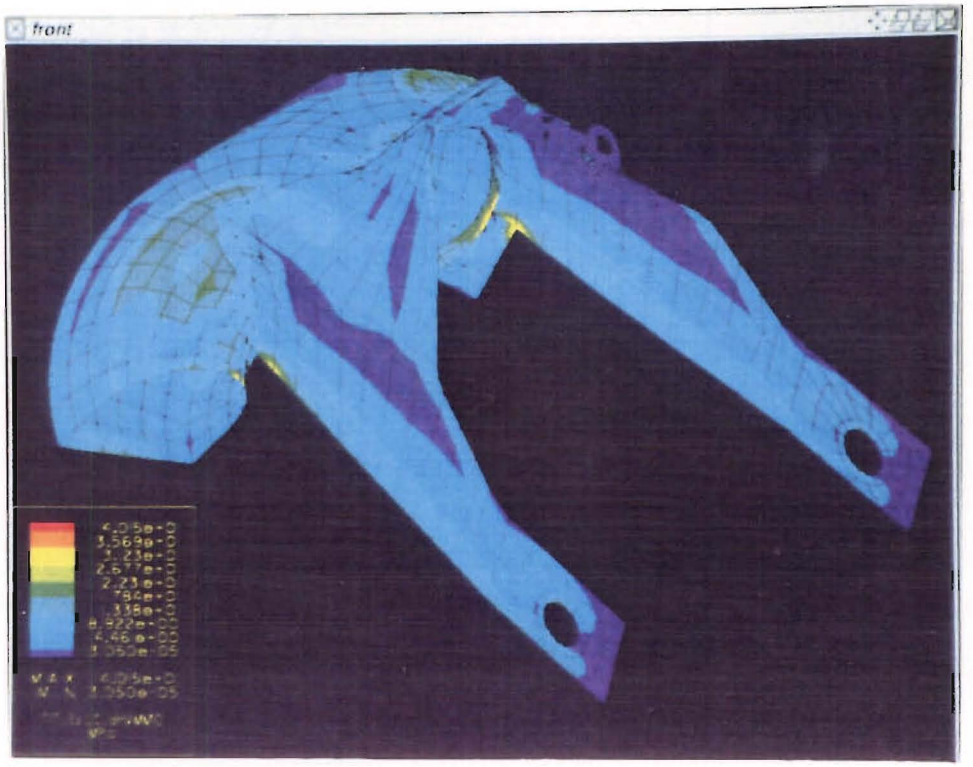

Figure E.2: 273 Reverse Duct; Isometric view–Loadcase One: HVMMID stresses

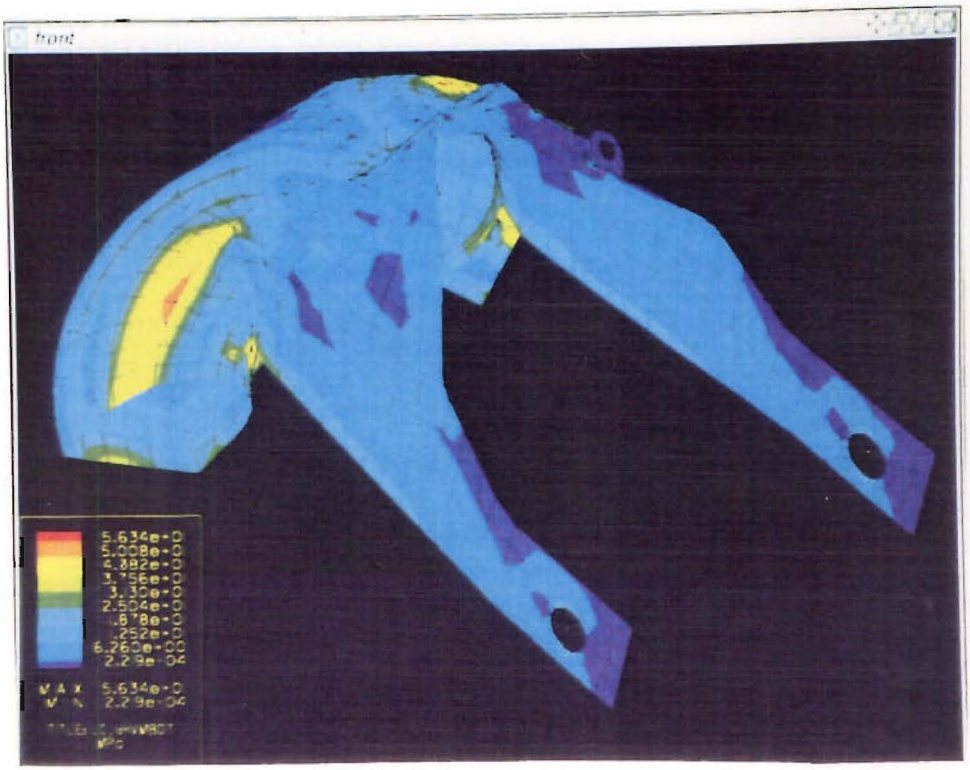

Figure E.3: 273 Reverse Duct; Isometric view–Loadcase One: HVMBOT stresses

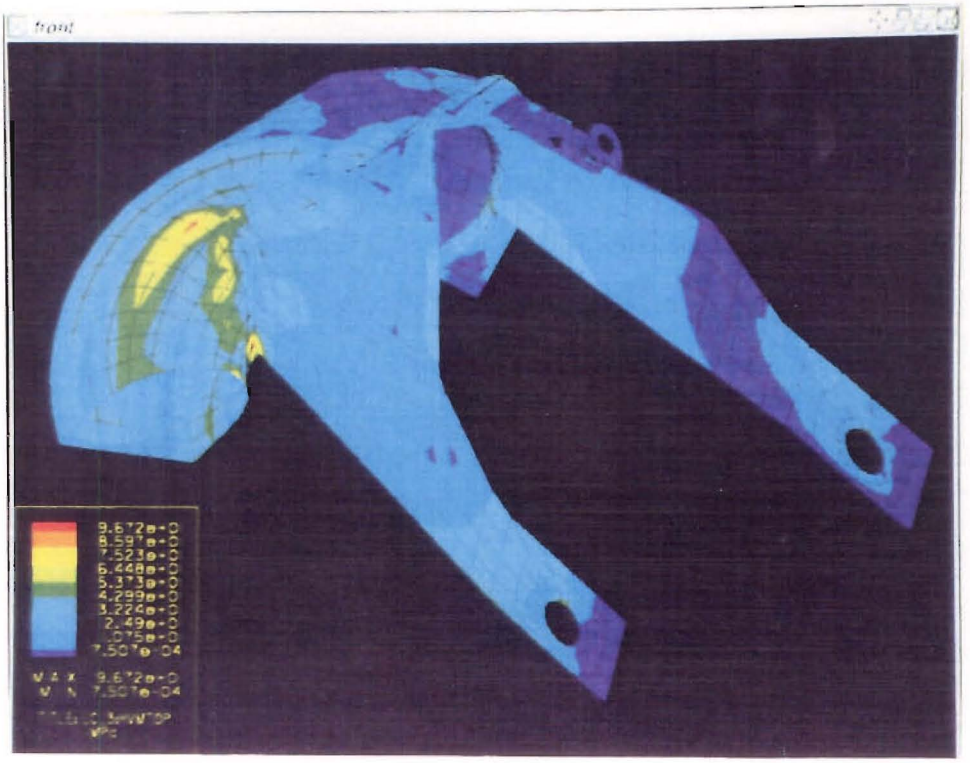

Figure E.4: 273 Reverse Duct; Isometric view–Loadcase Three: HVMTOP stresses

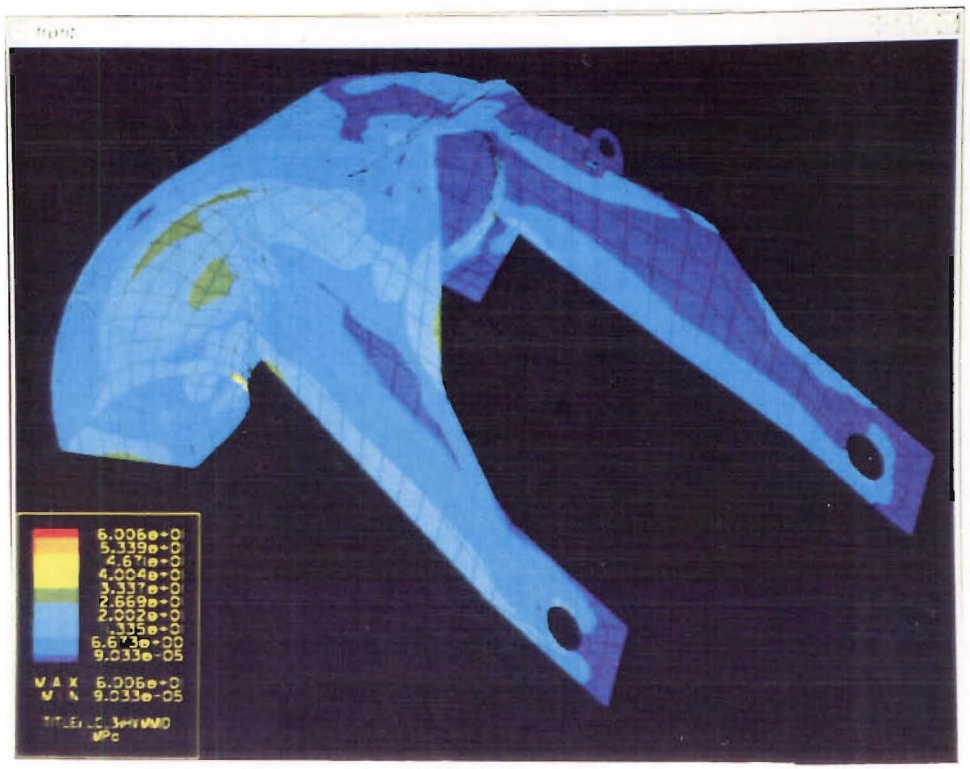

Figure E.5: 273 Reverse Duct; Isometric view–Loadcase Three: HVMMID stresses

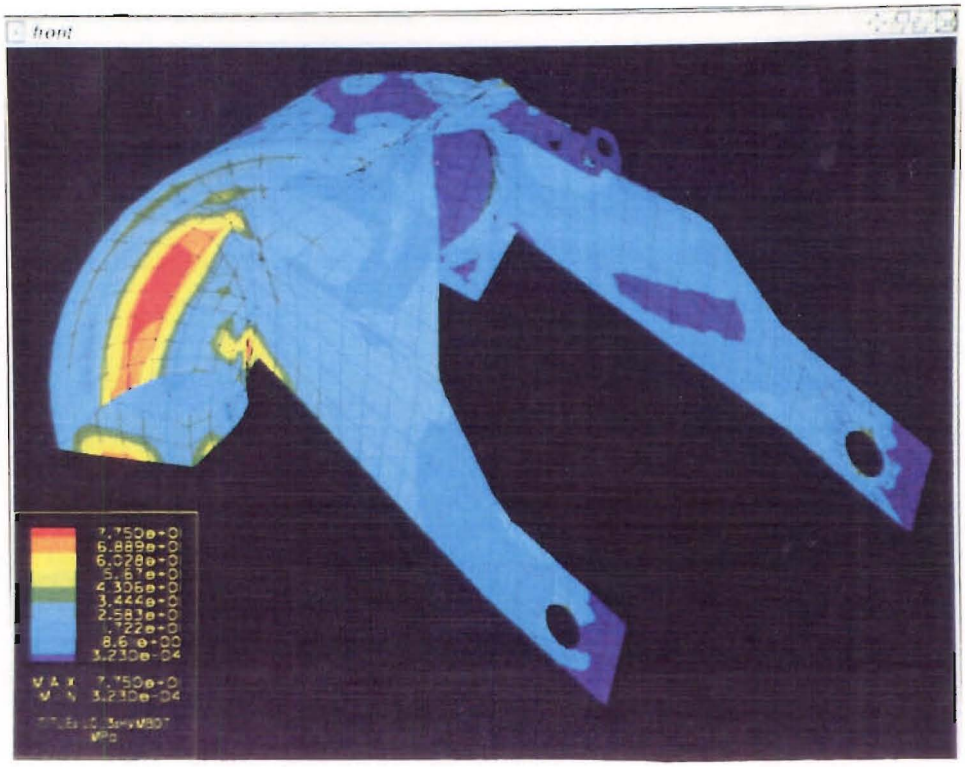

Figure E.6: 273 Reverse Duct; Isometric view–Loadcase Three: HVMBOT stresses

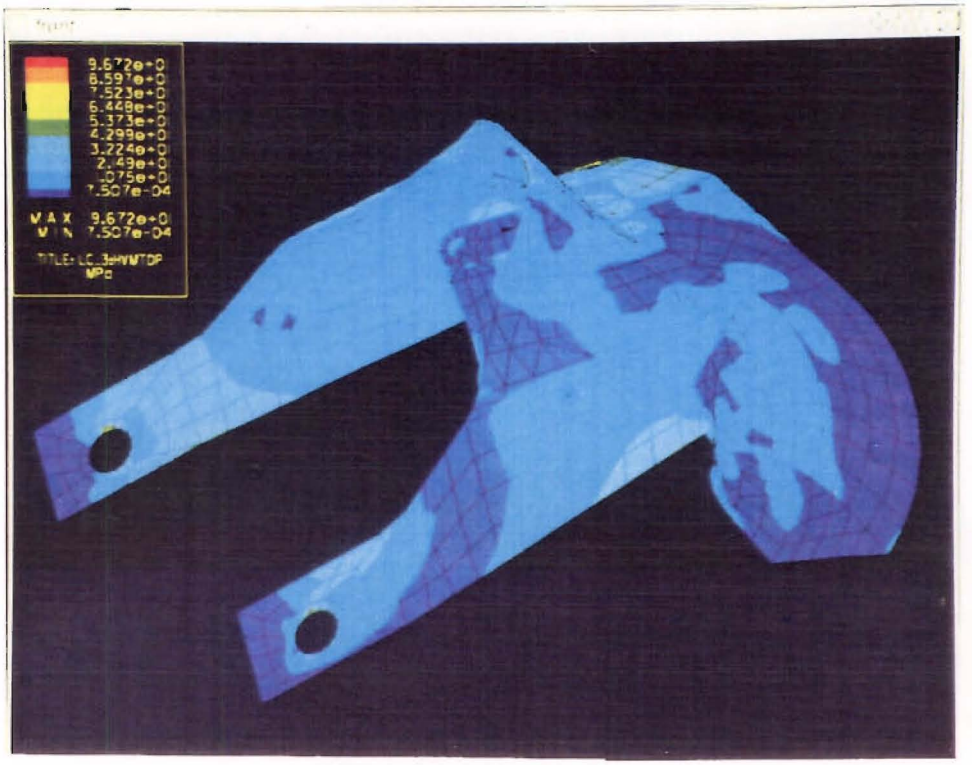

Figure E.7: 273 Reverse Duct; Alternate Isometric view–Loadcase Three: HVMTOP stresses

Figure E.8: 273 Reverse Duct; Alternate Isometric view–Loadcase Three: HVMMID stresses

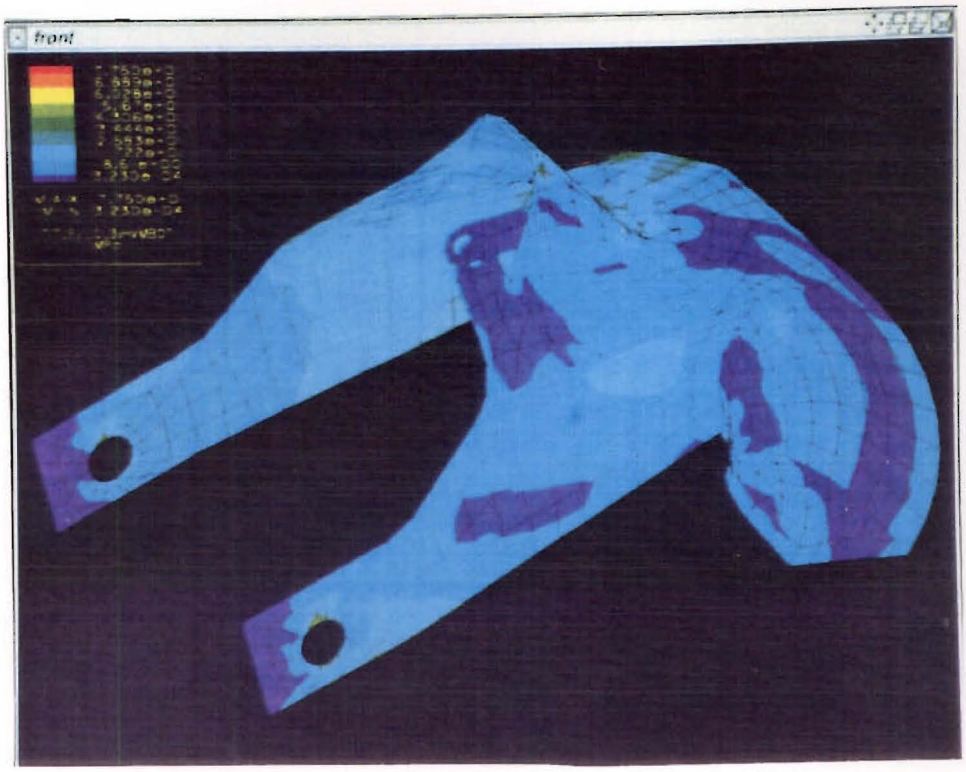

Figure E.9: 273 Reverse Duct; Alternate Isometric view–Loadcase Three: HVMBOT stresses

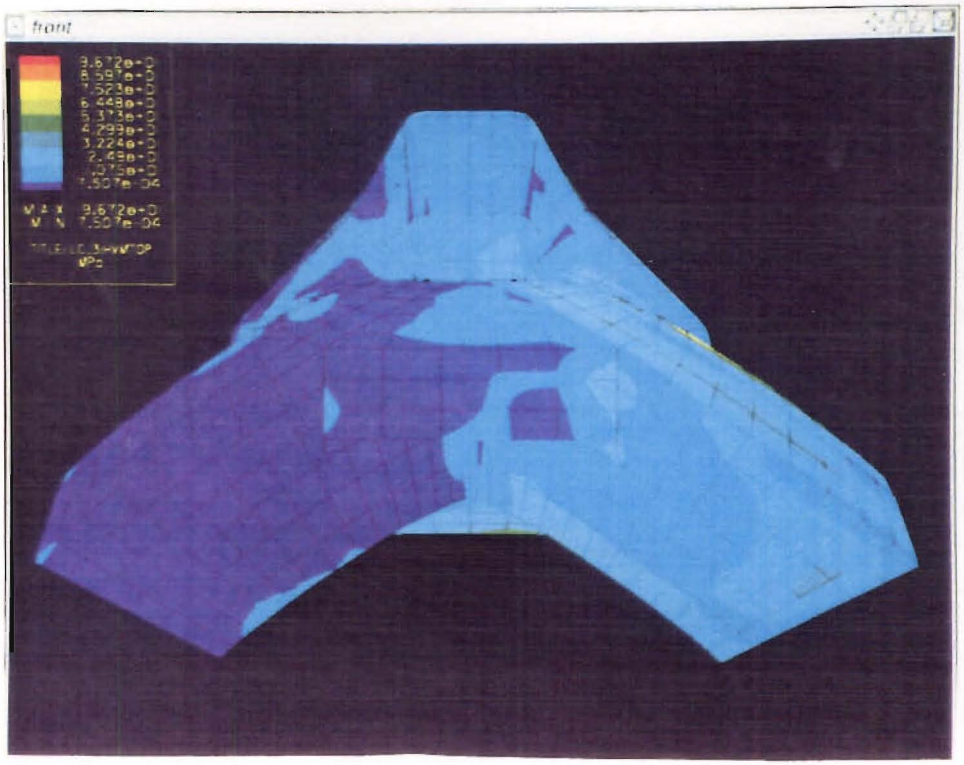

Figure E.10: 273 Reverse Duct; Rear View–Loadcase Three: HVMTOP stresses

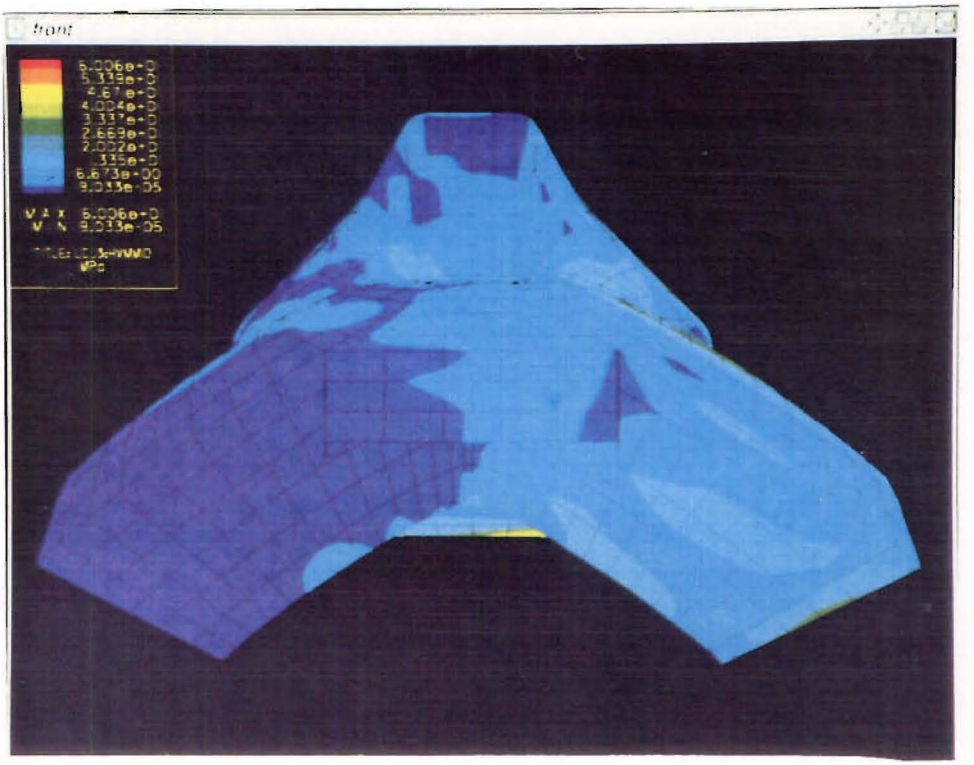

Figure E.11: 273 Reverse Duct; Rear View-Loadcase Three: HVMMID stresses

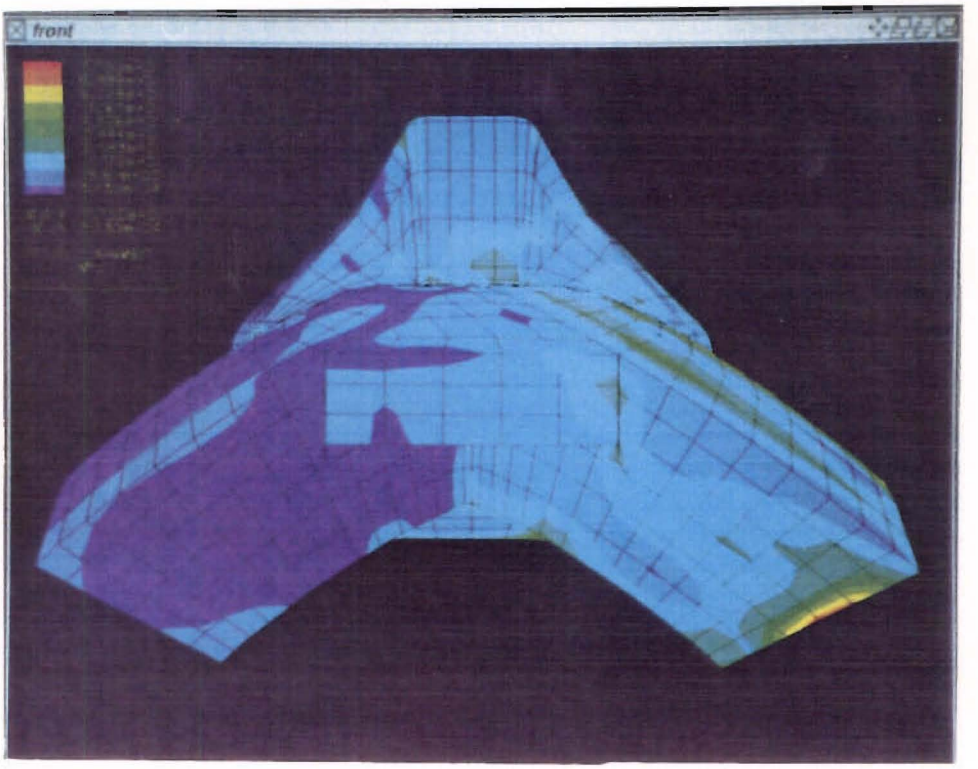

Figure E.12: 273 Reverse Duct; Rear View-Loadcase Three: HVMBOT stresses

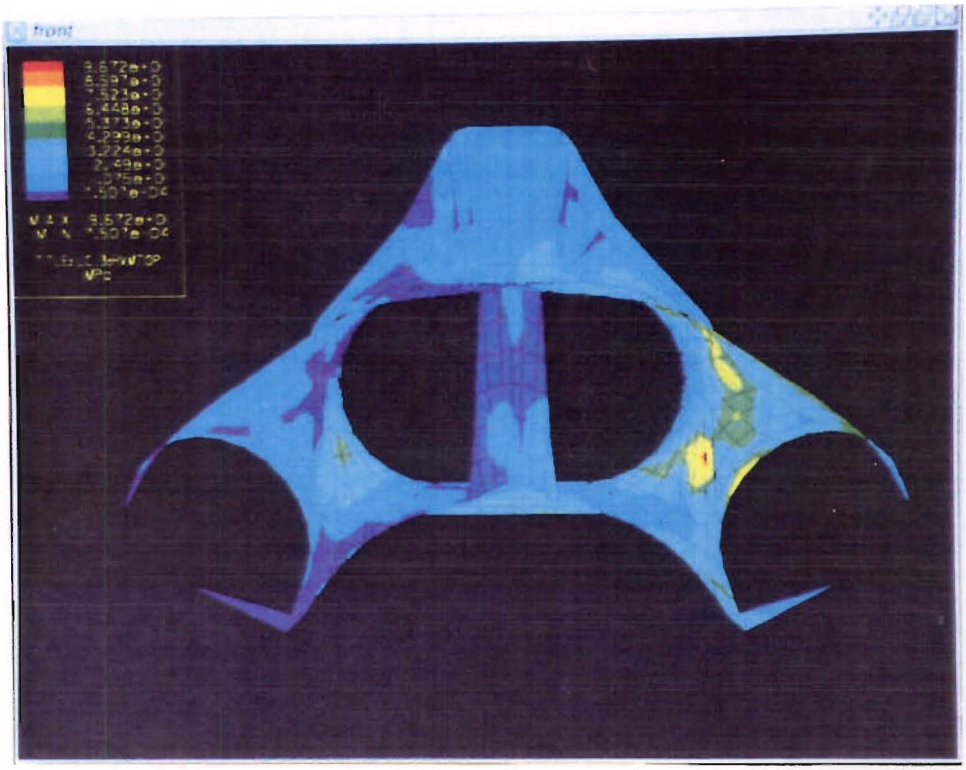

Figure E.13: 273 Reverse Duct; Cutaway rear view–Loadcase Three: HVMTOP stresses

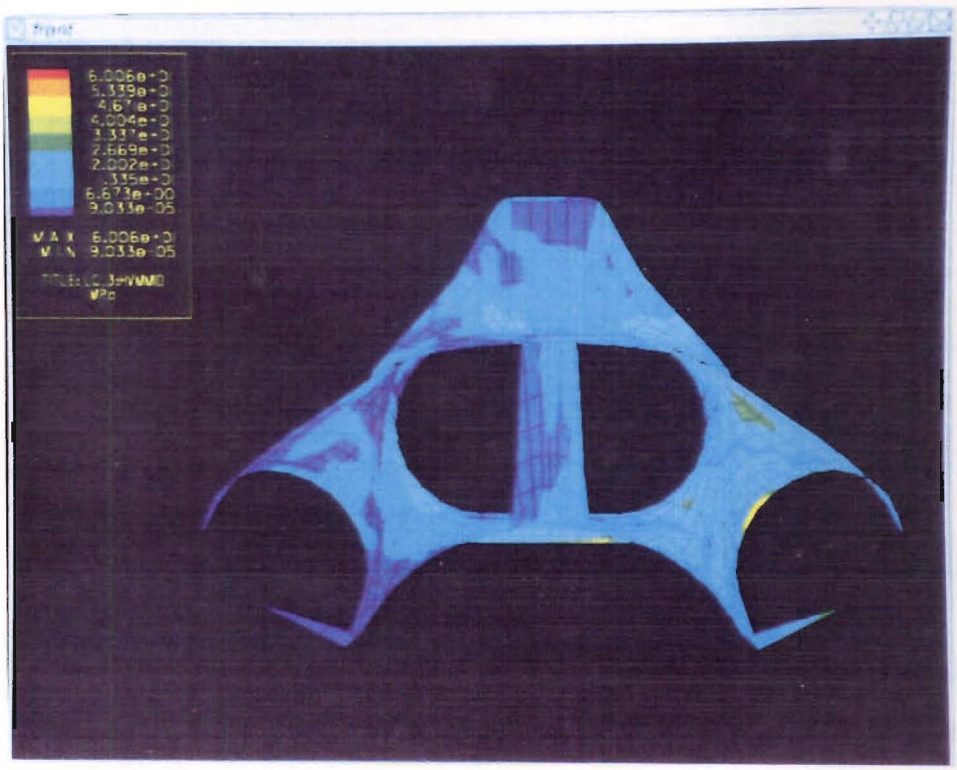

Figure E.14: 273 Reverse Duct; Cutaway rear view–Loadcase Three: HVMMID stresses

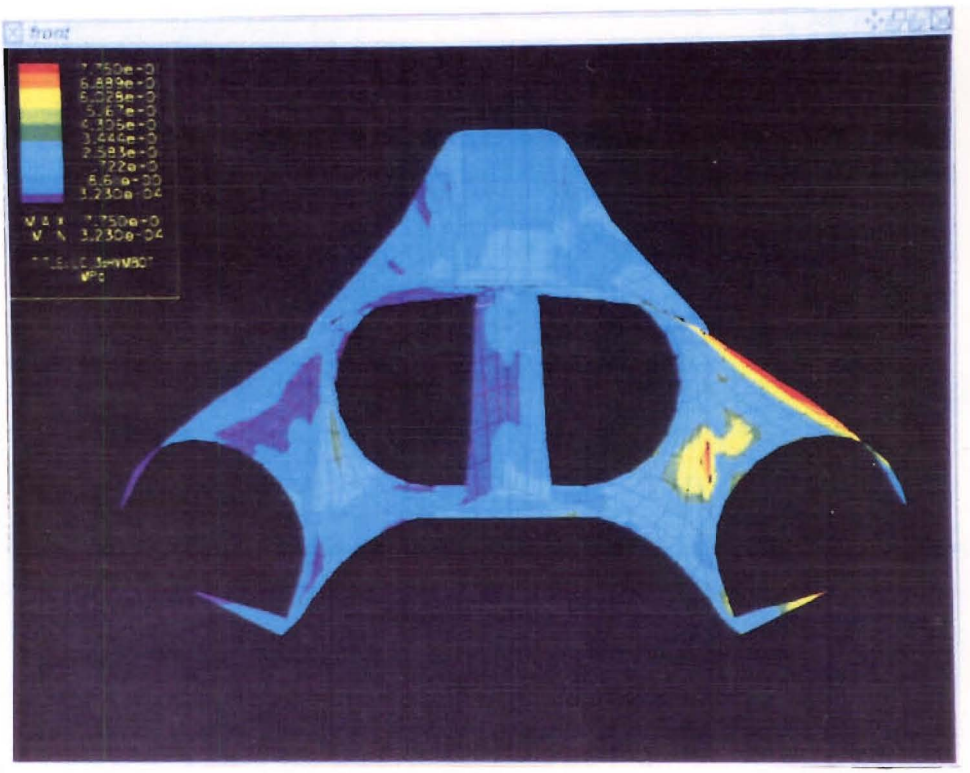

Figure E.15: 273 Reverse Duct; Cutaway rear view–Loadcase Three: IIVMBOT stresses

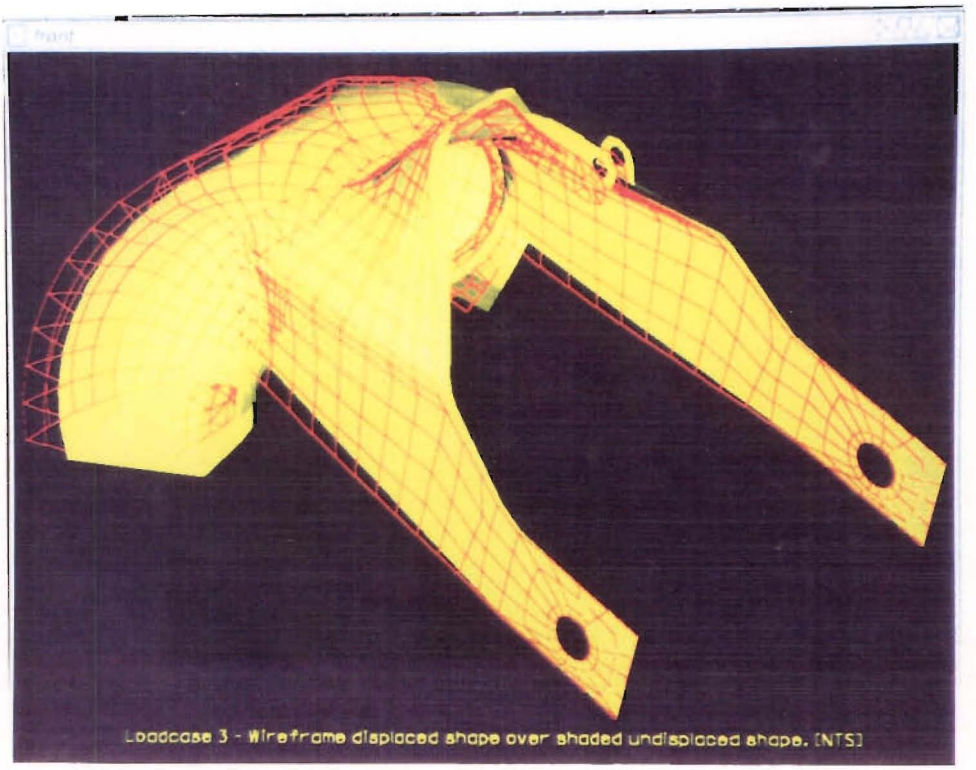

Figure E.16: Displaced shape of the 273 reverse duct–Loadcase Three

Appendix F

273 Reverse Duct Neutral Files.

The attached computer diskettes contains the ascii 'neutral' files for the two analyses of the C.W.F. Hamilton Ltd. 273 Reverse Duct. The files are stored in a 'Neutral' or PATRAN file format, and can be translated to an Intergraph I/FEM (version 1.04.01.18)[1] model for analysis using the "Translate Neutral File to Model" command.

[1]It appears that this model will not run on I/FEM version 2.0, due to some unspecified 'problem'.